MULTI-SOURCE PRECIPITATION ESTIMATION: FILLING GAPS OVER THE RADAR PRECIPITATION FIELD

by

KIBREWOSSEN B. TESFAGIORGIS

A dissertation submitted to the Graduate Faculty in Engineering in partial fulfillment of the requirements for the degree of Doctor of Philosophy, The City University of New York

2012

This manuscript has been read and accepted for the Graduate Faculty in Engineering in satisfaction of the dissertation requirement for the degree of Doctor of Philosophy.

Professor Shayesteh E. Mahani

Date | Chair of the Examining Committee

Professor Mumtaz K. Kassir

Date | Executive Officer

Supervisory Committee

Professor Shayesteh E. Mahani

Professor Reza Khanbilvardi

Professor Vasil Diyamandoglu

Dr. Marouane Temimi

Dr. Robert Rabin

The City University of New York

Abstract

MULTI-SOURCE PRECIPITATION ESTIMATION: FILLING GAPS OVER THE RADAR PRECIPITATION FIELD

by

Kibrewossen B. Tesfagiorgis

Adviser: Professor Shayesteh E. Mahani

Satellite Precipitation Estimates (SPEs) may be the only available source of information for operational hydrologic and flash flood prediction due to spatial limitations of radar and gauge products in mountainous regions. The present work develops an approach to seamlessly blend satellite, available radar, climatological and gauge precipitation products to fill gaps in ground-based radar precipitation field.

To mix different precipitation products, the error of any of the products relative to each other should be removed. For bias correction, the study uses a new ensemble-based method which aims to estimate spatially varying multiplicative biases in SPEs using a radar-gauge precipitation product. Bias factors were calculated for a randomly selected sample of rainy pixels in the study area. Spatial fields of estimated bias were generated taking into account spatial variation and random errors in the sampled values.

In addition to biases, sometimes there is also spatial error between the radar and satellite precipitation estimates; one of them has to be geometrically corrected with reference to the other. A set of corresponding raining points between SPE and radar products are selected to apply

linear registration using a regularized least square technique to minimize the dislocation error in SPEs with respect to available radar products.

A weighted Successive Correction Method (SCM) is used to make the merging between error corrected satellite and radar precipitation estimates. In addition to SCM, we use a combination of SCM and Bayesian spatial method for merging the rain gauges and climatological precipitation sources with radar and SPEs.

We demonstrated the method using two satellite-based, CPC Morphing (CMORPH) and Hydro-Estimator (HE), two radar-gauge based, Stage-II and ST-IV, a climatological product PRISM and rain gauge dataset for several rain events from 2006 to 2008 over different geographical locations of the United States. Results show that: (a) the method of ensembles helped reduce biases in SPEs significantly; (b) the SCM method in combination with the Bayesian spatial model produced a precipitation product in good agreement with independent measurements .The study implies that using the available radar pixels surrounding the gap area, rain gauge, PRISM and satellite products, a radar like product is achievable over radar gap areas that benefits the operational meteorology and hydrology community.

Acknowledgements

This research work has finally materialized with the support of many people. First and foremost, I wish to express my heartfelt gratitude to my advisers Prof. Shayesteh Mahani and Prof. Reza Khanbilvardi who guided me throughout my PhD study. Many thanks for the encouragement, support and invaluable assistance you offered me for the last four and half years.

Special thanks are due to my PhD defense committee members Professor Vasil Diyamandoglu, Dr. Marouane Temimi and Dr. Robert Rabin for their support and comments during my proposal defense and afterwards.

I am extremely thankful to Professor Nir Krakauer for his contribution in our research paper which is published in the journal of HESS. He also read and commented my PhD draft.

I would like to thank Robert Kuligowski, Robert Joyce and Yelena Yarosh for providing some of the necessary data. Thanks are due to Professor Ademe Mekonnen for his support and advice. Thanks to Dr. Shakila Merchant, Nitta Monteiro, Nida Jiwani, Eugen Leykin and Sanchia Peterson for administrative support. Thanks to friends, classmates and NOAA-CREST graduate students for the wonderful time I had. Alvaro, Ousmane, Dugwon, Cecilia and Hossein deserve special mention for cheering me up throughout those demanding years.

I feel especially indebted to my beloved fiancé, Meskerem Belay for the patience, support and perseverance she showed during the period of the research.

I extend my immense thanks to my parents Birsh and Sinkiye and also my brother and sister Abrish and Selamye for their moral support. I thank God for giving me all of you in my life.

Table of Contents

List of Tables

List of Figures

1. Introduction

1.1. General

Precipitation is an important part of the hydrologic cycle, and is the major source of fresh water for the environment. It is also a key forcing parameter for many hydrological, climatological and meteorological studies. Precipitation's impact on the environment is enormous: its deficiency can cause drought, while its abundance can result in flash floods. One way or another, precipitation can adversely affect human lives. Therefore, proper quantification, assessment and forecasting of precipitation both spatially and temporally are vital for engineers and water resource managers to make proper decisions.

Because precipitation depends on many atmospheric and microphysical processes, accurate prediction is difficult. Estimation of ongoing precipitation estimation is difficult because of the following factors. 1) There is not sufficient number of rain gauge station measurements to provide adequate spatial coverage in complex terrain, remote areas and open water bodies. In some areas even if gauges are sufficiently available, they suffer from under-catch, part of the precipitation carried away from the rain gauge because of wind. 2) Remote sensing (satellites and ground-based radars) can provide estimates of precipitation with improved coverage, but suffer from the following deficiencies: a) inadequacy of microphysical parameterization schemes in atmospheric precipitation models lead to inaccurate precipitation estimates in remotely sensed data (Clark et al., 2006); b) ground-based radar measurements in mountainous regions suffer from noise, bright band contamination and terrain echoes among other factors (Fulton et al.,

1998); c) non-unique rain rate--reflectivity relationship has created imprecise estimates in radars (Clark et al., 2006).

So far, more than 10 different algorithms have been developed to estimate precipitation (Levizzani 2003, Fulton et al., 1998). However, estimation with the required spatial and temporal resolution for hydrometeorological use is still a challenge at present time for the scientific community. Evidently, considering a better estimate of precipitation is still in demand, the National Aeronautics and Space Agency (NASA) is working on the Global Precipitation Measurement (GMP) mission, a satellite mission for better future precipitation estimation.

1.2. Precipitation Measurements

Precipitation measurements have a long history. The first rainfall measurement device was used in India in the fourth century BC (Stangeways, 2010). In the United States, scientists started recording precipitation via the Cooperatives Observer Program (COOP) since in the 1890s for climatological and agricultural purposes (Daly et al., 2007). Weather radars were introduced to measure precipitation in the 1950s. Later in the 1970s satellite information was started to be used to estimate precipitation. These measurement techniques and their principles to estimate precipitation are briefly explained as follows.

1.2.1. Rain gauges

The most traditional way of measuring precipitation is using ground-based gauges. It is a direct way of measuring precipitation by collecting the amount of precipitation in a standard

procedure. There are several types of rain gauges. Tipping buckets are one of the first scientific rain gauges (Figure 1-1). They are first used by the British in 1662. Tipping buckets remain one of the most commonly used gauges in the world. They have been used by the National Weather Service (NWS) for more than a century. Later in the early 1960s NWS implemented the more advanced Fisher-Porter design. The Fisher-Porter rain gauges are sometimes used for real-time data. These rain gauges are important for calibrating real time radar and satellite precipitation estimates, but they have limited spatial sampling. Generally Rain gauge measurements are relatively accurate but they are point based information. Rain gauges are mostly monitored manually and hence in general, there are not enough ground-based gauge networks available for areas with the heaviest precipitation, such as high mountains. And it is practically impossible to monitor rain gauges over large water bodies and remotely inaccessible areas. In addition, rain gauges suffer from wind effects, frozen hydrometeors, and uncalibrated tipping in heavy precipitation (Vasiloff et al., 2009).

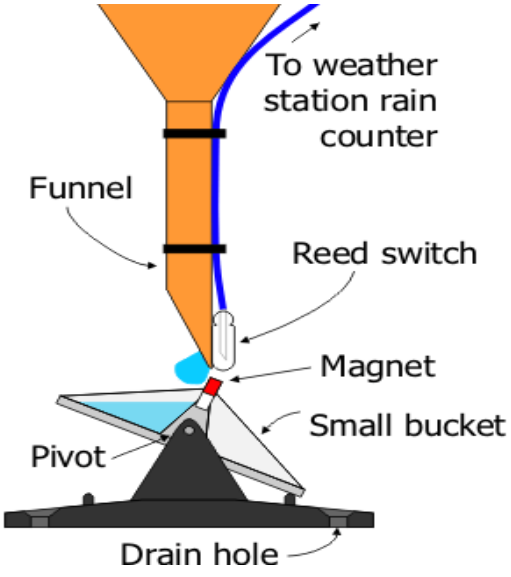

Figure 1-1 Automated tipping bucket rain gauge measurement
(http://www.malvernwx.co.uk/about.htm)

1.2.2. Radars

Because of the extensive coverage and high spatial-temporal resolution, radar based precipitation estimates are highly ingenious approaches to study the precipitation distribution of a certain region. Radars enable precipitation estimation through signal backscattering. In radars, precipitation is estimated using the Marshall and Palmer equation (Marshall and Palmer 1948). This equation is a power function given as $Z=aR^b$; where Z is the backscatter and R is the rain rate. The two parameters a and b are mostly in the range of 75-300 and 1-2 respectively, depending on the type of rain (converctive, stratiform or tropical storm) (Doviak and Zrnic, 1984, Smith and Krajewski, 1993; Lee and Zawadzki, 2005). The Weather Surveillance Radar-1988 Doppler (WSR-88D) uses a=300 and b=1.4. These values are recommended for summer deep convective and non-tropical convection precipitation formations. For orographic induced rainfall, a=75 and b=2.0 are recommended.

The first operational ground-based weather radar in the United States was installed in 1954 by the Army (http://celebrating200years.NOAA.gov/foundations/weather_obs/welcome.html). Now, the NWS has a network of more than 150 ground-based weather radars called NEXRAD (NEXt generation RADar) serving the continental United States. In 1997, NASA in collaboration with Japan Aerospace Exploration Agency (JAXA) launched the first space borne radar on board the Tropical Rainfall Measuring Mission (TRMM).

Radar precipitation estimates are considered as more direct and reliable than other remotely sensed estimates such as optical and infrared based satellite estimates (Gourley et al.,

2011; Tuttle et al., 2008). However, in mountainous regions, precipitation measurements from ground-based radar observations have particular difficulty in terms of: a) eliminating ground echoes caused by blocking of radar beams by high mountains; b) orographic enhanced precipitations occurs at relatively low altitudes which limits the range of usable reflectivity below the melting layer (Gourley et al., 2001). For instance, despite the availability of a dense radar network in the United States, the western river forecast centers rely heavily on gauge interpolated estimates because of limited radar coverage. c) Even if the problem of beam attenuation by heavy precipitation is solved by using 10 cm wavelength radars as in NEXRAD, radars suffer from anomalous signal propagation and bright band contamination. Bright band contamination occurs when radar beams intersect the freezing level of the cloud which can lead in overestimation of precipitation up to a factor of 10 (Gourley et al., 2001; Smith 1986). Quality control of the radar data can identify and eliminate contaminated data, leaving areas of missing data. Given the various sources of error in radar-based rainfall estimates, radar-only QPEs undergo considerable error correction before they are merged with the rain gauge measurements to produce usable products.

Problems in radars have continuously been addressed in different studies. The original WSR-88D algorithm have considered quality control for isolated targets and ground clutter, tilt test and anomalous propagation, and partial beam correction (Fulton et al., 1998). More recent studies developed a range dependent bias correction algorithm (Seo et al., 2002), ground clutter removal using the Radar Echo Classifier (REC) (Kessinger et al., 2000), Vertical Profile of Reflectivity (VPR) variability (Vignal et al., 2001) and Convective-Stratiform Separation Algorithm (CSSA) (Seo et al., 2002), which have been pivotal in addressing such difficulties

(see the respective references and therein for details).

At the NWS, the REC algorithm was implemented a few years ago. The VPR and range-dependent bias correction are not yet implemented. The CSSA is not yet implemented. However, the addition of dual-polarization capability on the entire network of NWS radars will be completed in 2-3 years. A fundamental improvement in accuracy of radar based QPE is expected with the dual-polarization. Use of the dual-polarimetric measurements provides more accurate estimates of QPE than Z-R relationships used with non-polarized radars. In addition, the measurements provide information on the classification of precipitation type (i.e, rain snow, hail etc). A Hydrometeor Classifier Algorithm (HCA) is scheduled for deployment for this purpose. Based on the dual polarization inputs, the HCA classifies hydrometeors for each radar bin. The implementation of the dual polarization is will also help classify different sources of errors in radar reflectivity data such as: attenuation, non-uniform beam filling, partial beam blockage, biological scatters and receiver noise (Ryzhkov et al., 2003; Schuur et al., 2003). This classification will improve radar precipitation estimation skills by ruling out unwanted radar beam reflectivity which should not be considered in precipitation estimation.

Through a thorough understanding of radar problems and their solutions, in the United States, radar based Quantitative Precipitation Estimates (QPEs) are arguably the best remotely sensed precipitation products. Radar QPEs are also important to validate satellite estimates (Krajewski and Smith 2002). Vicente et al., 1998 used collocated radar precipitation pixels to develop a relationship between Auto-Estimator (AE) (Vicente et al., 1998) rain-rate and cloud Brightness Temperature (T_b (10.7 micron)). Rozumalski (2000) used radar Stage-III to validate

the satellite product AE. Bias in radar Stage-III is better than AE (McCollum et al., 2002). McCollum et al., 2002 used gauge adjusted radar precipitation product to evaluate biases in different satellite precipitation products. Ebert et al., 2007 utilized daily accumulated radar precipitation to validate 12 different satellite QPEs (HE is one of them) over northwestern Europe.

1.2.3. Satellites

Using remote sensors mounted on Geostationary Operational Environmental Satellites (GOES) and low orbiting satellites, relevant source of precipitation information has been retrieved. Satellites provide infrared (IR), visible and microwave data which can be used for precipitation estimates (Figure 1-2). In mountainous regions where rain gauges are sparse, and radar gaps are prevalent, this information can be important for precipitation estimation in these areas.

The main principle in IR based precipitation estimates is to relate cloud-top properties and ground level precipitation. IR sensors do not give direct information about the physical characteristics of cloud. And hence, IR based precipitation estimates are indirect which makes them prone to various sources of errors. This inherent shortcoming in IR sensors hinders an accurate precipitation estimates. However, cloud-top information from IR sensors is important to analyze cloud-properties and improve weather forecast skills.

Precipitation estimates based on IR imagery from GOES would be useful to weather forecasters and water managers because their relatively higher spatial (4 km) and time resolution than Microwave based estimates facilitates hydrological prediction in comparison with the ones based on PMW from polar-orbiting satellites.

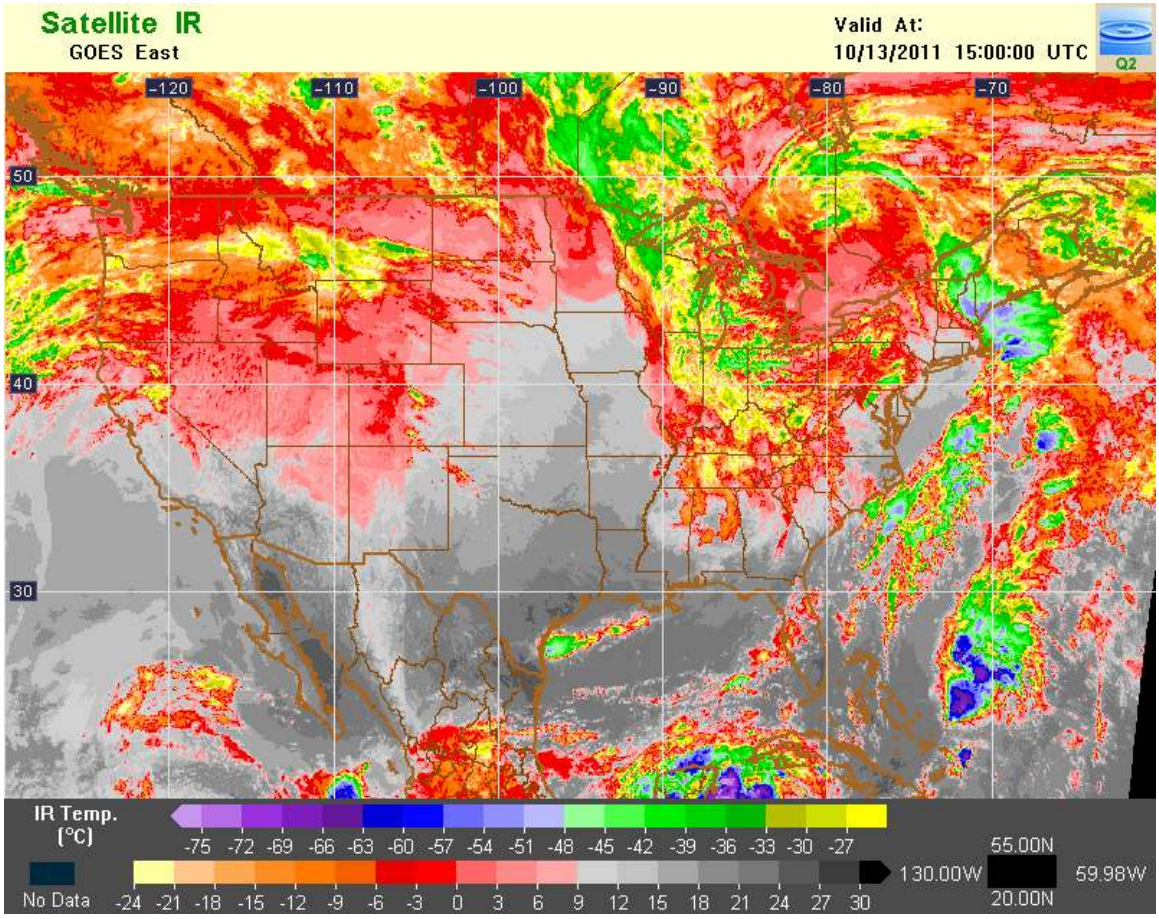

Figure 1-2 An InfraRed sample image from GOES-East (www.nmq.ou.edu)

In addition to IR information, Passive MicroWave (PMW) measurements from low orbiting satellites have been used for precipitation estimates for about three decades. Microwave frequencies from 10 GHz to ~150 GHz are generally used in precipitation estimates. Clouds, rain and snow manifest distinctive properties within this range of PMW frequency. Scattering is a dominant process in Microwave signals above 60 GHz whereas absorption is a dominant

characteristic below 22 GHz. At lower frequencies (below 22 GHz), ice above rain is transparent. These properties make microwave appealing in the field of remotely sensed precipitation retrieval. Sensors such as TRMM Microwave Imager (TMI), Advanced Microwave Sounding Unit (AMSU), Advanced Microwave Sounding Radiometer (AMSR) and Special Sensor Microwave/Imager (SSM/I) are the few examples used in microwave precipitation estimates. The spatial (12.5-25 km) and temporal (mostly two overpasses per day; one overpass per day for TRMM) resolution of Microwave data acquired from polar-orbiting satellites are poorer than IR imaging from GOES. Because of higher resolution than that of PMW, most of the satellite-based precipitation retrieval algorithms over the United States are still based on using IR at 10.7 micron wavelength from GOES.

There are several IR and Microwave based precipitation estimate techniques which have been developed. The first visible and IR precipitation estimation is back in the 1970s (Barrett 1970; Levizzani 2003). The first IR based precipitation estimates were based on cloud-indexing (Barrett 1970, Scofield and Oliver 1977, Arkin 1987). Cloud-indexing is prescribing precipitation estimates based on cloud types, threshold temperature and life-time of cloud. Arkin and Meisner 1987 introduced the GOES Precipitation Index (GPI), which estimates precipitation based on a threshold temperature of 235 K. Auto-Estimator (AE) (Vincete et al., 1998), one of the IR based estimates was developed for deep convective rain estimates. Later, Scofield and Kuligowski (2003) developed Hydro Estimator (HE) to solve AE's dependence on radar and gauges. Precipitation Estimation from Remotely Sensed Information using Artificial Neural Networks (PERSIANN) (Hong et al., 2004) and GOES Multispectral Rainfall Algorithm (GMSRA) (Ba and Gruber 2001) are also IR based products among others. At NWS, HE and AE are operational and available at hourly and 4 km spatial resolution. Products from Special SSM/I

(Ferraro et al., 1997), AMSU-B (Ferraro et al., 2000), Climate Prediction Center Morphing (CMORPH) (Joyce et al., 2004) and TMI (Kummerow et al., 2001) are worth mentioning satellite microwave based precipitation estimates.

To make satellite precipitation estimates more usable in flood forecasting and hydrological modelling, they must be "corrected" and/or combined with another reference such as radar and/or rain gauge measurements.

1.3. Statement of the problem

Despite the fact that there are various instruments and algorithms for precipitation estimations, many of them are not capable of providing a stand alone optimal estimation in certain regions. For example, PERSIANN and TRMM overestimate summertime precipitation over the central Unites States (Gottschalck et al., 2005); rain gauges suffer from under-catch under windy conditions (Vasiloff et al., 2009). Ebert et al. (2007) demonstrated that satellite based precipitation products perform variably when they are compared with ground-based measurements. Similar studies such as Fulton et al., 1998 indicated that radar products such as ST-II have their own problems while detecting precipitation (see Section 1.2.2).

Ground-based radar calibrated by rain gauge measurements, is the only reliable source of providing continuous reflectivity observation directly proportional to rain drop properties within and below cloud base at high spatial (up to 1 km) and temporal resolution (every few minutes) which is required for severe storm and flood related studies and applications. Thus, ground-based radar precipitation estimates are the most common precipitation product that is used by water

resources communities and scientists for various applications in comparison with satellite –based precipitation products.

However, because of limited coverage as shown in Figure 1-4 and 1-5, over mountainous regions such as the northwestern part of the United States where orographic effect creates heavy precipitation, radar estimates may not be usable in those regions (http://www.nws.NOAA.gov/oh/hrl/papers/2000mou/Jay/Jay00.html). Figure 1-4 and 1-5 which indicate seasonal variations of radar coverage are multi radar hybrid scan reflectivity images using the lowest available radar coverage. Hybrid scan reflectivity is a single layer representation of the lowest usable elevation scan (unblocked by terrain and below the height of the freezing level where a bright band might be present). Figure 1-4 illustrates the radar network coverage in the summer and Figure 1-5 illustrates wintertime radar coverage over the northwestern United States. In the cool season, in the western United States, melting level altitude is closer to the ground surface. Above this level the capacity of WSR-88D to estimate precipitation is limited (Westrick et al., 1999). This in turn decreases the effective radar coverage area significantly (Figure 1-5). This is also a common problem when the climatology is stratiform, which is a dominant case in the western United States (Westrick et al., 1999).

Therefore, to cover inaccessible regions not covered by the traditional ground-based radar and rain gauge networks, a more effective observing source and technique is required. Although satellites are the only possible source of collecting information with no spatial limitation, but precipitation estimates from satellite imagery (visible, infrared, and microwave) have greater uncertainties associated with the observing instrument as well as the relationship between precipitation and observations.

Lack of high resolution precipitation information, particularly for heavier precipitation amounts, can create large uncertainty in estimating precipitation and monitoring floods that might cause losses of lives and economic damage. The 1996 catastrophic flood in Oregon is an example for this (Westrick et al., 1999). Therefore, it is very critical to create a solution for covering radar gap areas with high resolution precipitation information that is not much less accurate than radar precipitation.

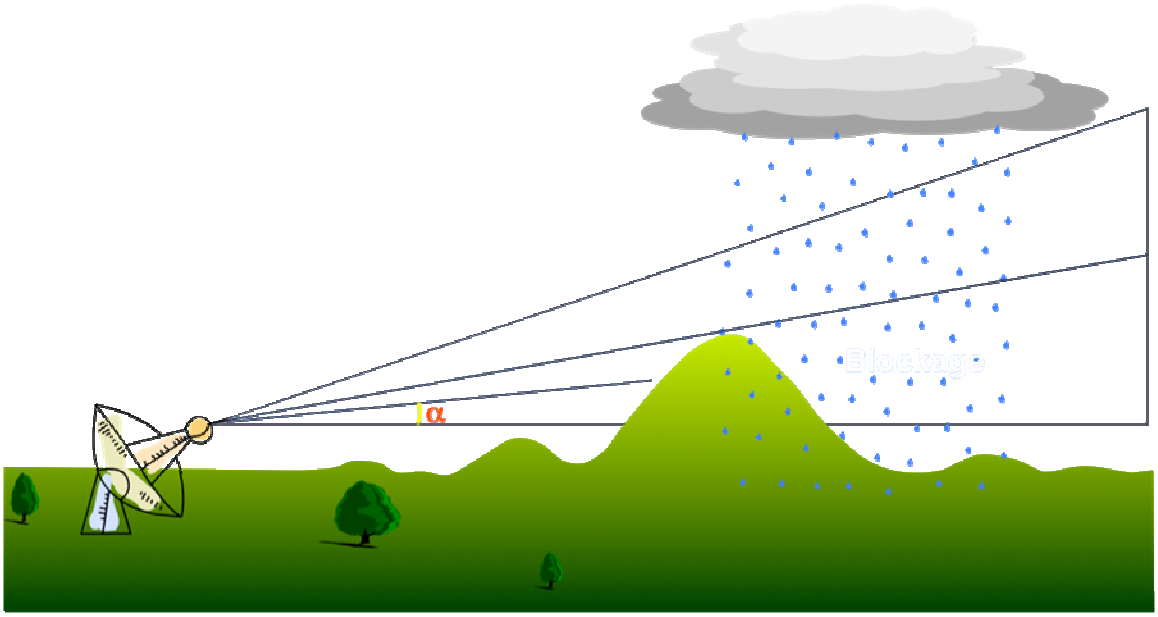

Figure 1-3 An illustration of the lowest three elevation scans of a radar over a mountainous area. In this example, the lowest elevation angle, α, is blocked by higher terrain.

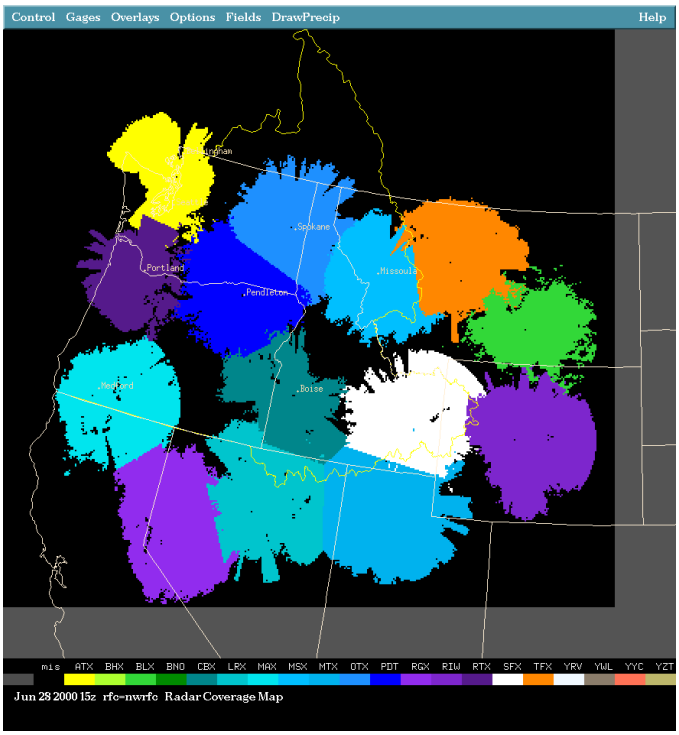

Figure 1-4 Radar Network gap coverage over the Northwestern U.S. in the summer (http://www.nws.noaa.gov/oh/hrl/papers/2000mou/Jay/Jay00.html)

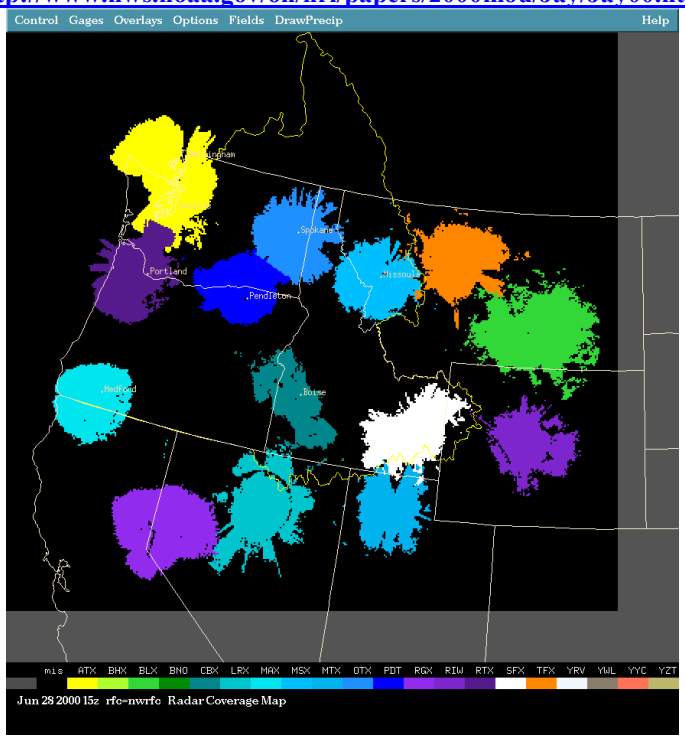

Figure 1-5 Radar Network gap coverage over the Northwestern U.S. in the winter (http://www.nws.noaa.gov/oh/hrl/papers/2000mou/Jay/Jay00.html)

1.4. Objectives

The objective of the present study is to generate high resolution precipitation estimates with better accuracy than IR based estimates for radar gap coverage. To cover inaccessible regions not covered by traditional ground-based radar and rain gauge networks, which is NOAA-NWS's interest, satellites seem to be the only possible source of collecting information with no spatial limitation. Because of greater uncertainties in comparison with radar measurements, the goal of this study is to enhance available satellite-based estimates for radar gap areas by using available radar, climatological Parameter-elevation Regressions on Independent Slope Model (PRISM) and Rain Gauge (RG) precipitation estimates around and in the gap area.

Therefore, the objective of this study focuses on: (1) improving hourly and daily satellite precipitation estimates, and (2) development of a merging algorithm to combine various precipitation data sources from rain gauges, satellite, climatology and radar, and (3) generate accurate precipitation estimation for the radar gap areas.

1.5. Project Description and Proposed Plan

Satellite and radar based products have differences in their measurements of precipitation. We expected higher correlations between them would be achieved with adjustment of one or the other. Specially in the process of merging two or more different precipitation products, their differences and sources of errors have to be clearly understood to achieve an optimal multi-source precipitation product. A closer look at and attention to details are required between satellite and radar precipitation products before the process of merging different

products. In this project, we observed that satellite products from NOAA/NESDIS produced on hourly basis manifested two classes of measurement errors in comparison with radar-gauge Stage-IV (ST-IV) product. These measurement errors are: (1) spatial error, and (2) intensity (magnitude or amplitude) error. The spatial error is characterized by a location difference between the measurement (satellite based product) and the 'truth' (radar based product). The position error may be a result of differences in viewing angle of the measurement and the truth, change of speed by the satellite, or difference in measurement times. Attenuation and non-Rayleigh scattering may cause distortion in returning satellite signals (Bolen and Chandrasekar 2000). Sensitivity of retrieval algorithms to relative location of the satellite can also be a reason for discrepancies between estimates of precipitation from ground-based radar and satellite observations (Grassotti et al. (1999)).

Intensity error is defined as the difference in intensity between the measurement and the 'truth' amounts at corresponding points (pixels). Intensity error can either be systematic and/or random errors. Systematic errors are errors caused by instrument and/or equation errors. The sources of random errors are unpredictable; and difficult to track down and adjust. Sometimes they can be caused by algorithms produce automated maps. Intensity error and bias are used interchangeably throughout this dissertation.

The aforementioned errors can be reduced to some extent. In the present study, a new method is proposed to correct intensity biases in satellite precipitation estimates. In this research, it is assumed that Stage-IV (ST-IV) can be used as a reference precipitation field against which to correct systematic errors in SPEs. Besides, quality controlled ST-IV is the best possible high

resolution (4 km, hourly) precipitation product that we could find. One reason for selecting ST-IV precipitation product is being aware that radar-only products suffer heavily from issues such as calibration, anomalous beam propagation, clutter, range dependent bias and bright-band contamination (Krajewski and Smith, 2002; Fulton et al., 1998). ST-IV product is adjusted for some of the mentioned error sources by implementing Radar Product Generator (RPG) adjustment algorithm, using hybrid scan construction, and more. It includes manual quality controlled product too.

In addition to intensity biases, satellite precipitation estimates suffer from spatial errors. To correct spatial errors, a method of alignment is proposed to reduce the mismatch between satellite and a corresponding radar precipitation estimates. The two mentioned methods are detailed in Sections 3.1 and 3.2. The corrected (spatially and intensity) satellite based precipitation estimate was merged with radar rainfall estimation using the method of SCM. This merging algorithm was found capable of extending radar information from pixels with radar rainfall measurements to the neighbouring pixels without radar precipitation estimates. Section 3-3 of this study focuses on development of a merging approach to combine SPE with available radar-based rainfall (RR) for improving SPE even over the radar gap coverage areas. The merging technique can successfully extend the patterns of RR from the surrounding pixels to the radar gap region. The SCM with different schemes is detailed in Section 3.3.1. And, finally, the merged satellite-radar rainfall product will further be merged with rain gauge measurements and PRISM using the spatial Bayesian approach which will be detailed in Section 3.3.2.

1.6. Motivation

The overall process of this study uses a collection of selected algorithms to produce a multi-source precipitation product over radar gaps. The motivation behind the selected methods is explained briefly as follows.

Image registration has been applicable in different fields of science and engineering to restore and align different images (data) (Zitova and Flusser, 2003). Different aligning techniques have been used to adjust spatial differences between remotely sensed data and the 'truth' (e.g. Bolen and Chandrasekar 2003). In this study, a linear image alignment (registration) is used to reduce spatial errors of SPE. Its simplicity and versatility makes it a prior choice for our application. Linear alignment produced a satisfactory result with less mathematical burden.

Most of the previously developed bias correction work assumed that the point-based observations of precipitation provided by rain gauges form the reference 'true' measurements against which to evaluate and correct SPEs and radar-based precipitation products. However, the rain gauge network is not always dense enough to accurately represent a region's precipitation, and errors can arise in using point rain gauges to represent precipitation of a radar or satellite pixel (Chumchean et al., 2003). In contrast, radar provides pixel-based areal precipitation measurements with better spatial coverage that is more comparable to the scale of satellite imagery. The United States has more independent radar coverage pixels than point rain gauges. Hence, there are smaller sampling and random errors (Xie and Arkin, 1997) in using merged radar-gauge products rather than point-based rain gauges alone particularly in areas where

gauges are relatively sparse. We therefore will use a merged radar-gauge precipitation product as a reference to detect and correct biases in SPEs.

Statistical approaches to merge different precipitation estimations have been demonstrated as one of the alternatives to obtain an optimal rainfall estimate (e.g. Sapiano et al., 2008). An advantage of a statistical methodology is that it optimally merges the inputs based on weights and errors associated with them. Thus, merging high resolution multi-source/multi-sensor information can help reduce bias and noise around radar gap areas.

The Successive Correction Method (SCM) is a method originally developed for data filtering. Its flexibility and usability in different schemes is the motivation behind using it to fill gaps (missing pixels) over the radar network. The Brandes and Single Optimal Estimation (SOE) schemes have been used to combine precipitation from different sources in previous studies. SOE has been operational at the NWS to combine radar precipitation estimates with gauges for more than a decade. This operational success makes it interesting to test it to combine radar with satellite precipitation estimates in this study. These schemes are modified to suit our purpose, successfully extend the patterns of radar precipitation estimates from the surrounding pixels to the radar gap region.

Rain gauges have been pivotal in precipitation measurements. Their accuracy at point measurements is very important in terms of assuring accuracy in multi-source precipitation estimates. Studies such as Wilson (1970) showed that 'radar precipitation estimates, when calibrated with gauge density as low as one gauge per 3400 km^2 are more accurate than estimates

from gauges alone spaced one per 860 km^2.' In addition to rain gauges, the climatological precipitation product PRISM may also provide physical and statistical information into the multi-source based estimate. To combine several data sources in one framework is challenging unless a more advanced mathematical approach is used. A linear Bayesian spatial model is developed to merge the available datasets. Statistical Bayesian spatial model approach is well understood and rigorously used by the scientific community. However, it is not an easy approach, moreover it is computationally expensive. The method's capability to ingest as many data as possible makes it a viable tool in the near future. In mountainous regions where rain gauges are sparse, statistical approaches such as Bayesian spatial model has demonstrated efficiencies in such conditions.

1.7. Background and Literature review

1.7.1. Spatial adjustment

Satellite precipitation estimates such as AE and HE undergo spatial adjustment known as parallax for convective clouds (Vicente et al., 2002, Kuligowski et al., 2003). Parallax error is a spatial displacement caused by the different sight angles of the top of the cloud. Even if, precautions and adjustments are made, spatial errors between satellite and ground-based precipitation observations still exist (Bolen and Chandrasekar 2003).

Spatial error has been the subject of several studies for more than a decade. Bolen and Chandrasekar (2003) used a quadratic least square approach to align space borne radar and ground-based radar. Anagnostou et al. (2000) used volume matching of reflectivity to compare space borne and ground-based radars. A method of Feature Calibration and Alignment (FCA)

has been employed by Grassoti et al. (1999) for integrating radar and satellite based precipitation estimates.

Grossatti et al. (1999) developed a new methodology, Feature Calibration and Alignment (FCA) to integrate radar based and satellite based precipitation estimates. The method adjusts both alignment (geolocation) and magnitude differences in satellite estimates using the method of variational approaches. Precipitation from SSM/I and radar occurring at the same time were used to develop the algorithm, they tested the technique on a number of satellite and radar rainy cases. They concluded that the method may be applicable to calibrate satellite estimates based on radars.

Bolen and Chandrasekar (2003) presented a method to align measurements from space borne radar (TRMM) with ground-based radar. The method aligns space borne measurements with ground-based measurements using an alignment equation originally developed by Schowengerdt (1997). It is a least square approach with parameters that account for shift in the latitude, shift in the longitude, rotation, scale and shear in the space borne measurements. Bolen and Chandrasekar (2003) used a quadratic version of the Schowengerdt's (1997) equation to align TRMM PR reflectivity with that of ground-based radar.

Nehrkorn et al. (2003) used the FCA method to characterize and analyze errors in the weather forecast. In Nehrkorn et al. (2003)'s work, an empirical regularization constraint is incorporated to the original FCA method to reduce its subjective nature. The study indicated that medium-term forecasts are subject to large scale phase (geolocation) and bias errors.

Ravela et al. (2007) proposed a technique that accounts both position and amplitude errors in data assimilation. Local displacements in current model state are aligned continuously with observations using field alignment. They demonstrated the method with examples, and showed that field alignment helped model performance.

Despite these attempts to correct spatial discrepancies, spatial mismatches between satellite and radar precipitation products continue to persist. In addition, efforts to correct high resolution geostationary satellite based precipitation estimates using ground-based radar networks have been limited. In our study, we propose spatial adjustment of a satellite based precipitation estimate by collocating with a ground-based precipitation estimate. This is a vital prerequisite step for merging.

1.7.2. Bias Correction

Systematic errors, commonly known as biases are the deviations from the true value. Biases in precipitation are found in many forms. For instance, sources of biases in radar can be improper Z-R (radar reflectivity-rainfall rate) relationship, evaporation of rain drops after they are intercepted by the radar signal, overshooting the cloud system, mis-calibrated radar (Doviak and Zrnic 1984) and so on.

Different authors proposed and exploited different bias correction techniques to improve precipitation estimations. Anagnostou et al. (1998), Smith and Krajewski (1990), and Seo and

Breidenbach (2002) used mean bias field estimation and correction approaches to solve the problem of biases in radar precipitation estimations in real time. In their approaches, their hypothesis was that estimated precipitation field from radar do not deviate from representative rain-gauge measurements under the radar umbrella.

Since satellite based precipitation estimates are uncertain and observations are indirect, they are prone to errors. Efforts have been put to quantify and correct these errors in satellite precipitation estimates (Boushaki et al., 2009, McCollum et al., 2002, Smith et al., 2006). Most of these works prioritize rain-gauges to correct the errors in satellite precipitation estimates. However, the rain-gauge network does not always accurately represent a region's precipitation distribution. For example, in mountainous regions, like in the north-western part of the United States where rain-gauges are sparse, many of rain-gauge based bias correction of satellite precipitation retrieval approaches have limited utility. In contrast, radars offer indirect precipitation measurements with better spatial coverage and more complete sampling than rain-gauges, which are direct point observations of precipitation. As part of the over all study, our objective is to improve satellite precipitation estimates using radar-gauge precipitation estimates over the radar gap. Rain gauge adjusted radar product provides a realistic areal and time representation for the study area when it is compared with rain-gauges. United States has more radar coverage pixels than point rain-gauges. Therefore, gauge-adjusted radar precipitation estimate provides a more realistic advantage than rain-gauges to correct biases in satellite products.

In general, since satellite-based precipitation products are estimates from indirect measures (e.g., IR cloud-top temperature), they are prone to errors greater than the ones for radar-based precipitation measurements. Thus, more accurate high-resolution precipitation products could be obtained by combining satellite-based estimates with radar-based ones, using the satellite imagery to fill in precipitation in areas where radar is not available. In merging satellite with radar estimates of precipitation, any bias in the satellite-based precipitation estimation must be quantified and corrected so that the merged product is, as far as possible, consistent.

A simple and widespread approach to reduce the error in one precipitation product relative to another, reference product is to multiply the precipitation from the first product by a "bias factor" chosen to optimize the correspondence of the two products where they overlap. Authors such as Ahernet et al. (1986), Anagnostou et al. (1998), Smith and Krajewski (1990), and Seo et al. (1999) estimated constant bias factors that were applied to the entire estimated precipitation field to correct biases in radar precipitation products, as compared to point-based observations from rain gauges. Seo and Breidenbach (2002) used a spatially varying bias factor to reduce biases in radar precipitation products against rain gauge observations with the hypothesis was that radar-gauge biases are variable, but spatially and temporally coherent. Efforts have also been made to quantify and correct biases in SPEs using rain gauge information (e.g. Boushaki et al., 2009 and Smith et al., 2006). McCollum et al. (2002) evaluated biases of SPEs using a gauge corrected radar precipitation product. In this research we propose a new approach which is detailed in Section 3.2 to improve biases in satellite-based estimates.

1.7.3. Merging Multi-Source Precipitation Data

Most research efforts on using multi-sensor data focus on calibrating or merging radar- or satellite-based precipitation with rain gauge observation to improve quantitative precipitation estimation (QPE) (Seo (1998b); Steiner, et al. (1999)) and forecast (QPF) due to the assumption that rain gauge observations can reliably account for the true values of point-based precipitation. There are ongoing research studies on merging satellite-based precipitation with rain gauge observations to adjust SPE bias. NWS-Office of Hydrologic Development (OHD) is working on integrating bias corrected SPE with rain gauge data to fill the radar gap coverage and create a radar mosaic algorithm to be implemented in the quantitative Multi-sensor Precipitation Estimation (MPE) algorithm (Kondragunta, et al., (2005)). The method applied for bias correction is similar to the one used for combining radar with rain gauge data (Seo and Breidenbach (2002a; Seo, et al. (1999)) to produce MPE, with the exception that radar precipitation measurements are replaced with satellite precipitation estimates. Similar multi-sensor merging approach was used for estimating more accurate stratiform rainfall in Arizona by Gourley et al. (2002) with consistent results. Satellite-based retrieved precipitation, after bias correction against rain gauge observation, was integrated with radar and rain gauge rainfall into the NWS-AWIPS by Fortune et al. (2002). The SIMAR program, has had the goal of merging satellite, radar, and gauge information to produce one field rainfall product for South Africa (Pegram et al. (2004)). Kriging was used in the merging approach of the SIMAR program to interpolate optimal rain-fields between rain-gauges at individual locations for converting point based observation to watershed based scale. Although multi-sensor precipitation estimation has thus been studied by several authors, they have not all reached a breakthrough to achieve the required optimal precipitation estimation over the radar gap. Besides, most of these studies

appear to ignore errors in remotely sensed precipitation products. Therefore, a multi-source algorithm that considers as many errors as possible and being capable of providing precipitation estimates in radar gaps would be beneficial to the hydro-meteorological community. In this paper, we are proposing to merge all the three sources of precipitation products, rain-gauge, radar and satellite. The method is detailed in chapter 3.

Seo (1998b) developed the method of Single Optimization Estimation (SOE) to merge radar precipitation products optimally with point rain gauge measurements. The study showed satisfactorily results for Oklahoma State. The method assumes that radar pixels are spatially and statistically correlated with rain gauges in a specified range (distance). He used exponential function to estimate spatial correlation of the precipitation process. From May 1996, the method is implemented at NWS River forecast centers to produce hourly multi-source precipitation products (NEXRAD).

CPC Merged Analysis of Precipitation (CMAP) precipitation estimation is a combination of rain gauge, both IR and MW satellite and model based products (Xie and Arkin 1996). In CMAP, ungauged pixels are estimated using the linear maximum likelihood technique using the rain gauges to calculate the random error. The data is available at NOAA/CPC since Jan 1979 at a spatial resolution of 0.4^{o} and 6 hourly (Gottachalk et al., 2005).

2. Case Studies and Data

2.1. Study Area

The area of this study is the western part of the United States, specifically regions afflicted by radar gaps. These specific study areas are described in chapters 4 and 5. The western United States, as shown in Figure 1-3 is afflicted by ground-based radar signal blockage in spite of the fact that U.S. has an enormous radar network. As a result, this region of the United States lack radar information about crucial weather features, such as heavy precipitation.

2.2. Data

For this particular study, high resolution satellite, gauge, climatologic and radar precipitation estimations are used. At NOAA-NWS, several hourly GOES IR based rainfall products are available; namely: HE (Scofield and Kuligowski, 2003), GMSRA (Ba and Gruber 2001), SCaMPR (Kuligowski 2002) and AE (Vicente et al., 1998). The performance of these various algorithms differ from one to another (Ebert et al., 2007). Therefore, we had to choose two of the best satellite precipitation estimates for our merging algorithm. Hourly, 4 km products of AE, GMSRA, HE, ST-IV and SCaMPR for the years 2006, 2007 and 2008 were obtained from National Environmental Satellite, Data, and Information Service (NESDIS).

Using the statistical parameters shown in Table 2-1, the different IR satellite precipitation estimates listed in the first column of Table 2-1 were compared with radar ST-IV. Using ST-IV as a reference for comparison, hourly precipitation data for the year 2006 involving more than 73.5 million raining pixels of ST-IV was investigated. Based on the results shown in Table 2-1

(see Apendix for definitions in the table), HE showed a better performance when it is compared with ST-IV and was selected for further analysis.

Table 2-1 Performance of the different GOES IR based precipitation estimates for 2006 in OK region

Satellite Rainfall Estimation	Bias Score	Probability of Detection	False Alarm Ratio
GMSRA	18.26	0.70	0.87
HE	3.80	0.45	0.65
SCaMPR	9.45	0.61	0.86
Auto-Estimator	4.10	0.32	0.70

2.2.1. Hydro-Estimator (HE)

HE (Scofield and Kuligowski, 2003), one of the satellite precipitation estimates which we used in this study, is based on one of the cloud-top IR and rainfall relationships. High resolution hourly HE product at 4 km × 4 km pixel size, uses the GOES IR window channel-4 (10.7 μm wavelength) as the main input data to estimate the rate of surface rainfall. HE was developed as an improvement to the original AE, which was intended for deep, moist convective systems (http://satepsanone.nesdis.NOAA.gov/PS/PCPN/HE.html). The HE algorithm identifies raining clouds based on both pixel brightness temperature (T_b) in GOES channel-4 and its value relative to its surroundings—pixels that are colder than their neighbors are presumed to be regions with updrafts and rainfall, while pixels warmer than the neighborhood average are associated with lower clouds and light or no rain. Rainfall rate is estimated as a function of pixel T_b, its

surrounding values, precipitable water, relative humidity, convective equilibrium level, and lower-tropospheric winds, and terrain is used to diagnose regions of terrain-induced updrafts and downdrafts. At the NOAA National Environmental, Data, and Information Service (NESDIS), HE has been an operational rainfall product since 2002, and has been available at a spatial scale of 4 km by 4 km and hourly time scale for CONUS since 2004.

2.2.2. Radar Stage-II (ST-II) and Radar ST-IV (ST-IV)

At NWS, there are four stages of radar-based rainfall products. References such as Fulton et al., 1998 and Lin and Mitchell 1999 contain details of how the different stages of radar products are produced. Briefly, Stage-I radar rainfall is produced for each radar scan at each radar site using the Z-R relationship. Hourly Stage-I products are generated by summing up the scan-wise accumulations. In the next step, the Stage-I products are adjusted for mean field bias using all the available rain gauges to produce bias-adjusted Stage-II (ST-II) rainfall products. The bias adjusted Stage-II products are further optimally merged with point rain gauges (Smith and Krajewski, 1991, Fulton et al., 1998, Seo et al., 1999). In Stage-III, at each NWS River Forecast Center (RFC), the Stage-II (radar-gauge) products from multiple radars are stitched together to cover the area under the respective RFC. At this stage, overlapping Stage-II products are optimally combined. In addition, Stage-III products undergo routine manual quality control to make sure that products are free from any obvious error (Fulton et al., 1998). The regional Stage-III products obtained from the 12 RFCs are further mosaicked to a national 4 km stereographic NWS's Hydrologic Rainfall Analysis Project (HRAP) grid at NCEP, forming the ST-IV product. ST-IV is thus ultimately generated from more than 3000 automated hourly rain

gauge observations and the WSR-88D radar based digital precipitation arrays (DPA) (Fulton et al., 1998) . The latest version of ST-IV contains HE and Mountain Mapper in the western part of the United States. Mountain Mapper is a combination of point rain gauges with climatological PRISM (Schaake et al., 2004). ST-IV precipitation product is available since 2001.

Radar based precipitation estimates are known to have problems including isolated targets and ground clutter, anomalous propagation, and partial beam reflection in mountainous regions (Fulton et al., 1998). Radar also suffers from range dependent attenuation (Young et al., 1999). However, composite products, such as ST-IV from NCEP, are manually quality controlled and corrected for these problems using direct rain gauge observations as one source of calibration.

In this work, it is assumed that quality controlled radar products using rain-gauge observations can be used as reference precipitation estimation sources to correct systematic errors in satellite rainfall estimations. Hourly radar ST-II and ST-IV, a mosaicked product over the CONUS with a spatial resolution of 4 x 4 km for the years 2006 to 2008 have been used in this study.

2.2.3. Climate Prediction Center Morphing (CMORPH)

CMORPH is a gridded precipitation product based on Microwave data from instruments aboard low-orbiting satellites with a secondary use of IR cloud imagery. CMORPH is based on both passive microwave data from low orbiting satellites and IR data from GOES satellite (Joyce

et al., 2004). CMORPH produces operational global (60^{o}N–60^{o}S) precipitation products at spatial resolution as high as 0.0728^{o} (~8 km at the equator) and half hourly time scale, which is the resolution we used. It combines the different existing microwave–based precipitation products from Special Sensor SSM/I (Ferraro et al., 1997), AMSU-B (Ferraro et al., 2000), and TMI (Kummerow et al., 2001). The effective temporal resolutions of these products are on the order of hours, corresponding to the overpass frequency of most of the low orbiting satellites. In the CMORPH algorithm these microwave based precipitation products are propagated backwards and forwards in time to calculate precipitation at a finer time resolution. The IR data is used to determine cloud evolution to propagate rainy pixels from the microwave products (Joyce et al., 2004). CMORPH has been operational and data are available since 2002 from the Climate Prediction Center (CPC) of the National Centers for Environmental Prediction (NCEP).

2.2.4. Rain-gauges

The NWS administers two types of rain gauges, manual (standard rain-gauges) and recording rain-gauges (Fisher-Porter recording gauges) (NWSI 10-1302) in the U.S. There are about 18,000 Cooperative Observing Program (COOP) gauges over the United States to measure daily precipitations (http://www.ncdc.noaa.gov/oa/climate/climatedata.html#hourly). There are about 6000 COOP gauges which are used to measure hourly precipitations. 2300 of these COOP gauges are Fisher-Porter rain-gauges to measure hourly precipitation (http://www.nws.noaa.gov/om/coop/newsletters/10winter-coop.pdf). These gauges measure daily, hourly and event based precipitation. We use the rain gauge data in the merging process.

They are assumed to represent a 4 km x 4 km grid. Independent gauge measurements will also serve for validation of the final algorithm.

2.2.5. PRISM

Parameter-elevation Regressions on Independent Slope Model (PRISM) has first been developed by the PRISM research group at Oregon State University for climatological studies (Daly et al., 1997). PRISM uses point data, digital elevation model and other climatologic as inputs to produce monthly climatological data temperature, precipitation, dew point and percent of average precipitation for the conterminous United States. The method in PRISM works in such a way that it assigns weight to ungaged locations based on their climatological similarities with the surrounding gauge stations. In PRISM elevation is the most important factor in precipitation distribution (Daly et al., 2002). The parameters in the regression equation are determined for each grid cell based on climate-regression function (Daly et al., 2002). The data is available at a spatial and time resolution of 4 km and monthly respectively at Oregon State University (PRISM Climate Group, Oregon State University, http://prism.oregonstate.edu).

For this study, averaged disaggregated monthly PRISM data is used. For instance, to produce a PRISM precipitation product for 30 March 2008: first, monthly PRISM data from 1998 to 2007 for the month of March is averaged which is the sum of the data divided by 10. Second, the averaged data is disaggregated to using daily rain gauge measurements. The disaggregation method is based on the method of partial fractions as explained in (Schaake et al.,

2004) Note that, rain used for calibration and validation were not used for the disaggregation purpose.

3. Methodology

To fulfil the objective of this study, the selected SPE (Section 2-2), RR, PRISM and RG will be combined through three steps, which are: 1) spatial and distribution adjustment of selected satellite-based precipitation estimates (HE) against radar ST-IV (ST-IV); 2) rainfall intensity bias correction of HE in comparison with ST-IV rainfall; and 3) development of a merging algorithm to combine spatial and bias corrected HE with available ST-IV to generate more accurate rainfall for radar gap areas. These procedures are explained in details in the following sections.

3.1. Spatial error correction

In this study, we employ the modified image alignment algorithm (Schowengerdt (1997)) to estimate the offset between the radar and the satellite rainfall measurement. The algorithm aligns satellite measurement field to the radar data at the same observation time by minimizing the spatial discrepancy. The method in this study calculates the displacement, scaling and the shear in the latitude- and longitude-direction, and establishes aligned field that best fit the radar data. This algorithm is using the alignment equations proposed in Schowengerdt (1997) and used by Bolen and Chandrasekar 1999. In an attempt to automate the algorithm for future use, our approach differs from that one in calculating the cost function, clustering analysis and the number of parameters calculated.

The first step in our approach is to pick corresponding coordinates in satellite and radar products. Because it is usually difficult to pick random corresponding coordinates in two

different rainfall products, we proposed a method of clustering rainy pixels in the same localities. The method of hill climbing (Lee et al., 2003) was used as a clustering analysis tool. Once the rainy pixels are clustered, corresponding peripheral contour coordinates in radar and satellite were picked up.

According to Schowengerdt (1997), corresponding coordinates of satellite based and ground precipitation estimates can be related using the equations:

$$lon(R) = \sum_{i=0}^{n} \sum_{j=0}^{n-1} a_{ij} \cdot lon_i(S) \cdot lat_i(S) \qquad 3\text{-}1$$

$$lat(R) = \sum_{i=0}^{n} \sum_{j=0}^{n-1} b_{ij} \cdot lat_i(S) \cdot lon_i(S) \qquad 3\text{-}2$$

Here, n is the degree of a polynomial; *lat* and *lon* are the latitude and longitude respectively; S and R refer to satellite and radar coordinates respectively; a and b are adjustment coefficients. Bolen and Chandrasekar (2003) used a quadratic function with n equal to 2 to match TRMM satellite radar with ground-based radar. In our study we propose a linear Schowengerdt's equation with n equal to 1 to correct the spatial misfit between a satellite and a radar product. We have tried Equations 3-1 and 3-2 with n equal to 2, however the results are not notably different from using a degree of n equal to 1. n equal to 2 improved False Alarm Ratio (FAR) by 1 % better than n equal to 1. Therefore, we opted to use a linear registration with a degree of n equal to 1 with less mathematical burden. For a given list of independent corresponding coordinates of radar and satellite precipitation pixels, Equations 3-1 and 3-2 in a sense of linear regression model can be written as:

$$\begin{bmatrix} lon_1(R) \\ lon_2(R) \\ \vdots \\ lon_{s-1}(R) \\ lon_s(R) \end{bmatrix} = \begin{bmatrix} 1 & lon_1(S) & lat_1(S) \\ 1 & lon_2(S) & lat_1(S) \\ \vdots & \vdots & \vdots \\ 1 & lon_{s-1}(S) & lat_{s-1}(S) \\ 1 & lon_s(S) & lat_s(S) \end{bmatrix} \begin{bmatrix} a_0 \\ a_1 \\ a_2 \end{bmatrix} + \begin{bmatrix} \varepsilon_1 \\ \varepsilon_2 \\ \vdots \\ \varepsilon_{s-1} \\ \varepsilon_s \end{bmatrix} \quad 3\text{-}3$$

$$\begin{bmatrix} lat_1(R) \\ lat_2(R) \\ \vdots \\ lat_{s-1}(R) \\ lat_s(R) \end{bmatrix} = \begin{bmatrix} 1 & lat_1(S) & lon_1(S) \\ 1 & lat_2(S) & lon_1(S) \\ \vdots & \vdots & \vdots \\ 1 & lat_{s-1}(S) & lon_{s-1}(S) \\ 1 & lat_s(S) & lon_s(S) \end{bmatrix} \begin{bmatrix} b_0 \\ b_1 \\ b_2 \end{bmatrix} + \begin{bmatrix} \varepsilon_1 \\ \varepsilon_2 \\ \vdots \\ \varepsilon_{s-1} \\ \varepsilon_s \end{bmatrix} \quad 3\text{-}4$$

M and *N* are called the design matrices of a linear regression system. The rows of *M* and *N* are the terms of the model evaluated at the predictors. To fit the model to the data, the system must be solved for the coefficient values in *A* and *B*. They can be obtained by using the method of least-squares. We propose to use the algebraic least-square problem minimization $\left\| M\hat{A} - lon(R) \right\| \to \min_{\hat{A}}$ and to $\left\| M\hat{A} - lat(R) \right\| \to \min_{\hat{B}}$ solve for the unknown parameters. To stabilize the least square, additional term of Tikhonov regularization $\lambda^2 \left\| L_x M\hat{A} \right\|^2$ is added to the least square problem (Johns and Mandel (2007)):

$$\left\| M\hat{A} - lon(R) \right\| + \lambda^2 \left\| L_x M\hat{A} \right\|^2 \to \min_{\hat{A}} \quad 3\text{-}5$$

$$\left\| N\hat{B} - lat(R) \right\| + \lambda^2 \left\| L_y N\hat{B} \right\|^2 \to \min_{\hat{B}} \quad 3\text{-}6$$

The added regularization term $\lambda^2 \left\| L_x M\hat{A} \right\|^2$ gives a prior assumption about the desired solution of A and B, the displacement is assumed to be small. Here λ is a smoothing parameter.

In least-square normal equations, the solution of the above equations can be solved as:

$$\left(M\hat{A} - lon(R)\right)^T Q^{-1}\left(M\hat{A} - lon(R)\right) + \left(r_k - L_x M\hat{A}\right)^T D^{-1}\left(r_k - L_x M\hat{A}\right) \to \min_{\hat{A}} \qquad 3\text{-}7$$

$$\left(N\hat{B} - lot(R)\right)^T Q^{-1}\left(N\hat{B} - lat(R)\right) + \left(r_k - L_y M\hat{B}\right)^T D^{-1}\left(r_k - L_y M\hat{B}\right) \to \min_{\hat{B}} \qquad 3\text{-}8$$

where D is a given symmetric positive definite covariance matrix, D^{-1} plays a generalized role of the parameter λ in Tikhonov least square regularization (Johns and Mandel 2007). This is like working on two least squares in a hierarchical manner, one $M\hat{A} - lon(R)$ and another $r_k - L_x M\hat{A}$ with error covariance *D*. r_k is sampled from $N(\mu L, D)$. *D* is a diagonal matrix with non-zero elements $d_{ii} = |z_i|/(2h)^2$ (Johns and Mandel (2007), where $z = \mu L$. Q is spatial error covariance and is the same for the above two formulas, unlike *D* which is different for x and y. Q can be generated using the exponential correlation function as shown in Section 3.2. In our case, *h* can be the variance, σ^2, in the x and y directions and,

$$L_y M = \begin{bmatrix} (lat_1(R) - lat_1(s))/h_y \\ \vdots \\ lat_s(R) - lat_s(s))/h_y \end{bmatrix} \qquad 3\text{-}9$$

$$L_x M = \begin{bmatrix} (lon_1(R) - lon_1(s))/h_x \\ \vdots \\ lon_s(R) - lon_s(s))/h_x \end{bmatrix} \qquad 3\text{-}10$$

We calculate the right hand side of Equation 3-7 and 3-8 first, then use the output *A* and *B* values to produce a new *M* matrix and calculate *A* and *B* once again using the left hand side part of the equation to have the final *A* and *B* values. (Note that we are calculating A and B twice and the second one is our final result).

In our case study, there are one space borne and two ground-based measurements at our disposal. ST-IV and rain-gauges are ground-based, whereas satellite based HE are space borne measurement. The rain-gauge measurements are very scattered in space and represent point measurements, and there are only a few measurements with positive rainfall rate at each measurement time. Because it is a point measurement, estimating the position error of satellite products is more complex than with radar. Therefore, in Section 4-1, we will estimate the error statistics for the satellite-based measurement, HE, using a radar based product, ST-IV.

3.2. Bias correction of Satellite Rainfall Estimates Using Radar ST-IV Rainfall

In our proposed approach the underlying assumption is that satellite rainfall biases are spatially variable. This highly variable nature of rainfall biases in satellite products has led us to propose a real time bias correction algorithm. It is ideal to make bias corrections of satellite products using rain-gauge measurements. However, rain gauges are point measurements and they are not always available in an extended spatial coverage. Therefore to augment the spatial difficulty in rain-gauges we recommend using ST-IV radar product to correct HE.

In this study, we consider bias adjustment via spatially variable bias factors, where the SPE field at a given time step is corrected through multiplying by a field of bias factors. The spatial field of bias factors is estimated from selected radar-gauge precipitation estimate divided by the SPEs for the same pixels to obtain a spatially distributed sample of bias factors. To reduce sampling errors, bias factors are randomly selected all over the study area (Smith et al., 2006). In the current study, pixel bias factors are sampled randomly over the study area. A bias factor spatial field is constructed based on the sampled values by weighting based on a negative power

of the distance to the sample points. To reduce the effect of random error in the bias factors for individual pixels, our approach relies on pre-smoothing the sample values by averaging across an ensemble where they are perturbed with a spatially correlated noise component. We compare this procedure of estimating the bias factor field to (a) a spatially varying bias factor field constructed from the sample points without the pre-smoothing; and (b) a spatially uniform bias factor field based on either (1) the mean or (2) the maximum bias factor in the sample. We use two operational SPEs, HE and CMORPH, as the products to be corrected, and the NEXRAD ST-IV radar-gauge composite product as the reference. Our test site is Oklahoma State, in the south-central USA, and we consider 5 rainy days in 2006 that represent different seasons. The area is one with good rain gauge and radar coverage and is intended to provide a preliminary test of our method for correcting bias in satellite-based precipitation estimates. This study is intended to show the feasibility of bias correction for satellite rainfall products, which can be applied operationally, even in areas and times where radar coverage is limited so that radar overlap with the satellite product is only partial.

Both HE and ST-IV data are in polar stereographic projection. They are converted to a regular grid of 4 km × 4 km resolution using a simple average of the data within a 4 km square grid cells.

In all the analysis involving CMORPH, ST-IV data at a 4 km spatial resolution is averaged to 8 km × 8 km to match up the resolution of CMORPH.

In the following, we describe the proposed approach for bias correction along with the simpler methods with which we compare our approach.

3.2.1. Bias Factor

The bias factor is defined as the ratio of a true value to the corresponding biased value. Bias is adjusted by multiplying the values from the biased field by the bias factor.

According to Anagnostou et al. (1998), the area-mean bias ratio is defined as the ratio of the true mean area rainfall to the mean area of 'biased' estimates. Thus, following the same definition, the maximum ratio bias factor will be the ratio of the area maximum of the true values to the maximum of the biased data field.

With the assumption that the rain gauge observation is the true and radar-based measurement is the biased rainfall information, the mean bias ratio is written as (Anagnostou et al., 1998):

$$B_h = \frac{\sum_{i=1}^{n} G_h(x_i)}{\sum_{i=1}^{n} R_h^{'}(x)} \qquad 3\text{-}11$$

where $G_h(x_i)$ and $R^{'}_h$ are the gauge and radar measurements at location x_i and hour h. Therefore, the existing bias from the original SPE is corrected by multiplying each pixel value by the mean (or maximum) bias ratio.

3.2.2. Ensemble Bias Factor Field

Following the same definition, a bias factor or ratio between ST-IV and SPE products at a pixel level can be written as:

$$B(x_{k,h}) = \frac{R_h(x_k)}{S_h(x_k)} \qquad 3\text{-}12$$

where $R_h(x_k)$ and $S_h(x_k)$ are the ST-IV (the 'true' measurement in this study) and satellite measurements respectively, at location x_k and hour h.

From Equation 3-12 bias factors can be:

- Zero if the radar pixel is not rainy and the corresponding satellite pixel is rainy.
- A positive real number if corresponding pixels from ST-IV and SPE are rainy.
- Infinity if the ST-IV pixel is raining and the corresponding satellite pixel is not rainy.
- Undefined if both pixels from ST-IV and SPEs are not raining.

We kept only pixels that were rainy in both precipitation fields; hence all our sample bias factors had positive values. A pixel is considered rainy if it registers a rainfall value of greater than 0.1 mm/hr (Dai et al., (1999)). A maximum of 150 (for HE) and 100 (for CMORPH, with its coarser resolution) bias factors were used for evaluation depending on the areal coverage of rain with in the study area. The process of selecting pixels for the estimation of the bias factor

field was as follows: (a) to ensure a fair spread of bias factors over the study area, 150 pixels for HE (100 in the case of CMORPH) are randomly picked regardless of their bias factor values; (b) the non-positive bias factors are discarded; (c) the process of randomly picking pixels continues until a total of 150 for HE (100 for CMORPH) positive bias factors is obtained; and (d) any closely located pixels, which would tend to occur whenever rain covers only a small part of the study area, were thinned out, potentially reducing the number of pixels retained below 150 for HE and 100 for CMORPH.

The bias factors obtained for a sample of pixels can have large scatter compared to the underlying bias field because of, for example, random error in the satellite radiances or radar backscatter. Generating an ensemble of perturbed bias factors that represents variability based on their estimated small-scale scatter can be useful in visualizing these errors, and the sample can be pre-smoothed by averaging across the ensemble.

Following the acquisition of the required number of bias factors, the ensembles of bias factors were created by following a similar procedure to that of Mandel et al. (2009). That work used Cholesky decomposition of the state covariance matrix to generate posterior ensembles in an ensemble Kalman filter. Germann et al. (2006b) used Cholesky decomposition of the error covariance to generate ensembles of radar precipitation fields. The method was found to be flexible to the space-time dependence of mean, variance, and auto-covariance of error in radar precipitation estimates (Germann et al., 2006b). A similar approach was adopted here to perturb the bias factors at known locations before spatial interpolation to produce the bias factor field was carried out.

In our ensemble generation, let *b* be a known *n* by 1 vector of the randomly sampled known bias factors. **M** is the initial perturbation matrix of size *n* by *N*, where *N* is the required ensemble size (100), and **M** is assumed to have the form,

$$\mathbf{M} = \mathbf{O} + \mathbf{G}$$

O is a matrix of size *n* by *N*. The columns of **O** are replicates of *b*. **G** is a matrix of independent random variables each drawn from $N(0, \sigma^2)$, a normal distribution with mean zero and unknown variance σ^2.

The initial perturbation matrix **M** is multiplied by the Cholesky factor **Q** of the spatial covariance matrix **C** to produce ensembles,

$$\hat{\mathrm{M}} = \mathrm{Q} \cdot \mathrm{M}; \mathrm{C} = \mathrm{Q} \cdot \mathrm{Q}^{\mathrm{T}}$$

$$C = \sigma^2 \cdot f(d_i - d_j)$$

where $\hat{\mathbf{M}}$ is the ensemble of perturbed bias factors, **C** is a positive definite matrix of dimension *n* by *n* n with the error covariance of each pair of sample points, assumed to be only a function of their separation $f(d_i - d_j)$. $\hat{\mathbf{M}}$ is thus a function of σ^2 as well as the parameters *p* and η introduced below.

A common correlation function, the exponential function without nugget effect (Kitanidis, 1986) with one unknown parameter was used as a spatial covariance estimator:

$$f(d_i - d_j) = \exp\left(-\frac{|d_i - d_j|}{\eta}\right)$$

3-13

where $|d_i - d_j|$ is the Euclidean separation distance in km between two bias factor sample pixels indexed at i and j, and η (km) is a range parameter.

The next step is to generate bias fields using each column of $\hat{\mathbf{M}}$. There are several spatial statistics approaches to generate spatial fields from point estimates of bias factors, including linear, kriging, spline and Inverse Distance Weight (IDW) (Cressie 1993). In this work, a multiplicative bias factor for the SPE was generated for each unknown pixel on an hourly basis using the IDW interpolation method by:

$$b(x_{i,h}) = \sum_{k=0}^{n} \frac{w_{k,h}(x)}{\sum_{k=0}^{n} w_{k,h}(x)} b(x_{k,h}) \qquad 3\text{-}14$$

$$w_{k,h}(x) = \frac{1}{D(x_{i,h}, x_{k,h})^p} \qquad 3\text{-}15$$

where $D(x_{k,h}, x_{k,h})$ is the distance from the unknown bias factor pixel $x_{i,h}$ to all known bias factor calculated pixels $x_{k,h}$. Values farther from a known value will tend toward the average of all the values (Shepard 1968). p >0 is an exponent, and n is the number of sample bias factors at hour h. Finally the bias corrected SPE is calculated as:

$$S_{cor,i,h} = \sum_{j=1}^{N} \frac{S_{i,h} \cdot b_{i,h,j}}{N} \qquad 3\text{-}16$$

where $S_{cor,i,h}$ is the bias corrected HE at hour h, $S_{i,h}$ is the HE at hour h and $b_{i,h,j}$ is the j-th member bias field at hour h. i is the pixel index in the rainfall field.

3.2.3. Parameter estimation

The previous section did not explain how to estimate the model parameters. The parameters, η, σ^2, and p have to be estimated to produce optimal bias correction. Parameter estimation was carried out separately for each day. Hourly ST-IV and SPE were aggregated to daily values before ratios of corresponding rainy pixels for parameter estimation were taken. In an operational setup, the parameters could be estimated using the previous 24 hours. Parameters could also be estimated on hourly basis.

For parameter estimation, the shuffled complex evolution optimization algorithm (Duan et al., 1993), originally developed for hydrologic modeling was used. In shuffled complex evolution, optimization starts by selecting the number of complexes (subgroup of sample set) and the number of points in each complex. The number of points in each complex should be greater than the number of dimensions of the problem. (See Duan et al., 1993 for detailed explanation)

Depending on the complexity of the problem the number of input parameters to SCE may vary. For this particular study, we have used nine input parameters, Table 3-1 shows the input parameters and their values used for this study.

Optimum values for parameters were determined based on minimizing an objective function given by the Root Mean Square Error (RMSE) between the ST-IV and mean ensemble bias corrected SPEs for a 24 hour period (Equation 3-17).

Table 3-1 Input values for SCE (Duan et al., 1998)

NGS	number of complexes in a sample population
NPG	number of points in each complex
NPT	number of points in the entire sample population, NPT=NGS*NPG
NPS	number of points in each sub-complex
NSPL	number of evolution steps allowed for each complex before complex shuffling
MINGS	minimum number of complexes required, if the number of complexes NGS is allowed to reduce as the search proceeds
MAXN	maximum number of trials allowed before optimization is terminated
KSTOP	number of shuffling loops in which the criterion value must change by PECNTO before optimization is terminated
PECNTO	percentage by which the criterion value must change in KSTOP shuffling loops

$$RMSE = \sqrt{\frac{\sum_{h}^{m}\sum_{j=1}^{n}\left(R_{i,h} - S_{cor,j,h}\right)^2}{n \cdot m}} \qquad 3\text{-}17$$

where n is the number of corresponding rainy pixels, and R is the ST-IV rainfall at each pixel, and m is the number of the rainy hours in the rainy day.

3.2.4. Interpolation Bias Factor Field

For comparison, a pixel-by-pixel spatial interpolation of bias factors in the interpolation method is carried out using Equation 3-14, in addition to the mean and maximum ratio method bias factors. The interpolation method uses Equation 3-14 on the original sample bias factors without generating an ensemble. Bias corrected SPE is obtained using Equation 3-16 with N=1. We include the method of interpolation to show that improvements in bias and correlation coefficients are not only based on the results of accounting for spatial variation, but specifically on pre-smoothing the sampled bias factors through ensemble generation. Note that the only parameter involved in the method of interpolation is *p*.

The method of mean ratio works by multiplying the original satellite product by the mean of sampled bias factors. Similarly, the method of the ratio of maximums works by multiplying satellite products by the ratio of hourly maximum rain rates between the radar-gauge and the satellite estimates irrespective of their location.

3.3. Merging of the different precipitation products

3.3.1. Successive Correction Method (SCM): Merging satellite precipitation estimates with radar precipitation estimates

Synergetic effects of multi-sensor rainfall information from multiple in-situ (e.g., rain gauge) and remotely sensed (eg. Satellite and radar) sources may produce more accurate precipitation estimates over the radar gap than precipitation measured from individual source. In this study, a merging approach which is capable of generating gridded areal precipitation over

the radar gap areas by combining SPE with RR is proposed. The proposed merging approach is planned to be implemented with the NWS-MPE algorithm to make it able to generate merged rainfall for radar gap pixels instead of assigning only SPE to these pixels. This multi-sensor merging algorithm estimates rainfall amount for every missing pixel uses information from its surrounding pixels, located in a selected overpass window, and applying weighting factors on a window base analysis. For a given pixel, located at the center of the window, optimum weight is calculated considering the spatial availability of SPE and RR data as well as the distance between the center pixel and the neighboring pixels from the merging window. The window size has varied according to the size of radar gap area and the number of corresponding rainy pixels.

For quantitative integration of multi-sensor rainfall, first, the SPE data needs to be spatially and bias corrected. At the NWS-MPE, for local bias correction the ratio between the rain gauge mean values and the radar mean values within a circular window is interpolated to the entire analysis domain (Seo and Breidenbach 2002b). In this research bias correction of HE was done by the method of ensembles as explained in section 3.2 and published in Tesfagiorgis et al. 2011.

The bias corrected HE product is merged with that of the ST-IV so that gaps over the radar networks could be filled. The SCM, originally developed for data assimilation, has been implemented here. The SCM uses the information from available radar-gauge rainfall for pixels surrounding the gap area and satellite rainfall to fill the gap pixels (Mahani and Khanbilvardi 2009). The merged precipitation for any pixel in the gap area is calculated based on information from satellite pixels and known available radar pixels surrounding the missing pixels.

In SCM, the objective analysis procedure (Barnes 1960) was applied iteratively by making successive estimates. A two-dimensional domain was considered for analysis of the satellite-based precipitation estimates *(f_{SR})* with respect to the radar-based rainfall *(f_{RR})*. Satellite-based model output was identified as the background domain *($f_B = f_{SR}$)*, to be analyzed using RR as observation domain *($f_O = f_{RR}$)*, for generating new analyzed (merged) data values *(f_A)*. For every gap (missing) analysis of every grid-point, pixel *(k)*, a window centered at the pixel *(k)* was considered.

Window size should be selected with respect to the resolution, size of gap area, and accuracy for analyzed domain output. In the present study, various window sizes were tried to investigate the appropriate size of merging window for every case study. The window moves in four directions where its center grid was placed one by one on all pixels.

For this study three different schemes were considered to estimate a missing pixel in the SCM framework. The different schemes are explained in the following subtopics (3.3.1.1, 3.3.1.2 and 3.3.1.3).

3.3.1.1. Inverse distance scheme

• The weight factor with respect to the distances in an over-passing window was calculated using the following equation:

$$\text{if}: r_i < R \Rightarrow w_i = \frac{R^2 - r_i^2}{R^2 + r_i^2}, \text{and if } r_i \geq R \Rightarrow w_i = 0$$

where: *"w_i"* is the weight factor related to any observation pixel *(i)*,with available both satellite and radar rainfall amounts; *"R"* is the maximum distance from window center, pixel *(k)*; and *"r"* is the distance between analysis center grid, pixel *(k)*, and the observation pixel *(i)* inside the window, Equation 3-18. If *(x , y)* are the grid pixel coordinates, then:

$$r^2 = (x_i - x_k)^2 + (y_i - y_k)^2$$

•The merged value for center pixel (k), is calculated using the following Equation 3-18:

$$\Rightarrow f_{MR_k} = f_{SR_k} + \frac{\sum_{i=1}^{i=n} w_i \left(f_{RR_i} - f_{SR_i}\right)}{\sum_{i=1}^{i=n} w_i + \varepsilon_{RR}^2} \qquad 3\text{-}18$$

where: $f_{MR(k)}$ and $f_{SR(k)}$ are the analyzed merged and satellite-based precipitation estimates for the center pixel *(k)*, $f_{SR(i)}$ and $f_{RR(i)}$ are the satellite-based rainfall and radar rainfall for observation pixel *(i)* inside the window, *"n"* is the number of observation pixels with available both radar and satellite precipitation estimates inside the window, and ε_{RR} is the WSR-88D (observation instrument) error that was assumed to be zero *($\varepsilon_{RR} = 0$).*

3.3.1.2. Brandes' Scheme

In this study, the Brandes scheme of SCM is one of the schemes which has been adopted in this study. This method uses Barnes' (1964) objective analysis to move correction factors from rain gauges onto radar grids. In this study we use the Brandes (1975) scheme to fill gaps in radar precipitation field using satellite precipitation fields. Following a similar procedure as in section 3.3.1.1, each radar pixel inside the over-passing window receives a weight calculated

using the inverse exponential function. According to Brandes' scheme the weights of the overpass window is calculated as:

$$w_i = \exp\left(\frac{-d_i^2}{EP}\right) \qquad 3\text{-}19$$

where d_i is the distance between the unknown center grid k and the known grid i in A (over passing window). *EP* controls the degree of smoothing and it is advised to keep it as small as possible (Brandes 1975).

This scheme uses two passes of the overpass window on each missing radar grid. On the first pass, a first guess (*F1*) is calculated as:

$$F1 = \sum_{i=1}^{N} w_i R_i / \sum_{i=1}^{N} w_i \qquad 3\text{-}20$$

R_i is the radar precipitation at pixel i in the overpass window. On the second pass, $w_i = 0.5\exp(-d^2 / EP)$ and calculates each missing pixel using the following equation (Brandes 1975):

$$F2 = F1 + \sum_{i=1}^{N} w_i D_i / \sum_{i=1}^{N} w_i \qquad 3\text{-}21$$

where D_i is the difference between radar and the first estimates at known locations.

$$D_i = R_i - F1 \qquad 3\text{-}22$$

In our studies we calculated $D_i = R_i - S_i$. S_i is satellite precipitation at pixel indexed *i*.

3.3.1.3. Single Optimization Estimation (SOE)

Starting from a missing pixel surrounded by the maximum number of available radar pixels, the method continues calculating other missing pixels by moving the m×m over-passing window successively. The conditional expectation of rainfall at the gap pixel can successively be calculated by employing double optimal estimation as (Seo 1998-b):

$$E\left[Z_{u0}|z_R, z_S\right] = E\left[Z_{u0}|z_R, z_S, z_{u0} > 0\right]\Pr\left[Z_{u0} > 0|z_R, z_S\right] \qquad \textbf{3-23}$$

$$E\left[Z_{u0}|z_R, z_S, z_{u0} > 0\right] = E\left[Z_{u0}|z_{u0} > 0\right] + \sum_{i=1}^{n} \Gamma_{ri}\left(z_{ri} - E\left[Z_{ri}|z_{r0} > 0\right]\right) + \sum_{i=j}^{m} \Gamma_{sj}\left(z_{sj} - E\left[Z_{sj}|z_{r0} > 0\right]\right)$$

where $E\left[Z_{u0}|z_{u0} > 0\right]$ is the expected rainfall at u_0 (the first pixel in the gap), $E\left[Z_{ri}|z_{r0} > 0\right]$ is the expected radar rainfall at u_i and $E\left[Z_{sj}|z_{r0} > 0\right]$ is the expected satellite rainfall at u_j.

There is a direct alternative for estimation of $E\left[Z_{r0}|z_R, z_S\right]$**.** This simpler estimate of the expected precipitation at the missing pixel r_0 inside moving window are A can be written as (Seo 1998-b):

$$E\left[Z_{r0}|z_R, z_S\right] = E\left[Z_{r0}\right] + \sum_{i=1}^{n} \Lambda_{ri}\left(z_{ri} - E\left[Z_{ri}\right]\right) + \sum_{j=1}^{m} \Lambda_{sj}\left(z_{sj} - E\left[Z_{sj}\right]\right) \qquad \text{3-24}$$

Where, $E\left[Z_{ri}\right]$ and $E\left[Z_{sj}\right]$ are the unconditional expectations of radar and satellite at pixel *i* and *j* respectively, in area A (the centered window).

$$E\left[Z_{ri}\right] = E[Z_{ri} \mid z_{ri} > 0] \cdot \Pr[Z_{ri} > 0] \qquad \text{3-25}$$

Similarly,

$$E\left[Z_{sj}\right] = E[Z_{sj} \mid z_{sj} > 0] \cdot \Pr[Z_{sj} > 0] \qquad \text{3-26}$$

These unconditional expectations can be approximated as (Seo 1998b):

$$E[Z_{ri}] = m_r \cdot m_{Ir} \qquad 3\text{-}27$$

$$E[Z_{sj}] = m_s \cdot m_{Is} \qquad 3\text{-}28$$

Here, m_r and m_s are the mean of rainy radar and satellite pixels in A (overpassing window) respectively.

$m_{Ir} = n_{pr} / n_r$ and $m_{Is} = n_{ps} / n_s$

n_{pr} and n_{ps} are the number of raining radar and satellite pixels in A respectively. $n_s = n_r$ is the total number of pixels in A.

According to Seo 1998b the weights in Equation 3-24 can be estimated by minimizing the error variance $E[(Z_{r0} - E[Z_{r0}])^2]$. Hence,

$$(\Lambda_{r1}, \Lambda_{r2}, \cdots \Lambda_{rn}, \Lambda_{s1}, \Lambda_{s2}, \cdots \Lambda_{sn}) = [\mathrm{C}_{0R} \quad \mathrm{C}_{0S}] \cdot \begin{bmatrix} \mathrm{C}_{RR} & \mathrm{C}_{RS} \\ \mathrm{C}_{SR} & \mathrm{C}_{SS} \end{bmatrix}^{-1} \qquad 3\text{-}29$$

Where C_{0R} and C_{0S} are the unconditional covariances $\mathrm{cov}[Z_{r0}, Z_{ri}]$ and $\mathrm{cov}[Z_{s0}, Z_{si}]$ respectively. C_{RR} and C_{SS} are the unconditional covariance matrices $\mathrm{cov}[Z_{ri}, Z_{rj}]$ $\mathrm{cov}[Z_{si}, Z_{sj}]$ respectively. $\mathrm{C}_{RS} = \mathrm{C}_{SR}^{-1}$ is the unconditional cross-covariance $\mathrm{cov}[Z_{ri}, Z_{sj}]$.

The covariances are approximated in a similar way as in Seo 1998-b:

$$\mathrm{cov}[Z_{si}, Z_{sj}] = \sigma_r \sigma_s \left(m_{Ir} \cdot (1 - m_{Ir})\right)^{1/2} \cdot \left(m_{Is} \cdot (1 - m_{Is})\right)^{1/2} + \rho_c(|u_i - u_j|) \cdot \rho_{Ic}(|u_i - u_j|) + m_r \cdot m_s \cdot \left(m_{Ir}(1 - m_{Ir})\right)^{1/2} \cdot \left(m_{Is}(1 - m_{Is})\right)^{1/2} \cdot \rho_{Ic}(|u_i - u_j|) + \sigma_r \sigma_s m_{Ir} m_{Is} \rho_c(|u_i - u_j|) \qquad 3\text{-}30$$

Where: - σ_r and σ_s are the standard deviations of the radar and satellite precipitations.

- ρ_c is the spatial cross-correlation function (exponential was our choice) between the radar and satellite precipitation in area A.

The other covariace equations follow a similar formulation.

3.3.2. Bayesian Spatial Model

So far we were able to merge the radar precipitation field with that of satellite estimates. The method explained in this section introduces how rain gauge measurements are incorporated in the multi-source precipitation model.

Assuming a spatial Gaussian process in a linear spatial regression model, the random rainfall field *Z* can be given as:

$$Z(\beta_i, X_i) = \beta_1 X_1(s) + ... + \beta_p X_p(s) + \varepsilon(s) \qquad 3\text{-}31$$

Where X_i is a covariate and βi is model parameter; $\varepsilon(s) \sim N(0, cov(Z(s), Z(u))$.

In a Gaussian process the covariance matrix can be modeled as

$$Cov(Z(s), Z(u)) = \begin{cases} \delta^2 & \text{if } |s-u| = 0 \\ \sigma^2 \kappa_\theta(s,u) & \text{if } |s-u| > 0 \end{cases} \qquad 3\text{-}32$$

$|s-u|$ is a Euclidean distance between two locations s and u. δ^2 is the nugget.

Assuming an exponential variogram function, the correlation function can be given as:

$$\kappa_\theta(s,u) = \exp(-|s-u|/\eta) \qquad 3\text{-}33$$

The standard Bayesian theory indicates that the posterior of the parameters is determined by:

$$p(\beta,\sigma^2,\theta \mid Z)\,\alpha\, L(\beta,\sigma^2,\theta;Z)\pi(\beta,\sigma^2,\theta) \qquad 3\text{-}34$$

In a Guassian Probability distribution, the likelihood *L(.)* is given by:

$$\mathrm{L}(\beta(\sigma^2,\theta,\mathrm{Z}) = \frac{1}{\sqrt{(2\pi 2\pi|\Sigma_\theta|}}\exp\left[-\frac{1}{2\sigma^2}(\mathrm{z}-\mu(\varphi_{\mathrm{x}}))^{\mathrm{r}}\Sigma_\theta^{-}1(\mathrm{z}-\mu(\varphi_{\mathrm{x}}))\right] \qquad 3\text{-}35$$

$\pi(\theta,\sigma^2,\beta)$ is priors of parameters.

In a hierarchical Bayesian model, the joint posterior distribution in equation (3-36) becomes:

$$p(\theta,\sigma^2,\theta \mid Z)\,\alpha\; p_1(\beta \mid \sigma^2\theta;Z)p_2(\sigma^2 \mid \theta;z)p_3(\theta \mid Z) \qquad 3\text{-}36$$

Then predictive distributions at the unknown locations is calculated as:

$$p(z_0 \mid Data) = \int p(z_0 \mid Data,\beta,\sigma^2,\theta)p(\beta,\sigma^2,\theta \mid Data)d\beta d\sigma^2 d\theta \qquad 3\text{-}37$$

We assumed a stationary model setting to obtain $p(z_0 \mid Data,\beta,\sigma^2,\theta)$.

To model the Bayesian model we used 'BayesGeostatExact' and 'spPredict' functions in R (Finlety and Sudipto 2007). The 'BayesGeostatExact' produces the posterior samples of the regression parameters using prior assumptions for the input parameters. The 'spPredict' collects the posterior parameters, prediction coordinates and covariate values at the unknown location and produces values at new locations.

4. Results and discussion: a case study in Oklahoma

Because the study area has limited radar precipitation estimates and sparse rain-gauge distribution, the performance of our proposed work cannot be validated. Therefore, our algorithm should be developed in a region where we can get a good network of radar and rain-gauges. Thus, part of the Oklahoma state, south of the United States, geographically bounded by 34^{o}–37^{o} latitude North and 94.5^{o}-100^{o} longitude West was selected for algorithms development and validation.

4.1. Spatial error correction

The procedure of the spatial error correction technique is illustrated by the following example. A satellite and radar rainy case for June 16^{th}, hour 4 UTC is shown in Figure 4-1(a) and Figure 4-1 (b). The acquisition of the corresponding peripheral pixels of the clusters is shown in Figure 4-2. Using Equation 3-3 and 3-4, the required six parameters were calculated and listed in Table 4-1. The parameters represent the shift, scaling and shear in the longitude and latitude directions. These parameters were fed to the right hand side of Equations 3-3 and 3-4 to correct the latitude and longitude of each rainy pixels of the satellite product. The final output of the satellite rain field is warped to its original 4 km by 4km grid using the method of nearest neighbourhood technique, and the result is shown in Figure 4-3. The final image shows that there is spatial mismatch improvement in satellite rainfall estimate after the spatial correction algorithm is applied. The False Alarm Ratio (FAR) improved from 0.5 to 0.2 after spatial error adjustment.

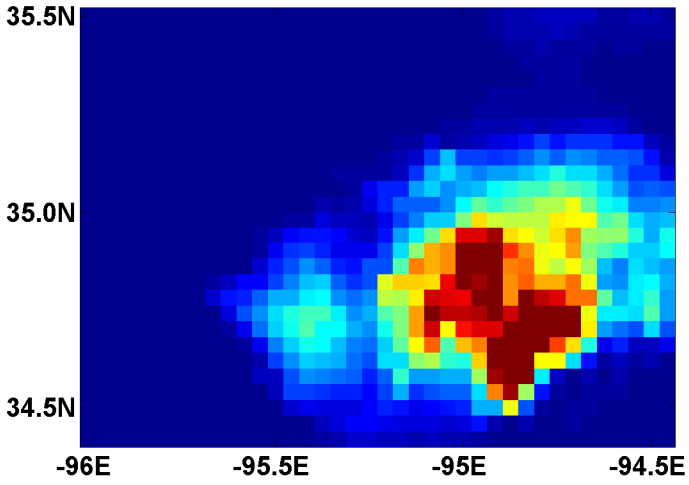

(a)

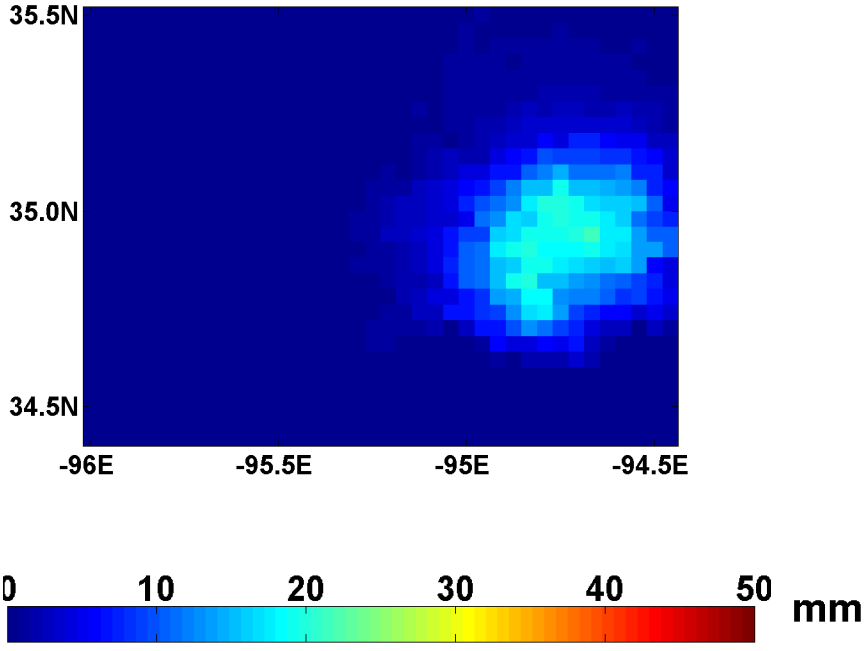

(b)

Figure 4-1 (a) and (b) are original ST-IV and HE respectively for June 16, 2006, 4 UTC.

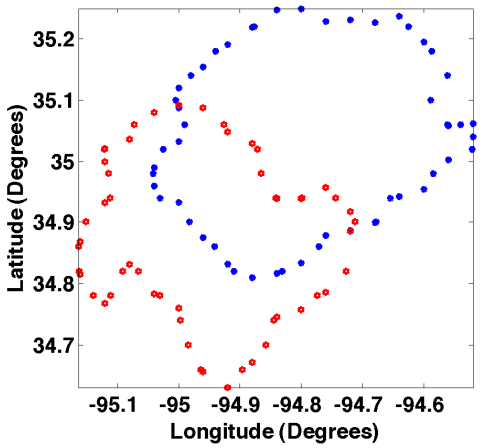

Figure 4-2 Selected corresponding rainy pixels for spatial correction analysis. Red is from ST-IV and blue is from HE pixels

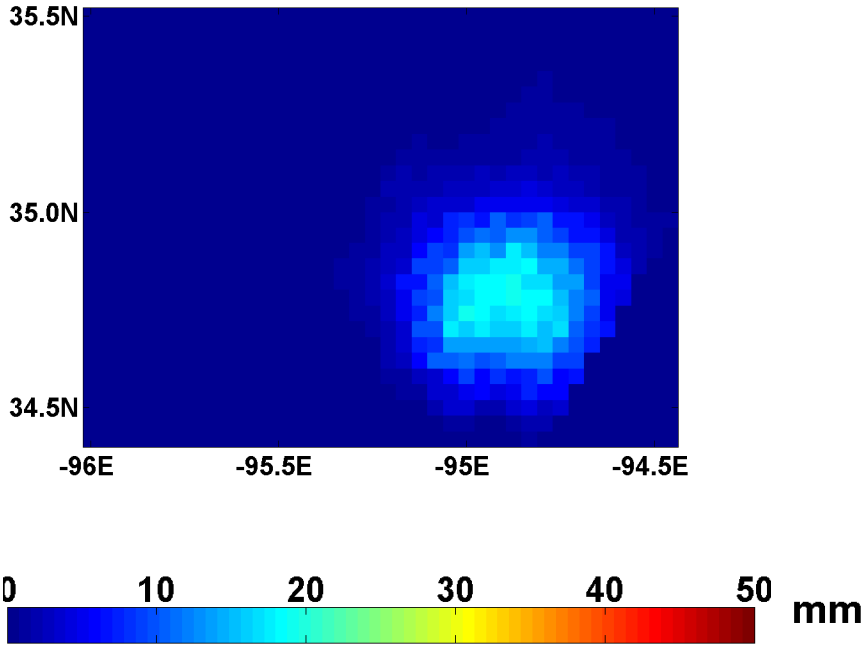

Figure 4-3 Spatially corrected HE for June 16, 2006, 4 UTC

Table 4-1 The different image analysis parameters and their values for case June 16, 2006, 4 UTC

Coefficients	Interpretations	Values for case (Degrees)
a_0	Shift in longitude	0.200
a_1	Scale in longitude	0.999
a_2	Shear in longitude	0.000
b_0	Shift in latitude	0.220
b_1	Scale in latitude	0.998
b_2	Shear in latitude	0.000

Well defined rainy storms as shown in Figure 4-1(a) and 4-1(b) are not that common, and getting corresponding coordinates in radar and satellite products makes the algorithm not practical in cluttered rainy cases. To mitigate the problem, obtaining the position error statistics is important, so that the adjustments can be applied in any circumstances. To do that, we plan to calculate the alignment statistics (A and B) with many well defined satellite measurements and collect their average position error parameters A and B in the latitude- and longitude- direction. With a collection of position errors, we plan to plot the histogram and estimate the position error statistics. In this paper, we plan to do seasonal calculation of the six parameters to be used in all rainy cases to correct spatial misfit in satellite precipitation estimates.

4.2. Bias correction

A maximum of 150 bias ratios (100 for coarser CMORPH)) depending on the areal coverage of storms were randomly picked up (see Figure 4-4 (a)) for analysis. Based on the bias

correction technique using ensembles explained in the methods section, hundred realizations of bias fields were generated for each rainy hour using the selected bias ratios and the optimized parameters for each 24 hour event period (Figure 4-4 (b)). Each generated bias field realizations or bias field ensemble member was multiplied by the original satellite precipitation estimates to generate one hundred simulated bias corrected HE for each hour. (d) The mean of the hundred realizations represents the final bias corrected HE (Equation 3-16) using the method of ensembles.

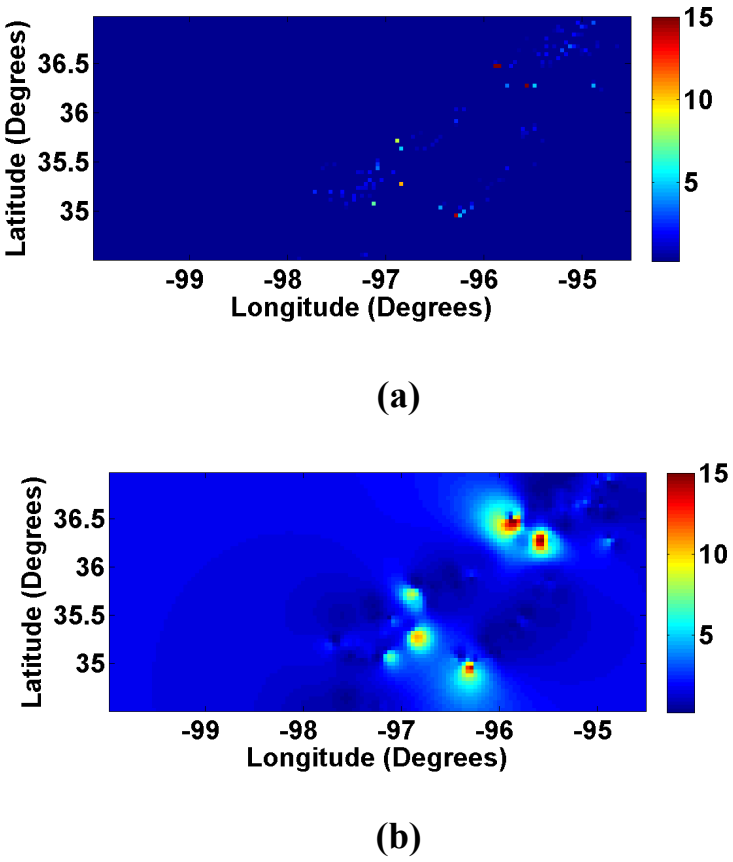

Figure 4-4 (a) 150 randomly chosen bias factors between the radar and satellite for hour 06071022. (b) A randomly generated ensemble bias field using the 150 bias ratios

The corrected satellite rainfall estimate using the method of ensembles was checked for its performance by comparing it with other bias correction techniques. The mean ratio and maximum ratio were taken as the bias correction factors for comparison. The method of mean ratio works by multiplying the original HE by the ratio of hourly mean of radar estimation to hourly mean of the satellite estimation. Similarly, the method of ratio of maximums works by multiplying HE by the ratio of hourly maximum rainy pixels between the radar and the satellite estimation irrespective of their location.

Four rainy representative days in 2006, one from each of the four seasons, were chosen for model evaluation. To better assess wintertime performance, which for SPE is generally poor, an additional winter case was chosen for overall evaluation of the model. The second and the last rainy events of the five events listed in Table 4-2 represent winter cases; event 1 is a spring case, event 3 is summer, and event 4 is a fall case.

Bias adjustment using the ensembles method requires obtaining the optimized model parameters, namely the range (η), the power-law exponent (p), and the variance (σ^2) based on m-hour aggregates of SPEs and ST-IV as explained in Section 3-2 (Equation 3-16). Table 4-2 lists the optimal values of the three parameters for each of the rainy days. These varied from one rainy event to another. For HE the variance range was from 0.5 (mm^2) for event 5 to 1.19 (mm^2) for event 4. The lowest power parameter of 2.7 was observed for event 5 while a maximum value of 4.44 was observed for event 1. The range parameter varied from 4.43 km for event 2 to 8.55 km (approximately 2 grid cells) for event 5.

After obtaining the optimized model parameters, the impact of the parameters was examined by varying each parameter about their optimal values while keeping the other parameters fixed at their optimal values. To demonstrate the influence of the parameters in the bias correction model, the RMSE versus the respective parameter for rainy hour 06071022 (YYMMDDHH) was plotted. Figure 4-5 and 4-6 show the response of the RMSE to variation of each parameter around their optimal values for HE and CMORPH respectively. Figure 4-5 shows that the model was insensitive to the power parameter up to a power of 4.5. For p values greater than 5 the model was acutely sensitive and the value of RMSE decreased steadily.

Table 4-2 Optimal parameters for the five rainy events in 2006 for HE (CMORPH).

Rainy Event	Rainy Period (YYMMDDHH)	Parameter		
		Range (η [km])	Variance (σ^2 [mm^2])	Power (p)
1	06031818–06031918	6.87 (37.5)	0.75 (0.54)	4.44 (1.73)
2	06020605– 06020705	4.43 (32.6)	0.75 (0.20)	4.07 (1.92)
3	06071021–06071121	6.58 (19.68)	0.85 (0.39)	3.23 (3.75)
4	06091008–06091108	6.59 (19.43)	1.19 (0.32)	4.09 (2.77)
5	06122902–06123002	8.55 (8.7)	0.50 (0.46)	2.70 (4.91)

A high value of the power parameter of inverse distance weight implies sharp non smooth variation among the interpolated pixels (Shepard, 1968). The range parameter that influences the spatial correlation function shows an increase in RMSE for values less than 4 km (the grid spacing of HE) and less steep increase at larger values. A similar parameter check for CMORPH

was carried out for the same rainy hour (Figure 4-6). The pattern of the parameters obtained for CMORPH has a similar nature to that of HE though with longer optimum η, which is of the order of 20 km. Figure 4-6 suggests that the optimal parameter set for CMORPH can be obtained from values η >19 km, p>3 and σ^2 <0.6 mm^2.

Following optimization and sensitivity analysis of model parameters for each rainy event, the performance of SPEs adjusted using the method of ensembles was evaluated by comparing it with that of the SPEs adjusted with the other bias correction methods mentioned. Figure 4-7 shows the mapped precipitation fields from HE and CMORPH before and after adjustment of biases, using various bias correction methods, are compared with ST-IV at hour 06071022. In this figure, bias corrected satellite estimates (left side for HE and right side for CMORPH) using the methods of (c) Maximum ratio (d) Mean ratio (e) Interpolation and (f) Ensembles are depicted. Figure 4-7a is ST-IV (8 km resolution left and 4 km resolution right) and Figure 4-7b is the original HE (left) and CMORPH (right). As shown in Figure 4-7c, the SPE corrected using the maximum ratio and ensemble methods gave a better estimate than bias corrected rainfall amounts using the methods of mean-ratio and interpolation.

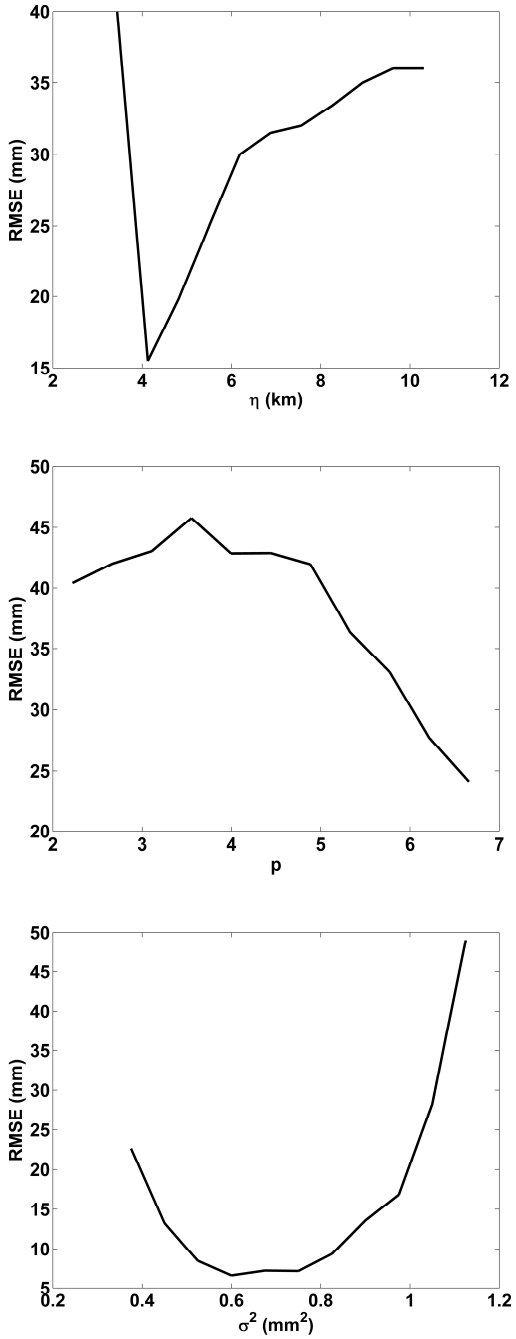

Figure 4-5 Parameter sensitivity check for HE for the range (η [km]), the power (*p*) and the variance (σ^2 [mm^2])

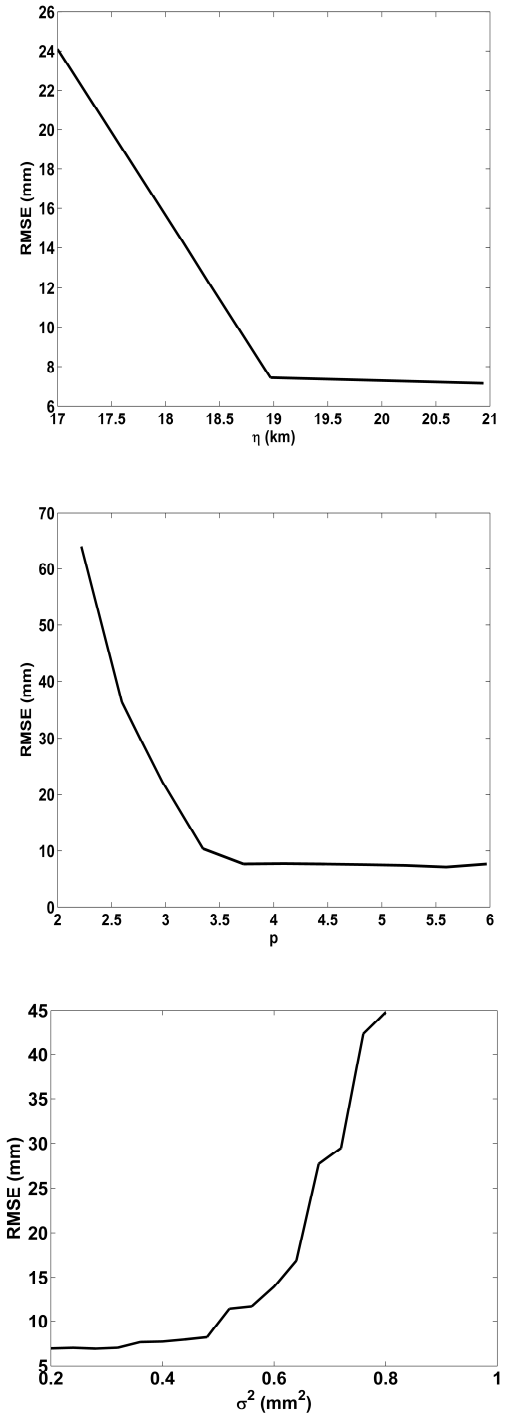

Figure 4-6 Parameter sensitivity check for CMORPH for the range (η [km]), the power (*p)* and the variance (σ^2 [mm^2]).

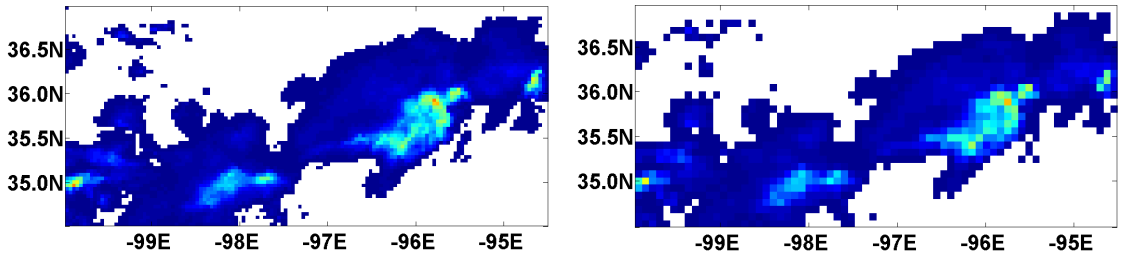
36.5N
36.0N
35.5N
35.0N
-99E
-98E
-97E
-96E
-95E

(a)

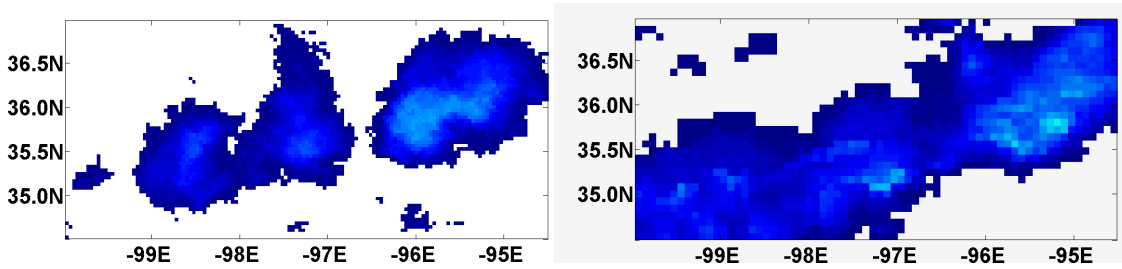
36.5N
36.0N
35.5N
35.0N
-99E
-98E
-97E
-96E
-95E

(b)

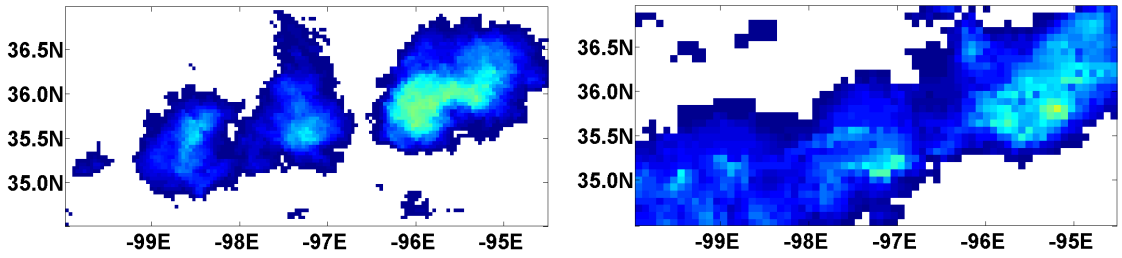
36.5N
36.0N
35.5N
35.0N
-99E
-98E
-97E
-96E
-95E

(c)

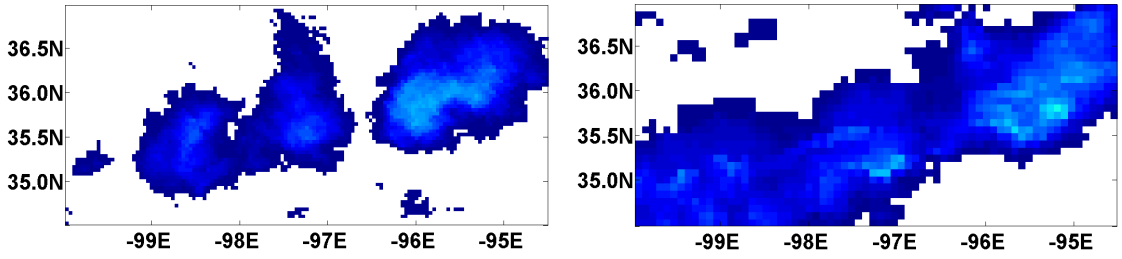
36.5N
36.0N
35.5N
35.0N
-99E
-98E
-97E
-96E
-95E

(d)

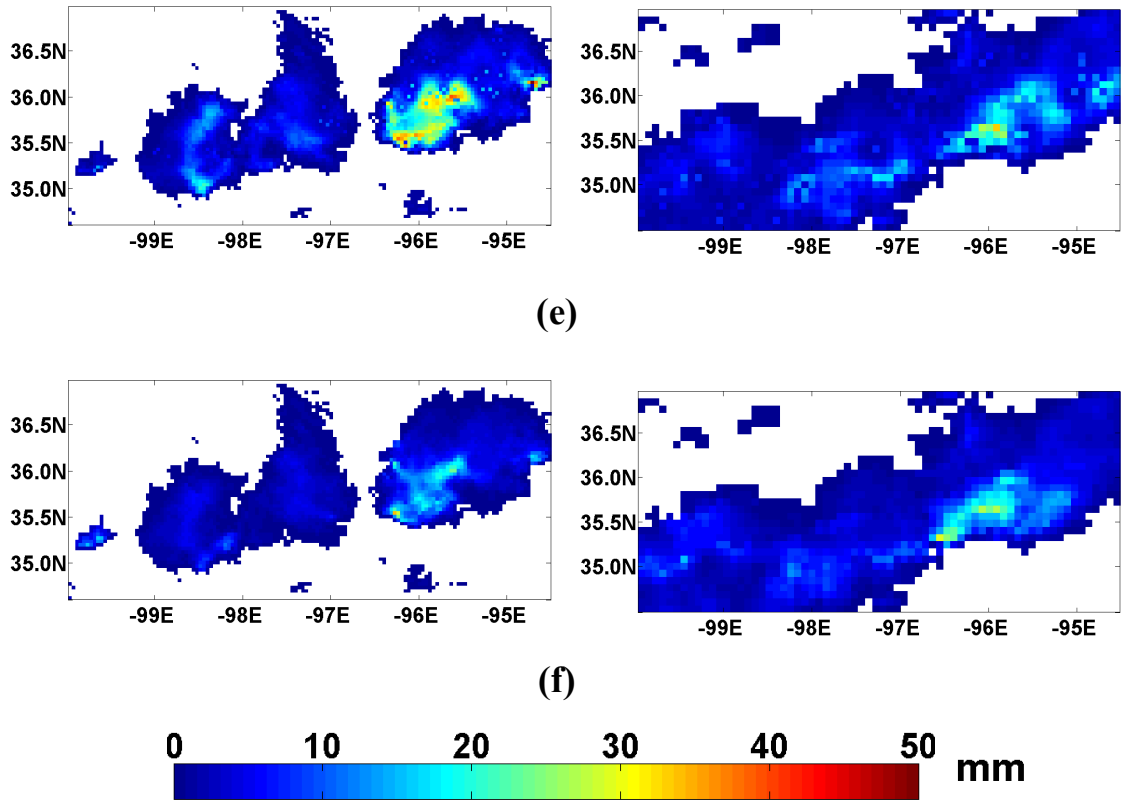

Figure 4-7 Bias corrected satellite estimates (left side for HE and right side for CMORPH) at hour 06071022 using the methods of (c) Maximum ratio (d) Mean ratio (e) Interpolation and (f) Ensembles. (a) is ST-IV (4 km resolution left and 8 km resolution right) and (b) is the original HE (left) and CMORPH (right)

Quantitative statistical evaluation criteria were calculated using reference ST-IV pixels which were not used for bias correction. Recall that the maximum number of pixels used for bias correction were 150 and 100 for HE and CMORPH respectively. The statistical criteria used for evaluation are hourly Bias ratio, the hourly RMSE and the hourly Correlation Coefficient (CC) corrected SPEs and ST-IV between the bias corresponding rainy pixels.

Hourly Bias ratio,

$$Bias\ Ratio = \frac{\sum_{j=1}^{n} R_j}{\sum_{j=1}^{n} S_{cor,j}} \qquad 4\text{-}1$$

The Hourly RMSE,

$$RMSE = \sqrt{\frac{\sum_{j=1}^{n} \left(S_{cor} - R\right)_j^2}{n-1}} \qquad 4\text{-}2$$

The hourly Correlation Coefficient (CC) between the bias corrected SPEs and ST-IV for corresponding rainy pixels,

$$CC = \frac{COV\left(S_{cor}, R\right)}{\sqrt{VAR\left(S_{cor}\right) \cdot VAR\left(R\right)}} \qquad 4\text{-}3$$

where j is the grid index, n is the number of all corresponding rainy pixels. COV(.) is the covariance between the simulated precipitation estimates and independent rain gauges. VAR(.) is the variance of the simulated rainfall field.

Figures 4-8 and 4-9 and Table 4-3 and 4-4 compare the performances of the bias methods using these performance criteria. The figures demonstrate the performance of the individual methods for each rainy hour. Table 4-3 and 4-4 summarize RMSE, correlation coefficient, and absolute difference for each event (from Table 4-1) for HE and CMORPH, respectively. In these tables, the hourly bias corrected products are aggregated to daily amounts for comparison. The relationship between ST-IV and the original SPEs before bias correction is also shown in these figures and denoted as 'Original'.

Table 4-3 Statistical outputs for five rainy hours each from the five rainy events of HE.

Statistics	Methods	Event 1	Event 2	Event 3	Event 4	Event 5
RMSE (mm)	Original	20.58	18.60	11.70	16.90	59.70
	Mean ratio	20.38	10.05	11.40	6.14	13.30
	Max ratio	21.10	8.26	11.10	9.06	21.60
	Interpolation	18.16	15.0	11.80	4.87	17.40
	Ensemble fields	17.70	7.90	9.30	4.30	10.61
Correlation Coefficient (CC)	Original	0.53	0.58	0.23	0.54	0.66
	Mean ratio	0.53	0.58	0.23	0.54	0.66
	Max ratio	0.53	0.58	0.23	0.54	0.66
	Interpolation	0.63	0.59	0.45	0.71	0.78
	Ensemble fields	0.65	0.59	0.47	0.79	0.81
Bias Ratio	Original	0.86	0.46	2.24	0.28	0.28
	Mean ratio	0.96	0.74	1.17	0.64	0.60
	Max ratio	0.93	1.50	1.10	0.69	0.55
	Interpolation	0.87	0.53	0.88	0.71	0.76
	Ensemble fields	0.98	1.20	0.94	0.82	0.78

Table 4-4 Statistical outputs for five rainy hours each from the five rainy events of CMORPH.

Statistics	Methods	Event 1	Event 2	Event 3	Event 4	Event 5
RMSE (mm)	Original	82.90	38.70	22.30	46.00	17.20
	Mean ratio	23.40	9.90	11.00	12.60	8.64
	Max ratio	18.10	11.3	10.20	10.00	8.70
	Interpolation	22.90	12.47	10.90	8.50	7.22
	Ensemble fields	16.70	6.80	7.30	7.50	6.27
Correlation Coefficient (CC)	Original	0.61	0.64	0.58	0.63	0.83
	Mean ratio	0.61	0.64	0.58	0.63	0.83
	Max ratio	0.61	0.64	0.58	0.63	0.83
	Interpolation	0.62	0.56	0.64	0.72	0.89
	Ensemble fields	0.67	0.71	0.67	0.76	0.89
Bias Ratio	Original	0.23	0.28	0.36	0.16	0.61
	Mean ratio	0.64	0.53	0.73	0.45	1.02
	Max ratio	0.78	0.34	0.64	0.53	1.05
	Interpolation	0.63	0.45	0.62	0.53	1.01
	Ensemble fields	0.80	0.96	1.08	0.60	1.01

Figures 4-9a-e and 4-10a-e, show Bias ratio, CC, RMSE and AD respectively. The two sets of Figures 4-9a-e and 4-10a-e are for HE and CMORPH respectively. In most of Figures 4-9 and 4-10, the original bias is below the red line. The red horizontal line in these figures represents the ideal (theoretical) value for the respective performance criteria. Thus, the satellite products overestimate the total areal precipitation (this doesn't mean the satellite products overestimate precipitation intensity at pixel level). From these figures, we note that the methods reduced biases variably. The method of maximum ratio effectively reduced biases in Figure 4-9b, a, d and e. However the maximum ratio is not a reliable method for bias correction in all cases as it lacks consistency in the other bias plots.

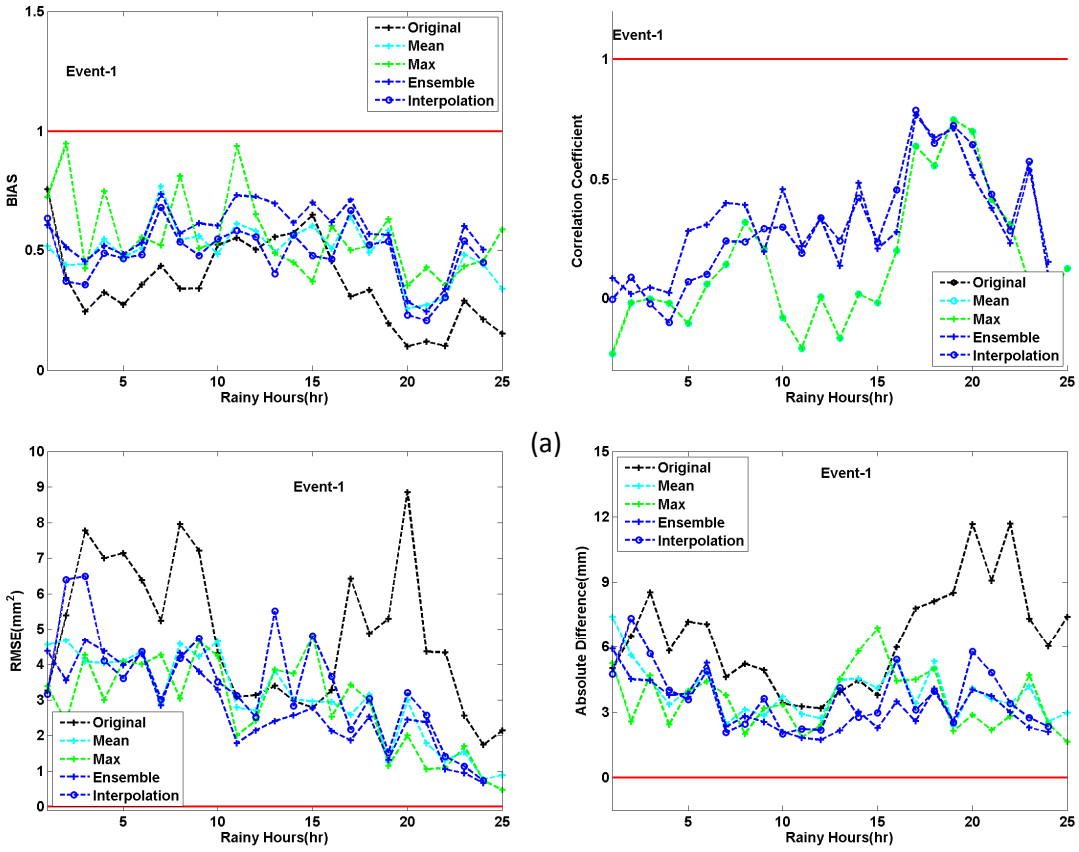
Event-1
Original
Mean
Max
Ensemble
Interpolation
BIAS
Rainy Hours(hr)
Correlation Coefficient
RMSE(mm^2)
Absolute Difference(mm)

(a)

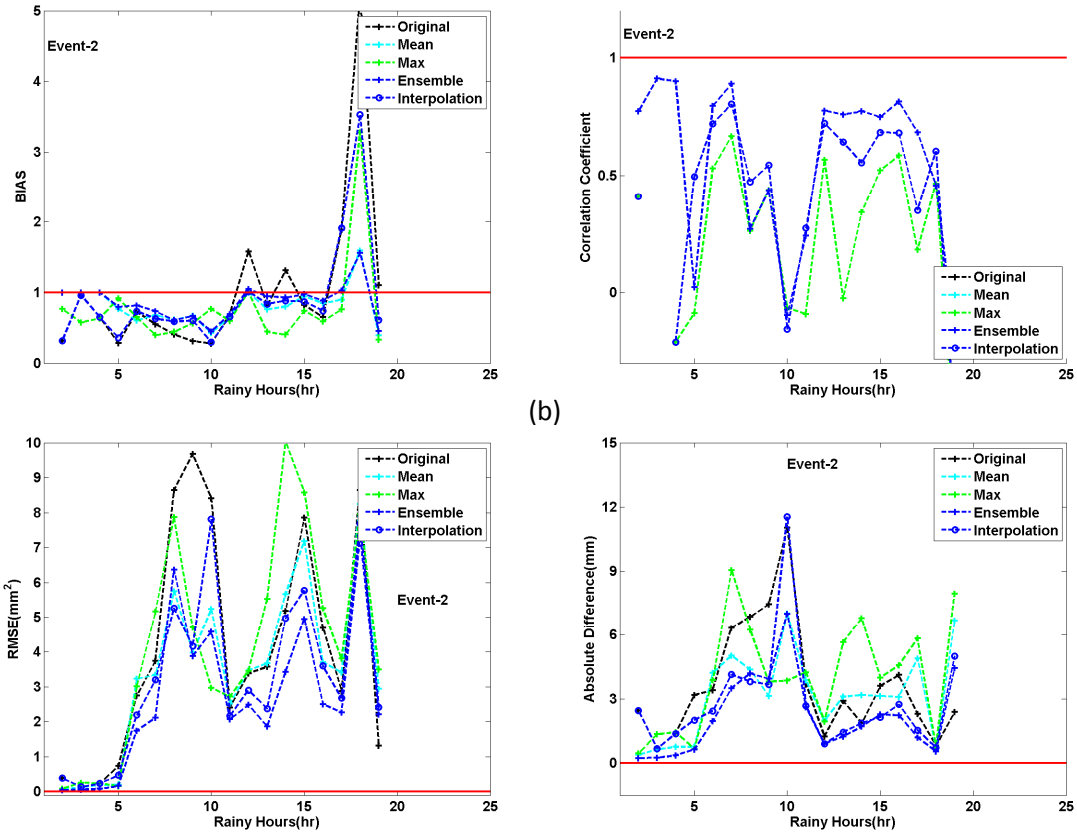
Event-2
Original
Mean
Max
Ensemble
Interpolation
BIAS
Rainy Hours(hr)
Correlation Coefficient
RMSE(mm²)
Absolute Difference(mm)

(b)

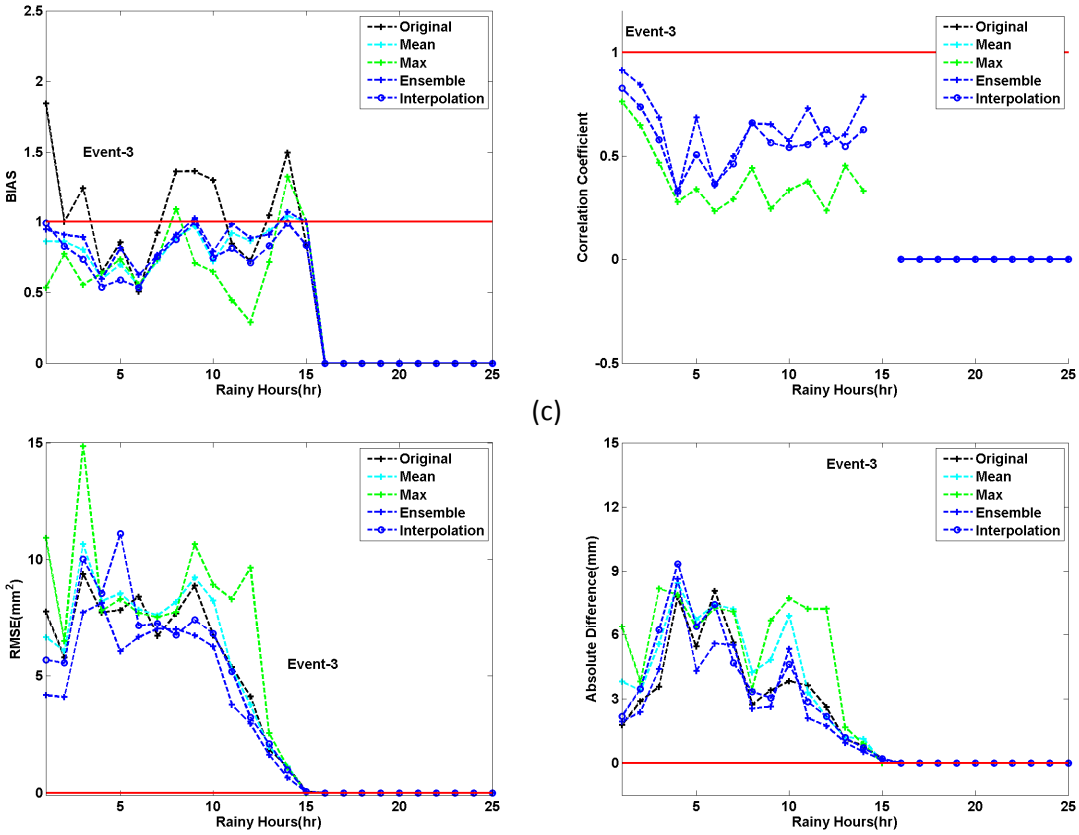
Original
Mean
Max
Ensemble
Interpolation
Event-3
BIAS
Rainy Hours(hr)
Correlation Coefficient
RMSE(mm^2)
Absolute Difference(mm)

(c)

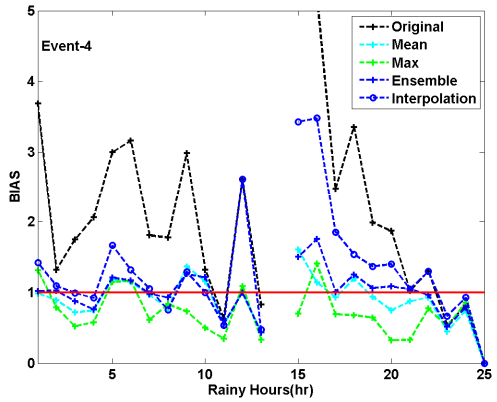
Event-4
Original
Mean
Max
Ensemble
Interpolation
BIAS
Rainy Hours(hr)

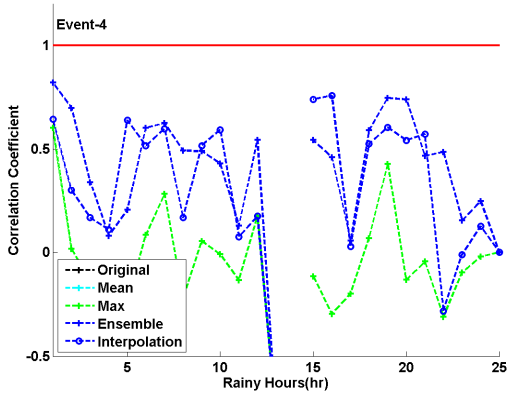
Event-4
Original
Mean
Max
Ensemble
Interpolation
Correlation Coefficient
Rainy Hours(hr)

(d

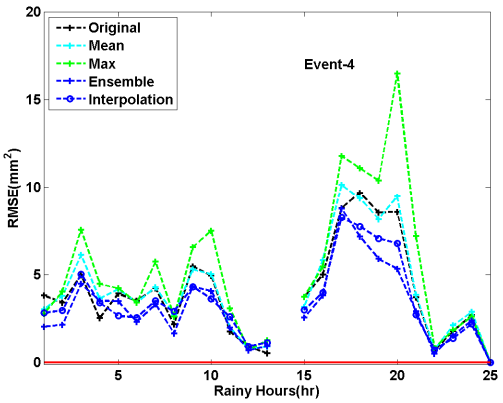
Original
Mean
Max
Ensemble
Interpolation
Event-4
RMSE(mm^2)
Rainy Hours(hr)

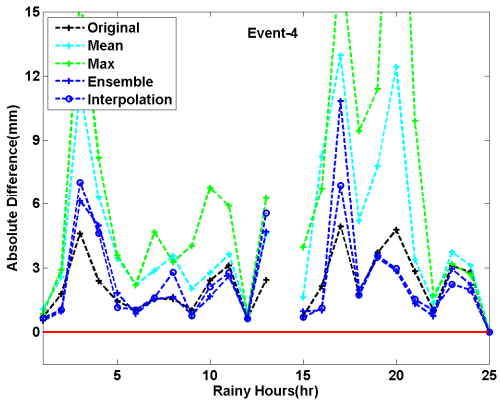
Original
Mean
Max
Ensemble
Interpolation
Event-4
Absolute Difference(mm)
Rainy Hours(hr)

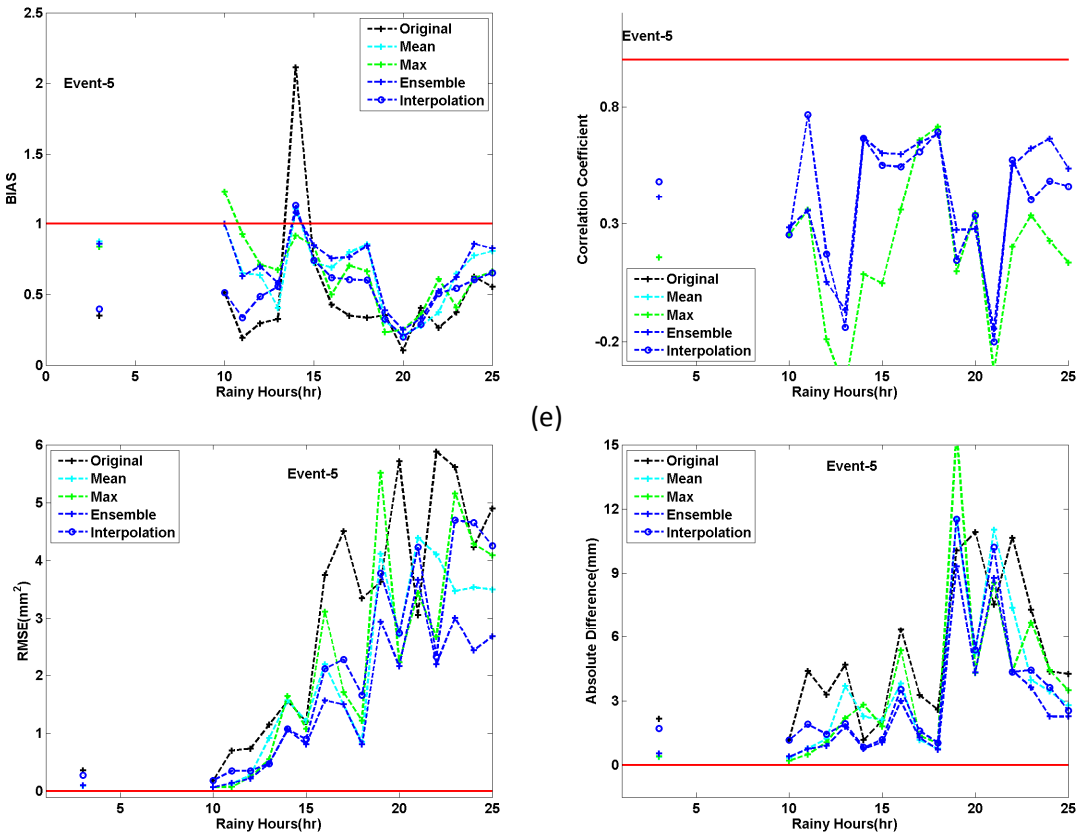

(e)

Figure 4-8 Evaluation criteria BIAS, Correlation Coefficient, Root Mean Squared Error (RMSE) and mean Absolute Difference for HE against ST-IV. (a) Event 1, (b) Event 2, (c) Event 3, (d) Event 4 and (e) Event 5.

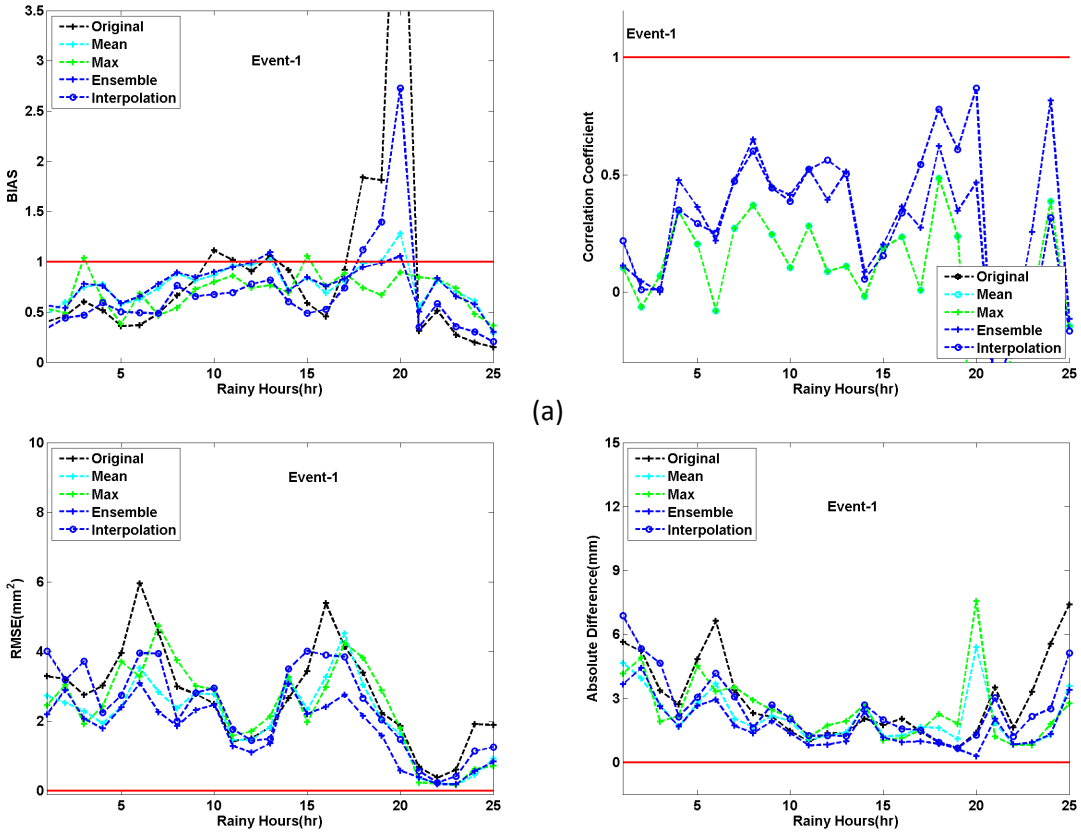
Original
Mean
Max
Ensemble
Interpolation
Event-1
BIAS
Rainy Hours(hr)
Correlation Coefficient
RMSE(mm^2)
Absolute Difference(mm)

(a)

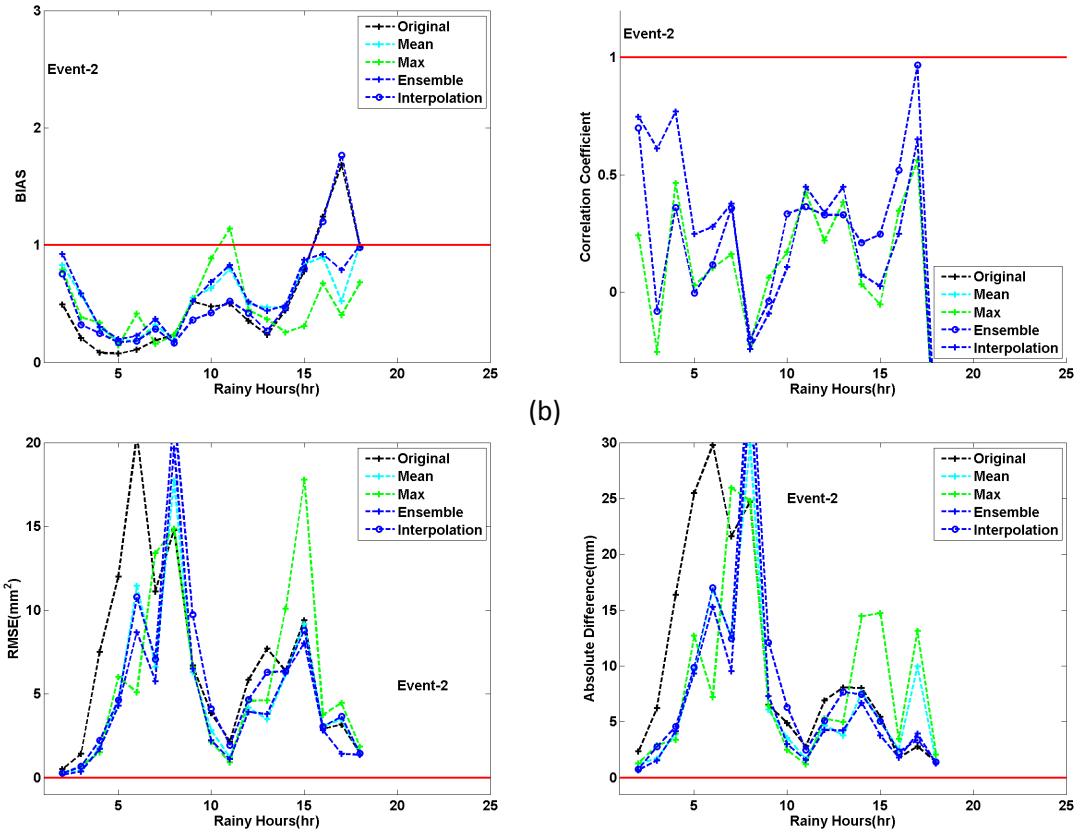
Event-2
BIAS
Rainy Hours(hr)
Original
Mean
Max
Ensemble
Interpolation
Event-2
Correlation Coefficient
Rainy Hours(hr)
Original
Mean
Max
Ensemble
Interpolation
RMSE(mm^2)
Rainy Hours(hr)
Event-2
Original
Mean
Max
Ensemble
Interpolation
Absolute Difference(mm)
Rainy Hours(hr)
Event-2
Original
Mean
Max
Ensemble
Interpolation

(b)

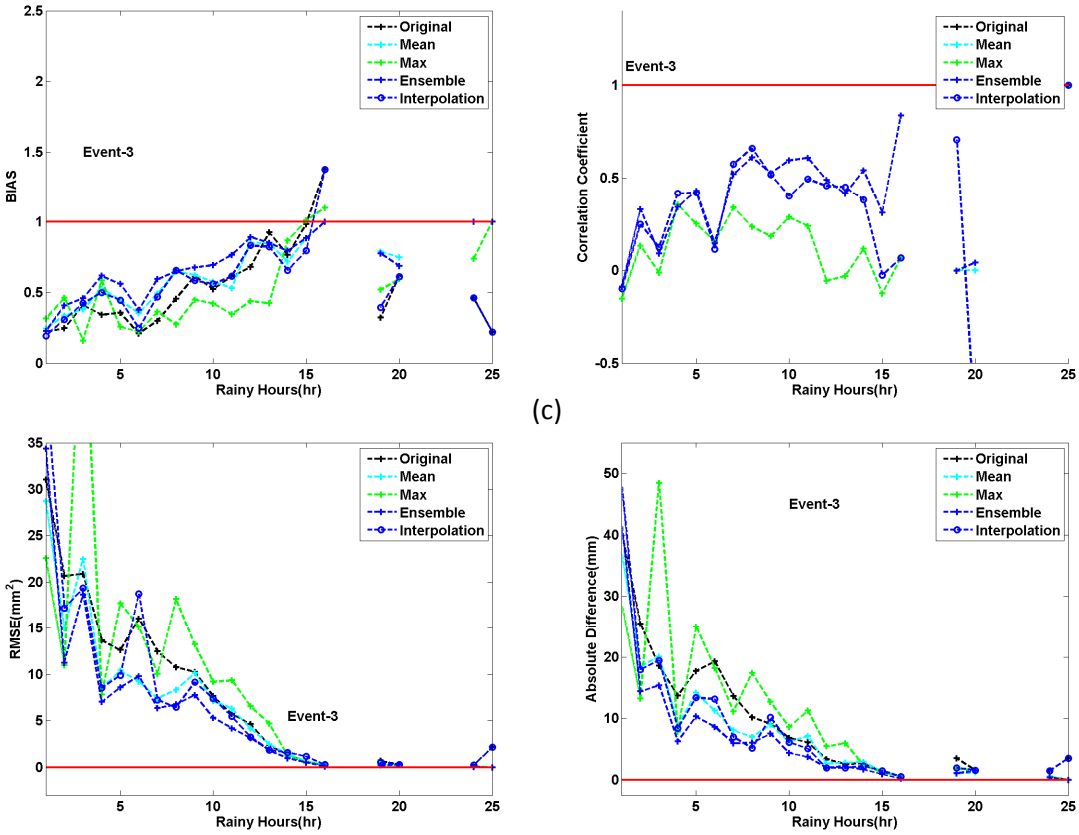
Original
Mean
Max
Ensemble
Interpolation
Event-3
BIAS
Rainy Hours(hr)
Correlation Coefficient
RMSE(mm^2)
Absolute Difference(mm)

(c)

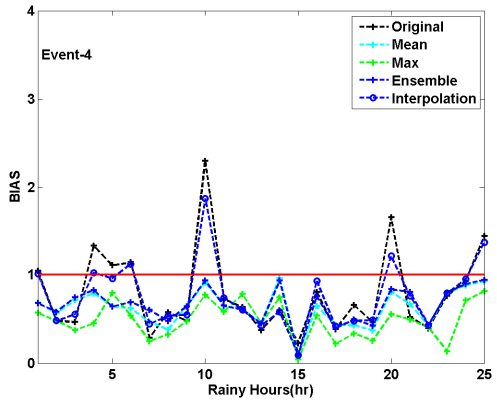
Event-4
Original
Mean
Max
Ensemble
Interpolation
BIAS
Rainy Hours(hr)

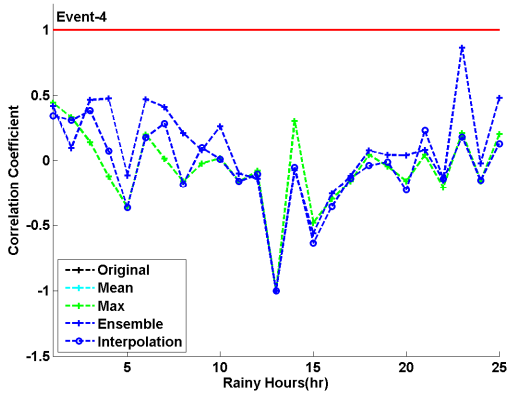
Event-4
Original
Mean
Max
Ensemble
Interpolation
Correlation Coefficient
Rainy Hours(hr)

(d)

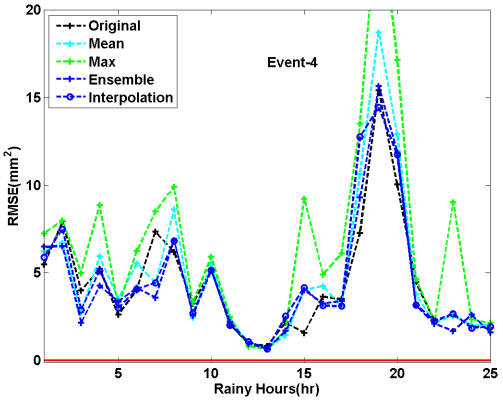
Original
Mean
Max
Ensemble
Interpolation
Event-4
RMSE(mm^2)
Rainy Hours(hr)

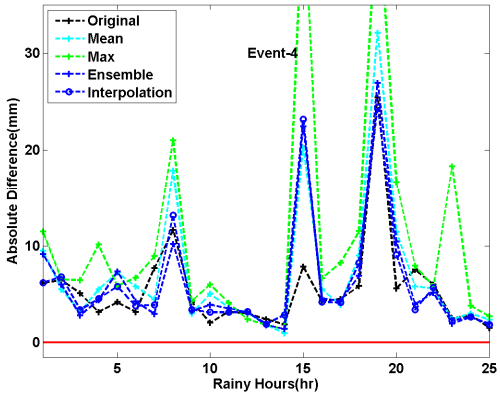
Original
Mean
Max
Ensemble
Interpolation
Event-4
Absolute Difference(mm)
Rainy Hours(hr)

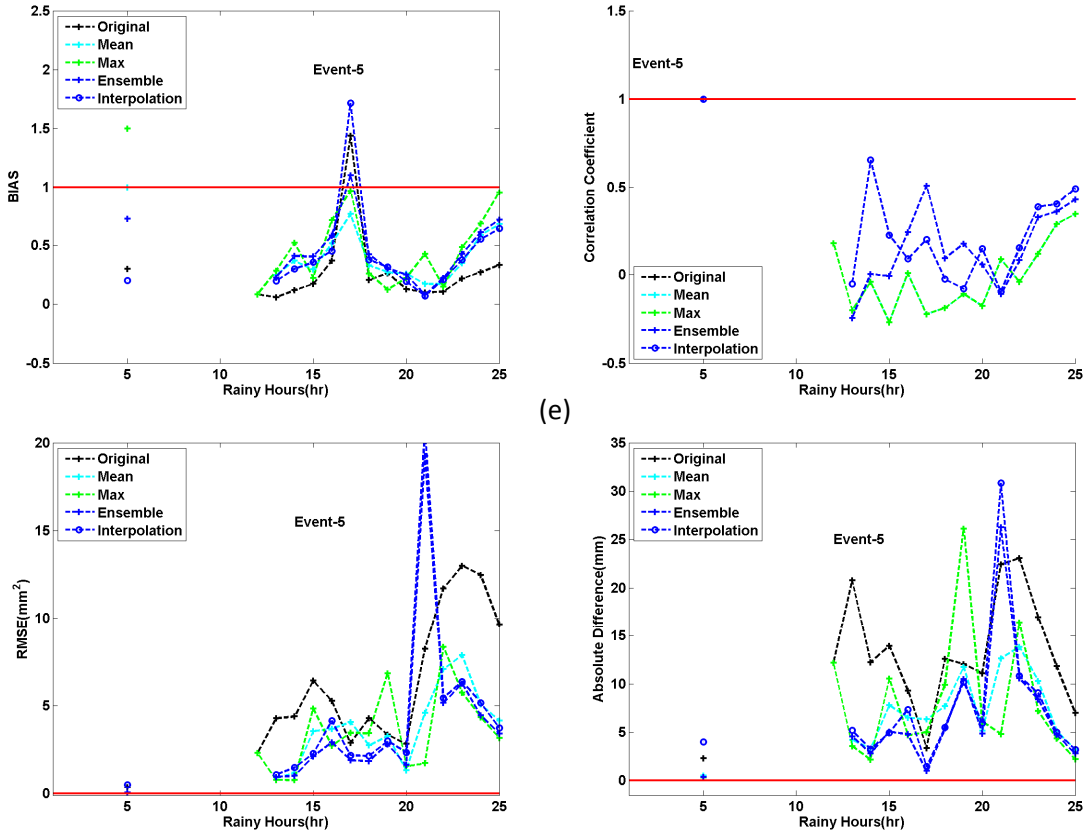

Figure 4-9 Evaluation criteria BIAS, Correlation Coefficient, Root Mean Squared Error (RMSE) and Absolute Difference for CMORPH against ST-IV. (a) Event 1, (b) Event 2, (c) Event 3, (d) Event 4 and (e) Event 5.

For instance, the method further degraded the satellite product in some cases (Figure 4-9c, d and 4-10c). The classic mean-ratio (mean field bias correction) method effectively reduced bias in almost all cases except a few (for example Figure 4-10a hour mark 14) when the sampled bias factors are not good representatives of the areal precipitation. In those cases bias ratios from the sample were mostly greater than 1 while the mean bias ratio for the whole region was less than 1. The method of interpolation also effectively reduced bias in satellite precipitation products. But

it was the method of ensembles which outperformed the rest. The performance of both the interpolation and ensembles methods is generally superior to the mean and maximum ratio methods, which use spatially constant bias factors.

Figures 4-8 and 4-9 also contain CC, RMSE and AD besides BIAS for each hour. Generally poorer correlation is observed in event 1 and event 5 (winter cases) which reflects poor estimation of precipitation in satellite products in the wintertime. The methods of maximum and mean ratio don't work well in terms of improving the correlation coefficient (CC). The method of ensembles tends to reduce AD and RMSE and improve CC better than interpolation without ensembles.

Figures 4-10 and 4-11 (from top to bottom), respectively illustrate scatter plots for HE and CMORPH at rainy hours 06071107, 06020619, 06091015, 06122923, and 06031906. These selected hours from each rain event shown in Table 4-2. The right side of Figure 4-10 and 4-11 represent the relationship after bias correction, and the left side represents values before bias correction. For each hour, the CC, RMSE and BIAS are shown as indicators of the overall performance of the ensemble bias correction method. The percentage improvement of the correlation coefficient varied from case to case. Both HE and CMORPH showed significant improvements after bias correction was made using the method of ensembles. For instance, for hour 06071107 the bias correction improved the correlation coefficient between the HE and ST-IV by 20 %. For cases with already higher correlation coefficient between the ST-IV and original

SPEs a lower percentage of improvement was observed than with low correlation between the original SPEs and ST-IV. The scatter plots indicate that our method has effectively improved the SPE in randomly picked hours in every season.

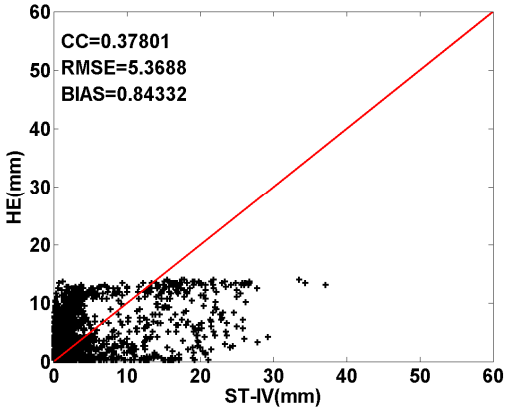
CC=0.37801
RMSE=5.3688
BIAS=0.84332
HE(mm)
ST-IV(mm)

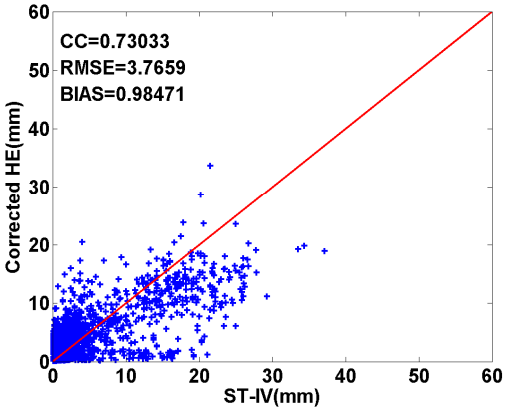
CC=0.73033
RMSE=3.7659
BIAS=0.98471
Corrected HE(mm)
ST-IV(mm)

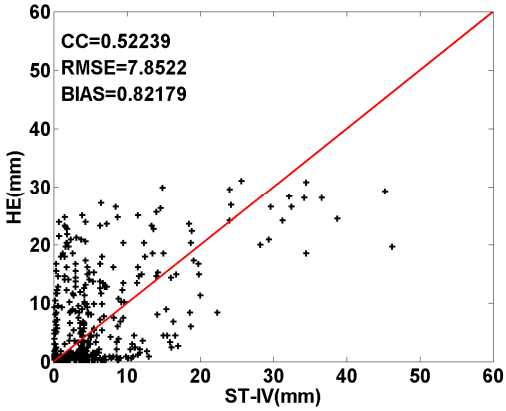
CC=0.52239
RMSE=7.8522
BIAS=0.82179
HE(mm)
ST-IV(mm)

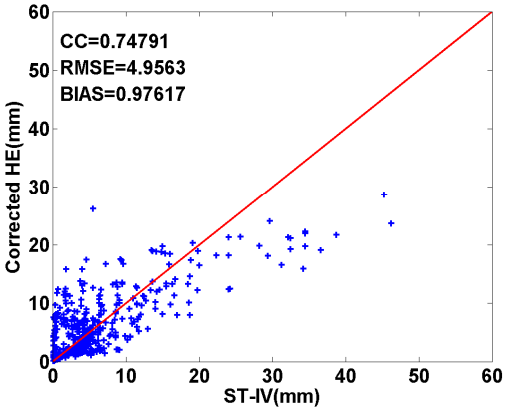
CC=0.74791
RMSE=4.9563
BIAS=0.97617
Corrected HE(mm)
ST-IV(mm)

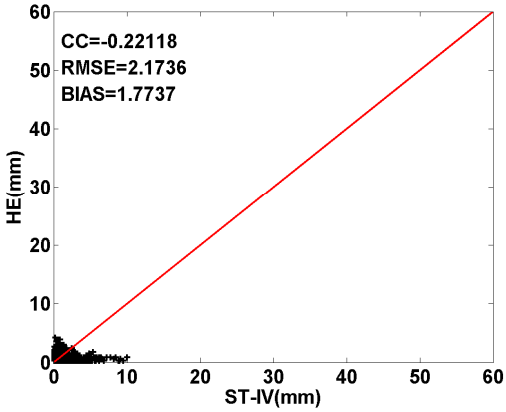
CC=-0.22118
RMSE=2.1736
BIAS=1.7737
HE(mm)
ST-IV(mm)

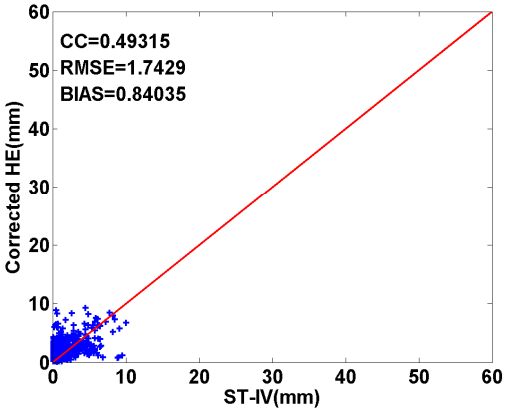
CC=0.49315
RMSE=1.7429
BIAS=0.84035
Corrected HE(mm)
ST-IV(mm)

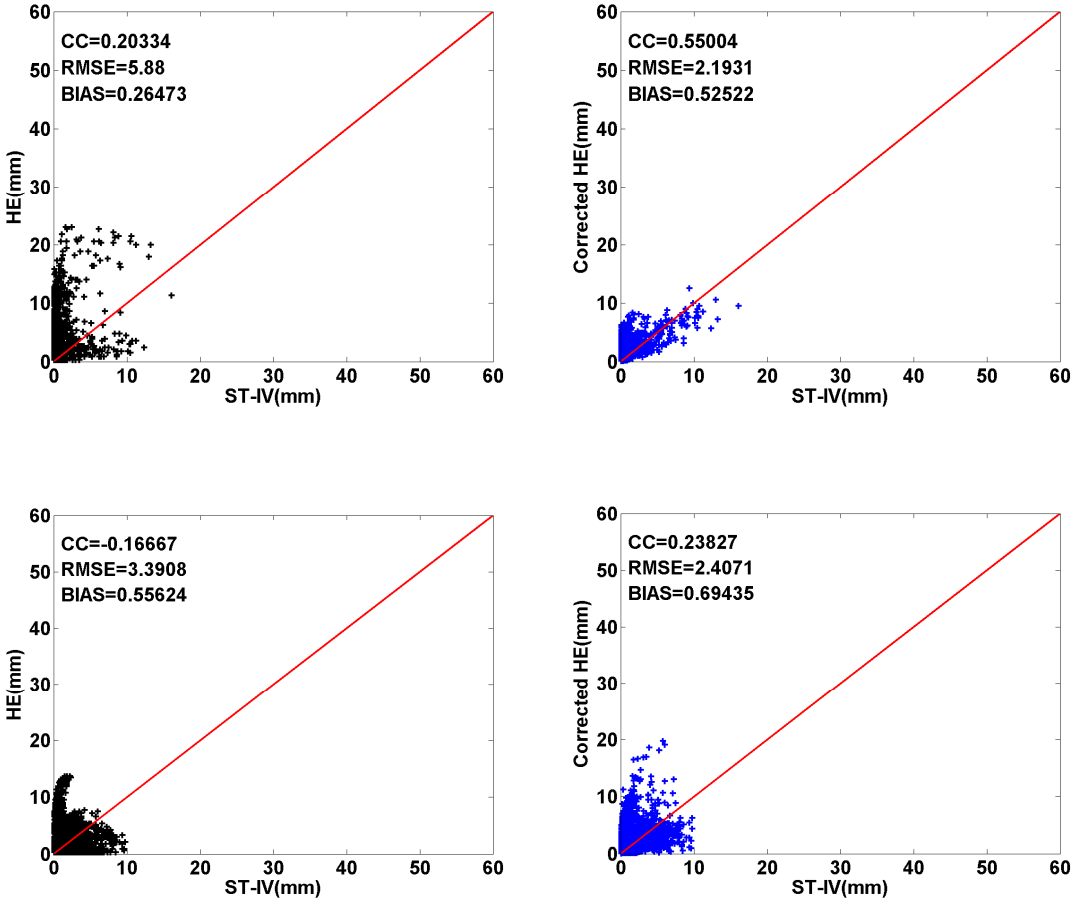

Figure 4-10 Scatter plot of radar-gauge (ST-IV) and satellite estimate (HE) before (left side) and after (right side) bias correction for 06071107, 06020619, 06091015, 06122923 and 06031906 (from top to bottom respectively). CC, RMSE and BIAS are the correlation coefficient, Root Mean Squared Error and Bias.

In most rain events it is observed that even though significant improvements are obtained by our approach of interpolation with ensemble pre-smoothing, systematic biases remain in the satellite products.

In the United States, radar and satellite products are available near real-time. This gives an advantage to radars to correct biases in satellite products over very sparse real time rain gauges. This work demonstrates that daily updates of parameters are sufficient to carry out bias correction in satellite products. The results showed that with only three parameters, the method

of ensembles provides useful bias correction and should be further tested, particularly in rain gauge sparse areas.

After further testing in more locations, the developed approach is intended to be implemented operationally along with existing operational satellite-based precipitation retrieval algorithms (such as HE and CMORPH) to correct biases and improve the resulting precipitation product. This is expected to improve the operational SPE products and reduce the differences between corresponding precipitation values produced by different algorithms, benefiting end users by providing improved quality precipitation information particularly over areas of sporadic or incomplete radar coverage.

The two SPE products selected for bias corrections are 1) Hydro-Estimator (HE), available in near real time (within ≈1 hour) and 2) CPC Morphing (CMORPH) available at ≈18 hour delay. Biases are computed and corrected against the operational merged radar-gauge rainfall product (ST-IV), which is also available within 1-2 hours (in preliminary form) to 18 hours (fully calibrated against gauge data). It is anticipated that the proposed method can be applied with 1 to 3 hour windows of both the satellite and radar-gauge products, depending on the areal coverage of precipitation (which controls the amount of overlap between the satellite and radar fields). Hence, bias-corrected HE or CMORPH precipitation fields could be produced within <24 hours.

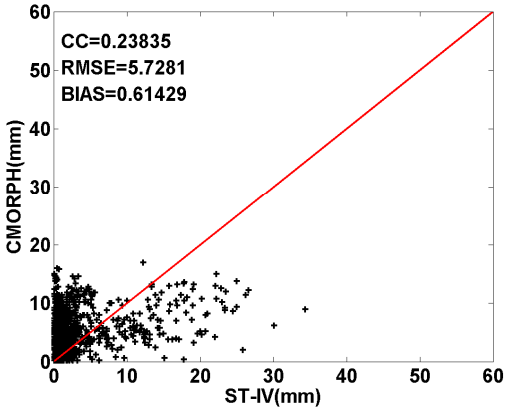
CC=0.23835
RMSE=5.7281
BIAS=0.61429
CMORPH(mm)
ST-IV(mm)

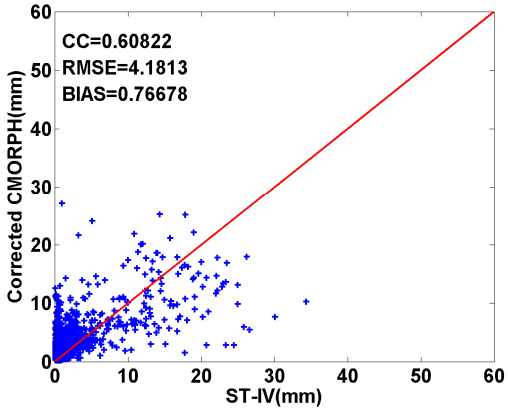
CC=0.60822
RMSE=4.1813
BIAS=0.76678
Corrected CMORPH(mm)
ST-IV(mm)

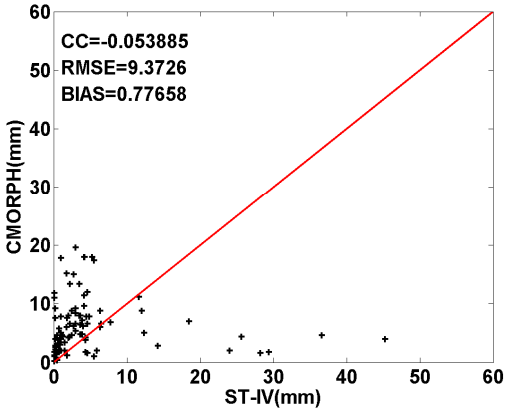
CC=-0.053885
RMSE=9.3726
BIAS=0.77658
CMORPH(mm)
ST-IV(mm)

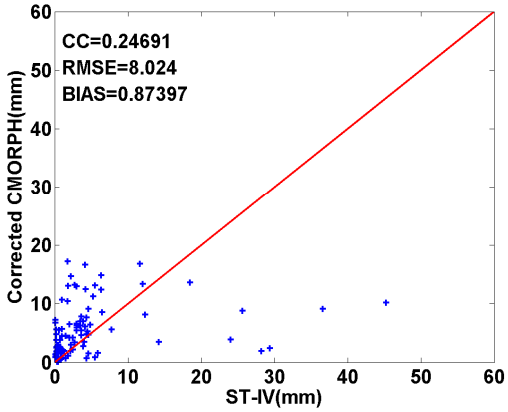
CC=0.24691
RMSE=8.024
BIAS=0.87397
Corrected CMORPH(mm)
ST-IV(mm)

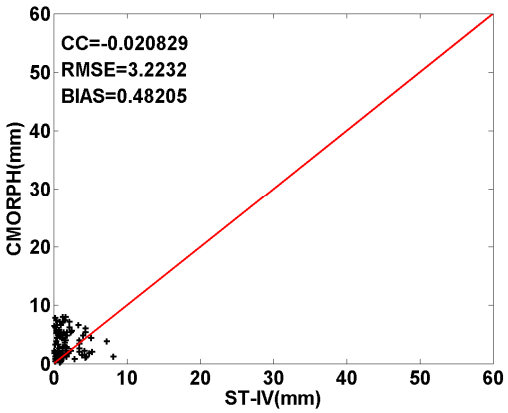
CC=-0.020829
RMSE=3.2232
BIAS=0.48205
CMORPH(mm)
ST-IV(mm)

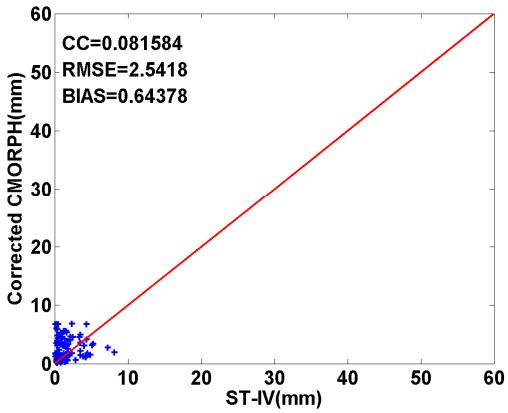
CC=0.081584
RMSE=2.5418
BIAS=0.64378
Corrected CMORPH(mm)
ST-IV(mm)

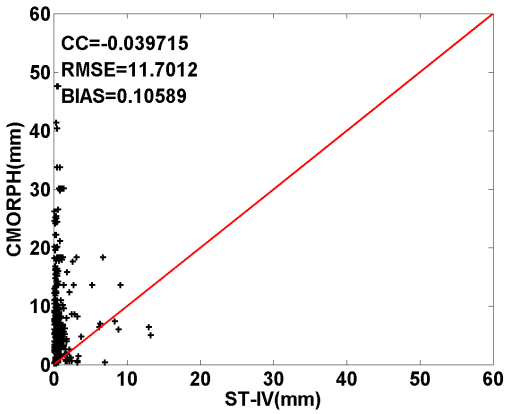
CC=-0.039715
RMSE=11.7012
BIAS=0.10589
CMORPH(mm)
ST-IV(mm)

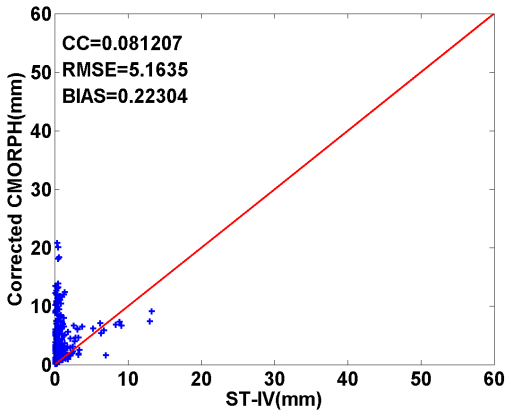
CC=0.081207
RMSE=5.1635
BIAS=0.22304
Corrected CMORPH(mm)
ST-IV(mm)

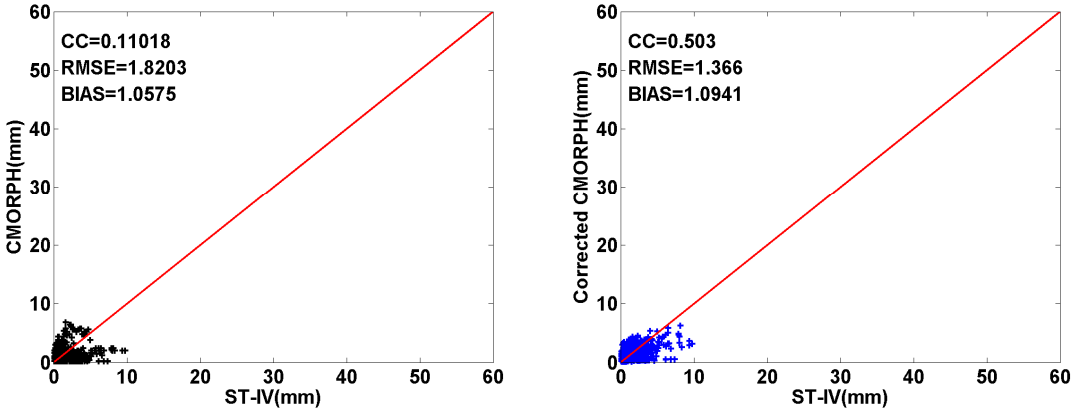

Figure 4-11 Scatter plot of radar-gauge (ST-IV) and satellite estimate (CMORPH) before (left side) and after (right side) bias correction for 06071107, 06020619, 06091015, 06122923 and 06031909 (from top to bottom respectively). CC, RMSE and BIAS are the correlation coefficient, Root Mean Squared Error and Bias.

In addition to the statistics explained in the above paragraphs, it was worthwhile to check the performance of the bias correction techniques in a time series frame-work. Four pixels were randomly selected from each season and their 24 hour rainfall time-series was depicted from Figures 4-12 to 4-15. The pixels were selected in such away that they were raining for a representative duration in the rainy events in Table 3. Figure 4-12, 13, 14 and 15 are time series for the selected pixels for events 2, 3, 4 and 5 respectively. We could not identify a rainy pixel for long enough duration to show the significance of the time series for event 1. Each figure shows the time series of hourly accumulated rainfall of STIV, HE, 100 ensemble members of the model and the mean bias corrected HE using the method of ensembles for the chosen pixel. The blue crosses represent the hundred ensemble members simulated using the ensemble bias correction method for the respective pixels in rainy events, where as the red crosses and the cyan triangles represent the original HE and ST-IV estimations respectively. The green crosses are the mean of the hundred blue crosses (ensemble members). As shown in the figures the green crosses (mean of the ensemble members) are closer to the cyan triangles (ST-IV estimates or

'true' estimates). Figure 4-12 shows that the mean of the ensembles reduced the over-estimation made by the original HE at hours 8, 9 and 10, and improved the underestimation at hours 13 and 14. Similar outputs were observed for cases in Figures 4-14 and 4-15. In Figure 4-14 and 4-15, the ensemble bias correction technique improved the satellite rainfall estimation in such away that the discrepancies between the radar and satellite precipitation estimates are reduced. In Figure 4-13, the method of ensembles over-estimated the rainfall at hour 24 and 25.

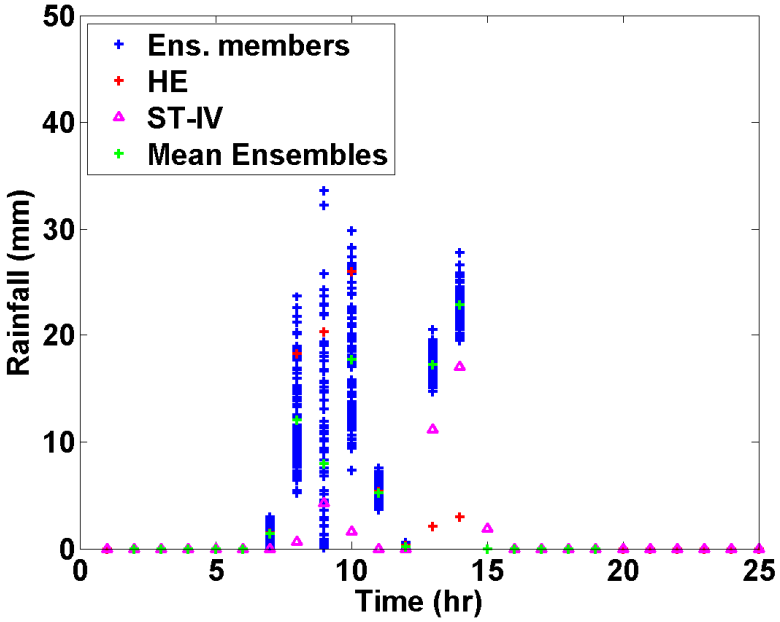

Figure 4-12 Time series of HE, ST-IV, bias corrected HE using Ensembles (Mean members), 100 realizations of ensemble members (Ens. members) for event 2.

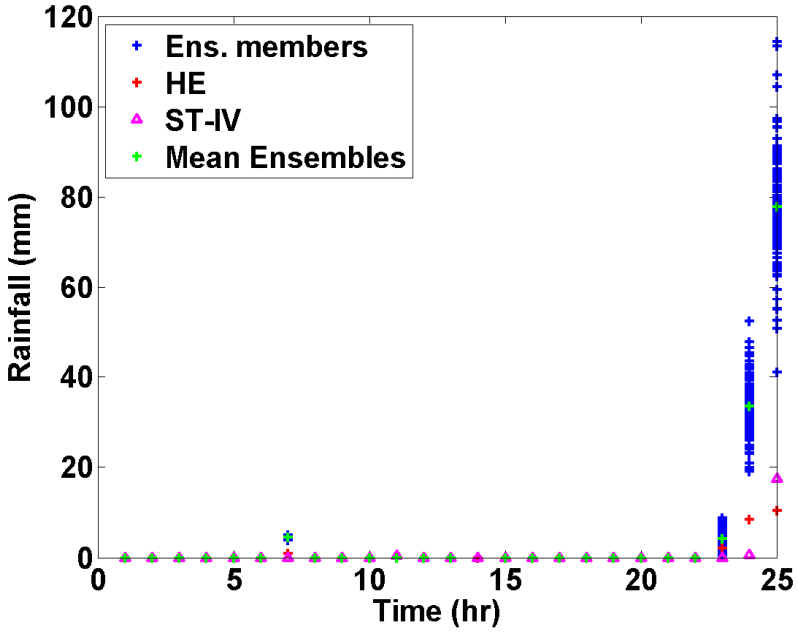

Figure 4-13 Time series of HE, ST-IV, bias corrected HE using Ensembles (Mean members), 100 realizations of ensemble members (Ens. members) for event 3.

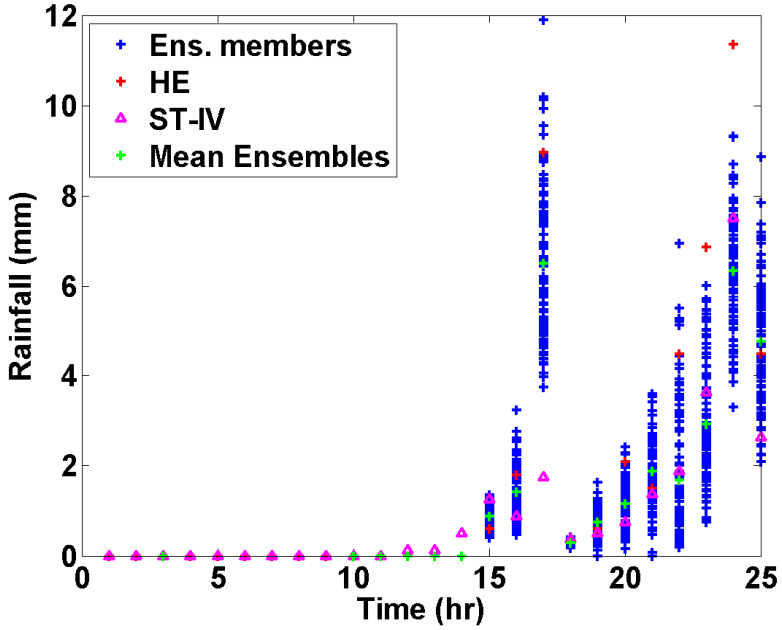

Figure 4-14 Time series of HE, ST-IV, bias corrected HE using Ensembles (Mean members), 100 realizations of ensemble members (Ens. members) for event 4.

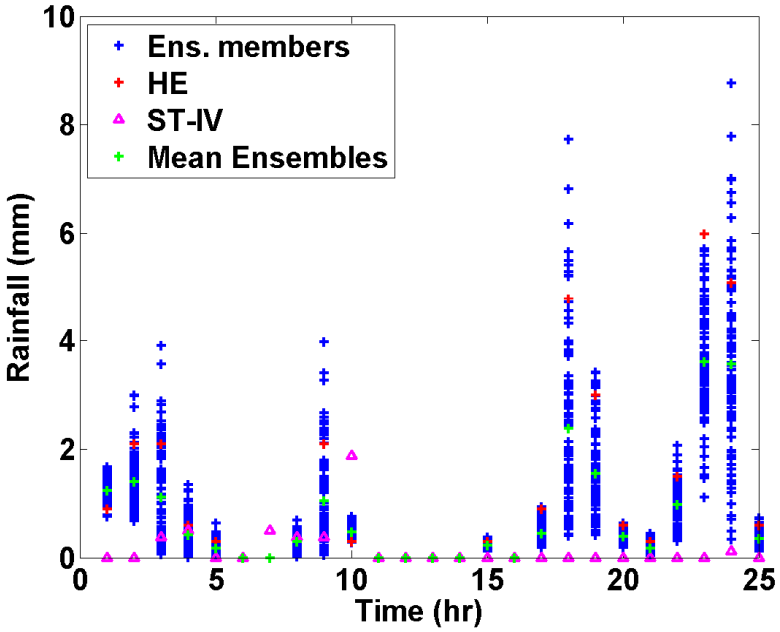

Figure 4-15 Time series of HE, ST-IV, bias corrected HE using Ensembles (Mean members), 100 realizations of ensemble members (Ens. members) for event 5.

4.3. Successive Correction Method (SCM)

The SCM schemes are tested by creating artificial radar gap areas by annulling some of the rainy pixels in the radar rainfall images. Several case studies are selected for merging RR rainfall with HE at hourly 4 km x 4 km resolution, using a merging window with various sizes, from 3 x 3 to 25 x 25 pixels. Radar gap areas with a size 0.5° x 0.5°, 1° x 1° and 1.5° x 1.5° was selected to study the performance, where RR was unavailable for some pixels or for a large area. In the case of an existing large radar gap area, rainfall was estimated only for the pixels with no radar data and RR assigned to the pixels outside the gap region to minimize bias of the generated rainfall. To estimate rainfall for every pixel with missing RR, its neighboring pixels with generated rainfall values within the merging window were also used in the merging process.

The window was moved from outside toward the gap area from four different directions (left, right, above, and below) to extend rainfall patterns from outside into the gap area from four different sides. Figure 4-16 shows a sample of moving window. In this figure, the yellow box represents a 9 × 9 moving window; the white area is the radar gap and the white pixel at the center of the yellow box is the first pixel to be estimated. Mostly, precipitation might not fully surround the gap area. In such cases, calculating the mean of the outputs from the different-direction can weaken estimates. Thus, the generated rainfall value for every pixel with no radar data is the maximum of four estimated values for that pixel when merging window moves over the gap area from four different directions. We considered the maximum value for the following reason: if the storm does not surround the gap proportionally, estimates made by moving the window from the non-raining side will definitely be small. Thus, maximum of the four outputs from SCM will give a better out put than the average of the four.

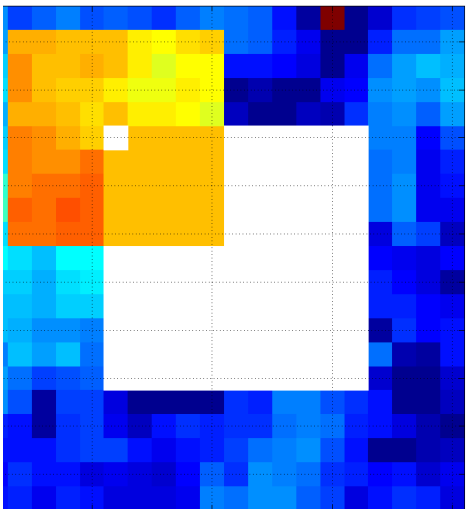

Figure 4-16 An illustration of a moving window in the Successive Correction Method. The yellow box represents a 9 × 9 moving window; the white area is the radar gap surrounded by available precipitation data and the white pixel at the center of the yellow box is the first pixel to be estimated.

The above two steps have been applied to fill artificially created gaps of size 0.5 × 0.5, 1.0 × 1.0 and 1.5 × 1.5 degrees over the ST-IV rainfall field (Figure 4-17). Since the true precipitation rainfall field in a true gap is unknown, an artificial gap is created at the center of the ST-IV field. A precipitation field is reproduced in the gap using the Brandes scheme explained in the previous Chapter. The original ST-IV in the gap is used to validate the merged product (reproduced product). A sample of the original ST-IV and HE products for 2006122905 UTC is shown in Figures 4-17a and 4-17b respectively. As Figure 4-17 illustrates, there is a considerable discrepancy between the original ST-IV and HE.

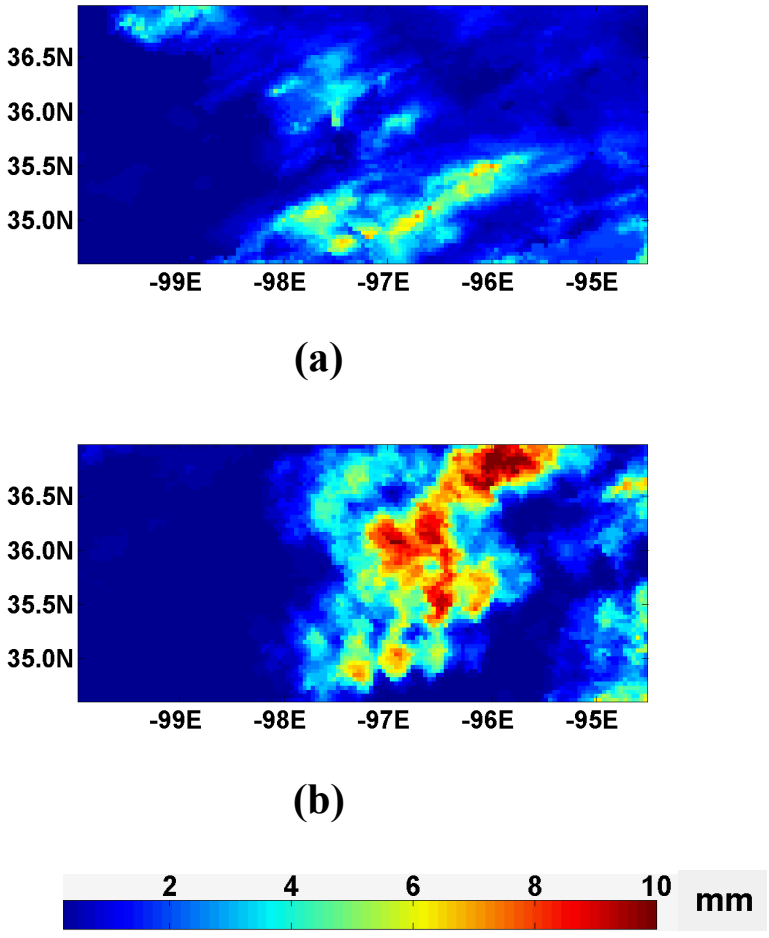

Figure 4-17 (a) Original radar-gauge Stage-IV (ST-IV); (b) Original satellite based Hydro-Estimator (HE).

To reduce this discrepancy, a bias correction of HE was needed against ST-IV.

The bias corrected HE is merged with ST-IV to produce a gap free product. In the SCM scheme, different overpass window sizes result in different accuracies. We tried different sizes of windows to obtain optimal merged product. For this study, an overpass window of size 9 pixels by 9 pixels was used for analysis. Figure 4-18 (right) is a result of merged estimates of radar-gauge and satellite products.

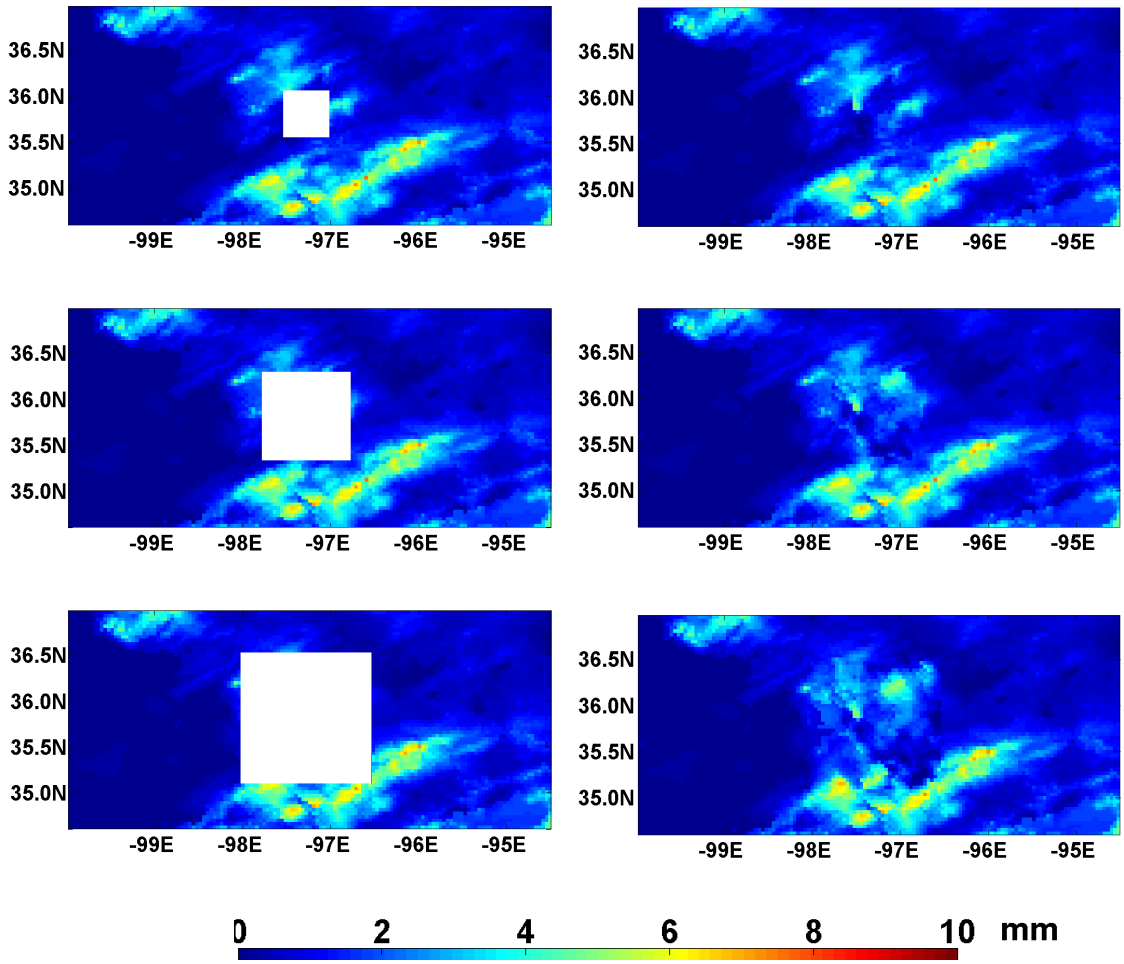

Figure 4-18 ST-IV with an artificially created gap of size 0.5 by 0.5, 1 by 1 and 1.5 by 1.5 degrees (Left). ST-IV with generated merged product for gap area using SCM method (Right).

Correlation coefficients and RMSE are used to evaluate the performance of the merging procedure. Correlation coefficients between ST-IV and original HE, between ST-IV and bias corrected HE, and between ST-IV and the merged product for the three gap areas with sizes of: 0.5 × 0.5, 1 × 1 and 1.5 × 1.5 degrees can be compared (Figures 4-19, 4-20 and 4-21). From these figures, we noted that bias correction could improve HE by up to 30%. It is also observed that the merged product could produce a higher correlation coefficient than that of bias corrected HE when it is compared with the original ST-IV. From these figures, we note that the merged products have less bias than the original HE when it is compared against the original ST-IV.

The accuracy of SCM depends on the size of the window we use. To get an optimal window size, we plotted correlation coefficient calculated between the SCM outputs and the original radar versus the window size (as shown in Figure 4-25 and 4-26). For the particular case we picked a window size of 9 by 9 (36 km by 36 km) gave an optimal output. For the rest of the studies, we used an overpass window of size 11 by 11.

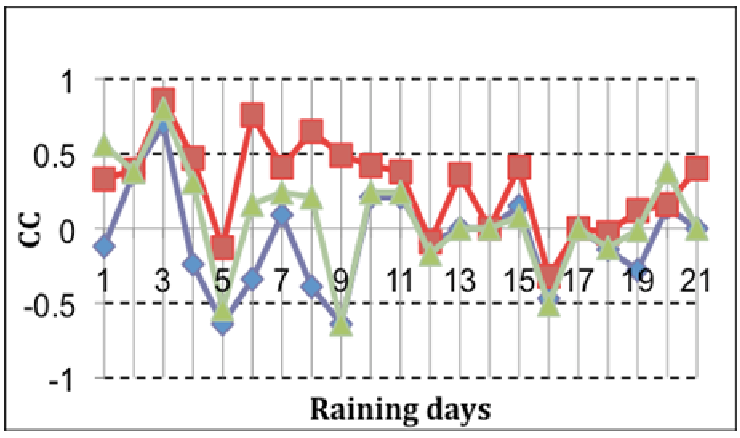

Figure 4-19 Blue, Green and Red demonstrate correlation coefficients between the ST-IV and Original HE, ST-IV and bias corrected HE, and ST-IV and the Merged product respectively, for 21 hours of 2006122902-2006123002 UTC over a gap area size of 0.5 × 0.5 degrees.

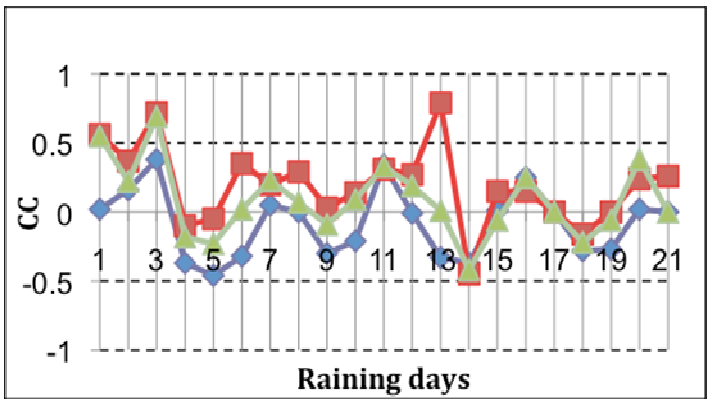

Figure 4-20 As Figure 4-19, except the size of the gap is 1 × 1 degree.

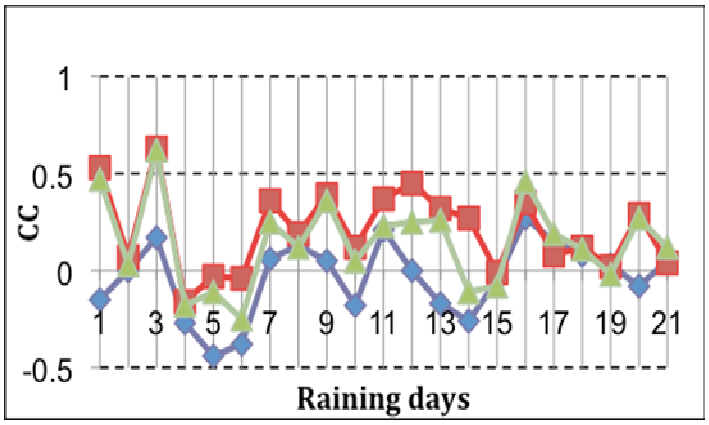

Figure 4-21 As Figure 4-19, except the size of the gap is 1.5 × 1.5 degrees.

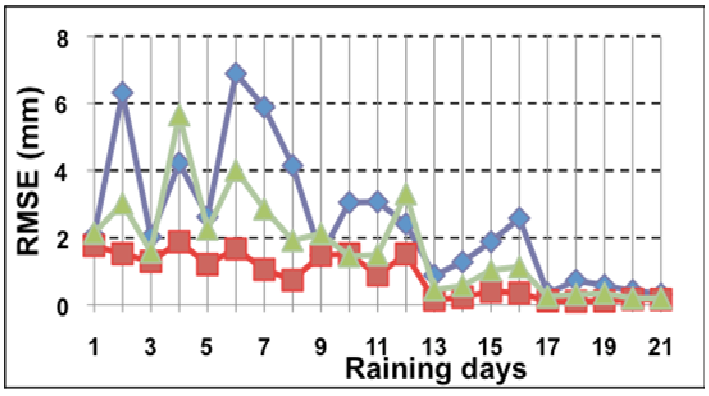

Figure 4-22 Blue, Green and Red demonstrate RMSE between the ST-IV and Original HE, ST-IV and bias corrected HE, and ST-IV and the Merged product respectively, for 21 hours of 2006122902-2006123002 UTC over a gap area size of 0.5 × 0.5 degrees.

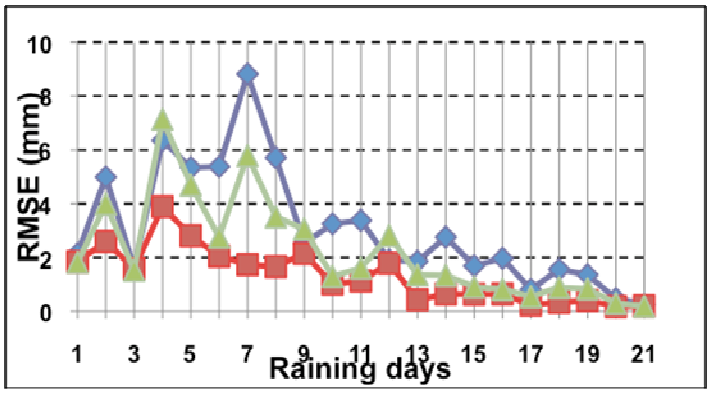

Figure 4-23 As Figure 4-22, except the size of the gap is 1 × 1 degree.

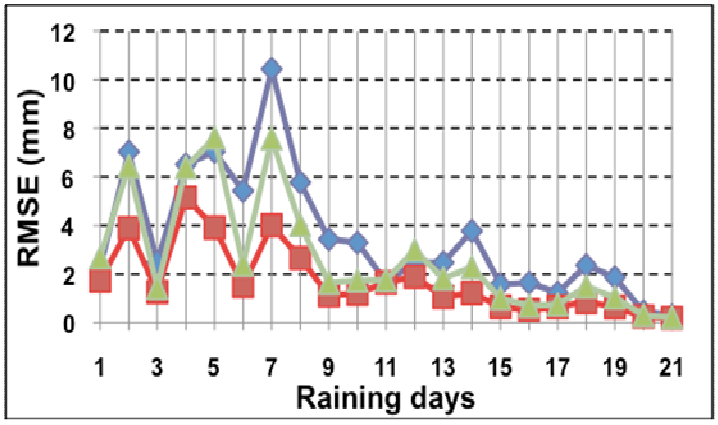

Figure 4-24 As Figure 4-22, except the size of the gap is 1 × 1 degree.

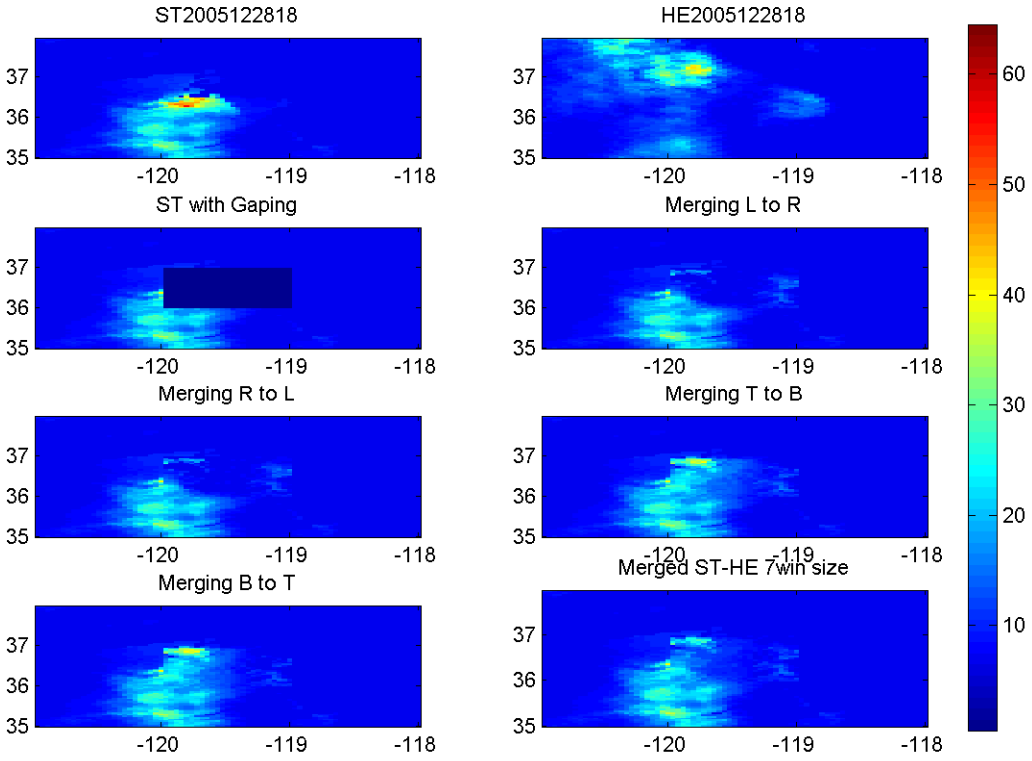

Figure 4-25 The SCM approach. R to L, L to R, B to T and T to B refer right to left, left to right, bottom to top and top to bottom respectively. the lowest right image shows the mean of the others using a 7 by 7 merging window

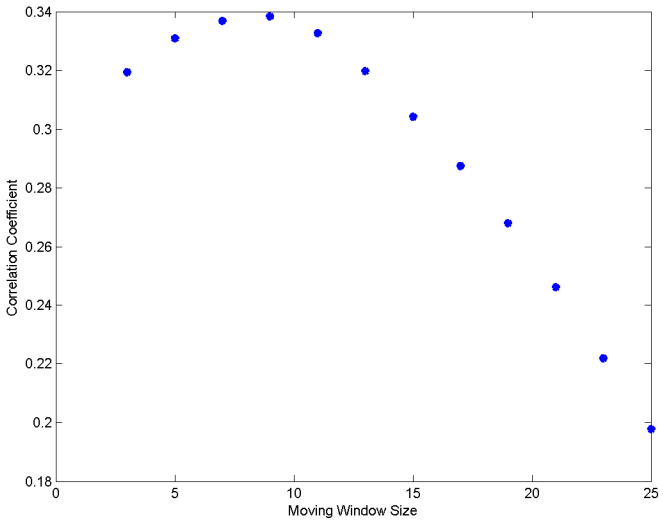

Figure 4-26 Moving window size versus correlation coefficient

4.4. The Bayesian-SCM Model

4.4.1. Covariate preparation

In a Bayesian spatial model, covariates are supplemental data which are known at each grid point with the required temporal and spatial resolutions. They are selected based on availability.

The radar data with missing pixels and monthly PRISM cannot be used directly as covariates. The only data that can be directly used in the analysis is HE, the rest of the covariates need modifications and are developed as follows.

a) ST-II as a covariate

The HE product is merged with that of the ST-II to fill gaps over ST-II. We implemented the Successive Correction Method (SCM), originally developed for data assimilation to calculate missing pixels. The SCM uses the information from available ST-II pixels surrounding the gap area and satellite rainfall to fill the gap pixels (Mahani and Khanbilvardi 2009).

Assume a selected moving window size m×m with its center at u_0, the merged precipitation for any missing pixel centered at u_0 in the gap area is calculated based on information from satellite pixels and known available radar pixels with in the window.

Starting from a missing pixel surrounded by the maximum number of available radar pixels, the method continues calculating other missing pixels by moving the m×m window successively.

For this study, the Brandes scheme of SCM has been adopted (Brandes 1975). In addition, we implemented the method of Double Optimization Estimation (DOE) (Seo 1998b) in the SCM frame work to fill gaps over the radar network. Because of its operational success we prefer to use DOE to fill gaps over the radar network.

b) PRISM as a covariate

One of the covariates for this study was the mean PRISM climatological monthly precipitation. For this study, monthly precipitations from PRISM are averaged for past 10 years prior to the year considered in the study before they are used as a covariate for this study. The averaged monthly PRISM products are disaggregated into daily by calculating percentage partial fractions using the daily gauge measurements (Schaake et al., 2004). Percentage partial fractions are calculated for the monthly averaged data using the method explained as in (Schaake et al., 2004). The percentage partial fractions are multiplied by the monthly averaged PRISM products to calculate the required daily PRISM covariate.

Whenever rain-gauges are available, we plan to incorporate them in a multi-source rainfall estimation model. According to Wilson (1970), "a single rain gauge and radar estimate provides a better estimate in an area as large as 3400 km^2 than a single gauge in an area of 800 km^2." For this reason we will incorporate rain-gauges in our multi-source model in a Bayesian

frame-work.

4.4.2. Parameters and Priors

The next step is to assign priors for the parameters. The unknown parameters, βs, σ^2, and range parameter η should be assigned. It is assumed that priors are conjugate with posteriors, such that posteriors and priors have the same distribution.

We used an independent prior distribution for β and σ^2.

$\beta \sim N(\mu, \sigma^2)$

$\sigma^2 \sim IG(\sigma^2 | a, b)$

To avoid dependence of the posterior on the initial values, a 'burn-in' period of 1000 was used.

To model the spatial model we used 'bayesGeostatExact' (Andrew and Sudipto 2007) in R to determine posterior of the parameters. It is a Bayesian spatial linear model with fixed semivariogram parameters. The fixed parameters to model the spatial field in 'bayesGeostatExact' are (spatial range) and the ratio between δ^2 and partial-sill. We calculated the fixed parameters from the experimental variogram using rain gauges. For our choice of the experimental variogram, we employed the exponential experimental variogram shown in Figure 4-27.

Assuming an isotropic one dimensional variogram which represents the spatial roughness of a spatial data set quantitatively.

$$\hat{\gamma}(|h|) = \frac{1}{2n(|h|)} \sum_{i=1}^{n(|h|)} z(x_i + h) - z(x_i))^2 \qquad 4\text{-}4$$

Where x_i is the location of gauge *i* and x_i+h is the locations at distance h from location x_i. The variograms are produced using the daily mesonet datasets. Out of the total 120 Mesonet rain gauges, we have picked 60 of them to develop the variogram.

The most ideal condition is to calculate the parameters for each rainy day. But from feasibility and efficiency point of view, it is better to determine this parameter using all rainy days using the mesonet rain gauge points. Instead we consider the mean of all the daily variograms. The red line in Figure 4-27 is the mean of the the blue semi-variances.

Referring Figure 4-27, a more conservative choice of η (spatial range) 5 km was used. The parameter α which indicates the ratio between nugget (δ^2) (30 mm^2) and partial-sill (150 mm^2) 1/5 was used (Figure 4-27). The numbers in this figure represent selected rainy days.

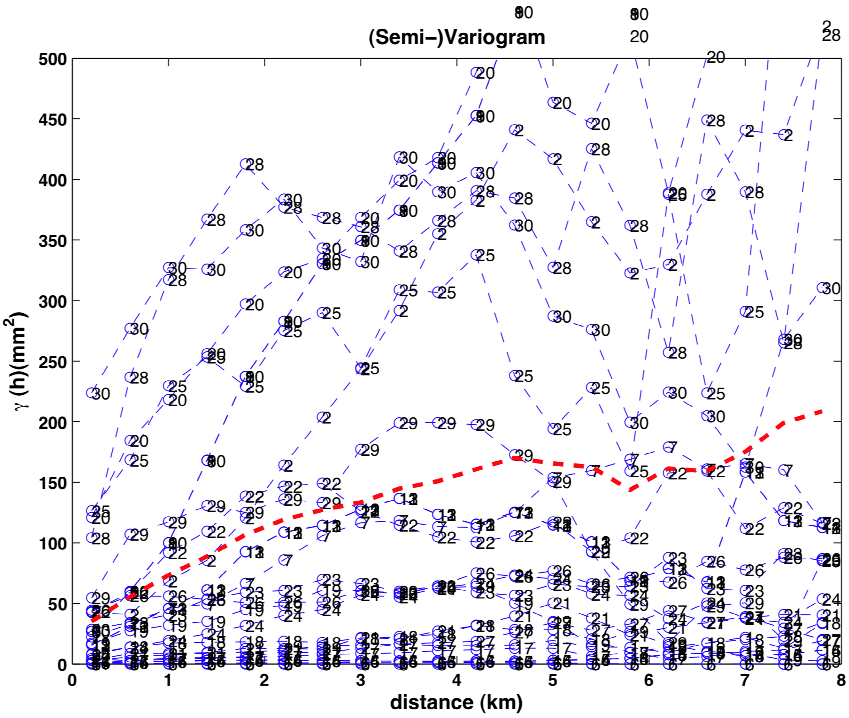

Figure 4-27 Experimental semivariogram using Mesonet rain gauges.

A prior of an inverse gamma function with shape 1 and rate 1 was used for the σ^2.

10000 posterior samples were collected for each daily simulation. The β multivariate normal mean vector hyper prior is (1,1,1). β multivariate normal precision matrix hyperprior is diag(1,1,1). We have applied an exponential covariance model.

The function 'spPredict' in R is used to make predictions at unknown locations. The function collects the posterior predictive samples of the new locations given by the 'bayesGeostatExact'.

Out of the previously used 21 daily data previously used, 9 daily rainy days in 2006 (0110, 0128, 0319, 0320, 0323, 0504, 0508, 0509 and 0617) considered for model calibration and validation. These rain gauges are based selected based on the number of rain gauges available for that particular day. We considered a minimum of 17 gauges are required for calibration.

In the Bayesian model, the posterior of the parameters are collected from the model based on 10,000 samples. In some cases, the number of rainy rain gauges are relatively small, however satisfactory results are still obtained in such cases. This is consistent with previous studies De Oliveira et al. (1997).

Quantitative statistical evaluation criteria (Correlation coefficient, Bias and Nash-Sutcliffe Efficiency) were calculated using reference gauges which were not used for model calibration. Figures 4-30 to 4-33 and Table 4-5 compare the performances of the multi-source method using these performance criteria. Table 4-5 summarize these statistical criteria. In this table, the daily statistical criteria are averaged for the study period. The figures demonstrate the performance of the Merged product, ST-II and HE for each rainy day.

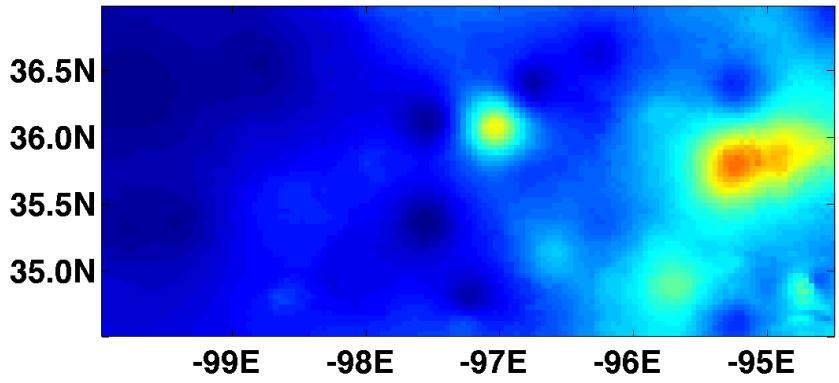

Figure 4-28 A merged product for 20060504.

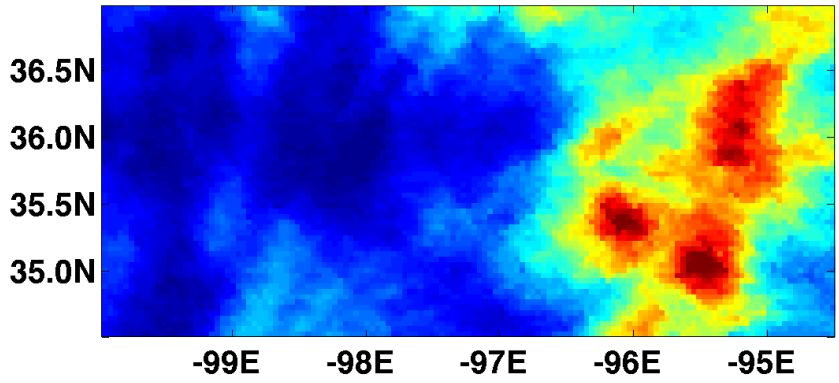

Figure 4-29 Satellite Precipitation product Hydro-Estimator for 20060504

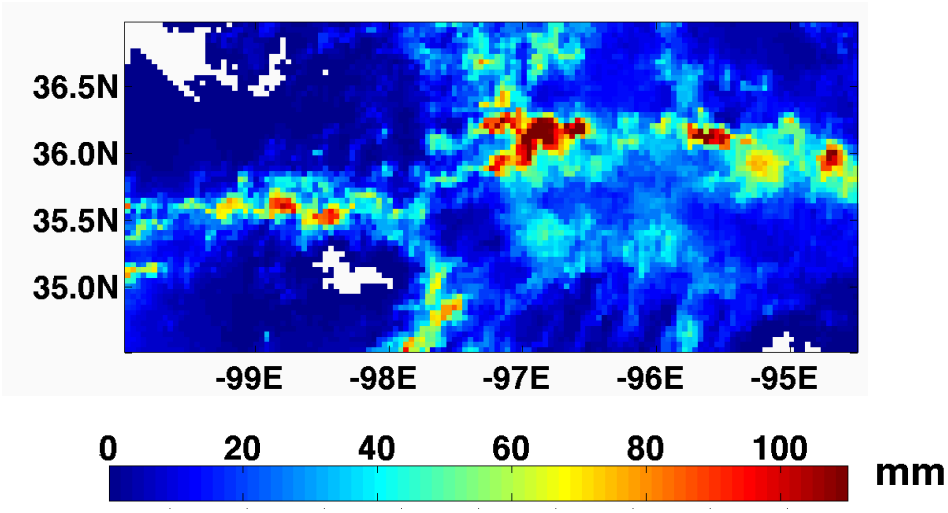

Figure 4-30 Radar product Stage-II for 20060504

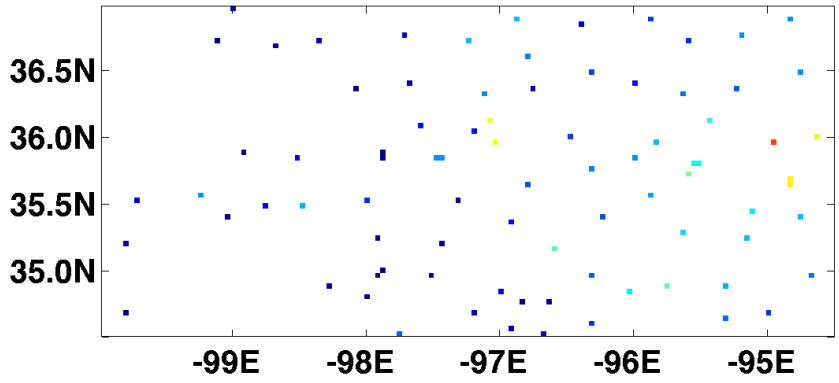

Figure 4-31 Mesonet Rain gauge network and their measurements for 20060504

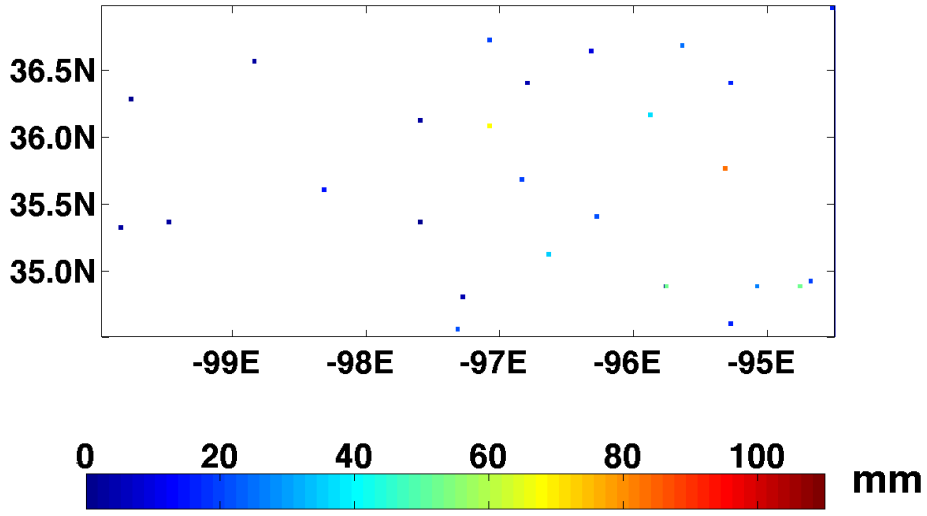

Figure 4-32 COOP rain gauges for 20060504

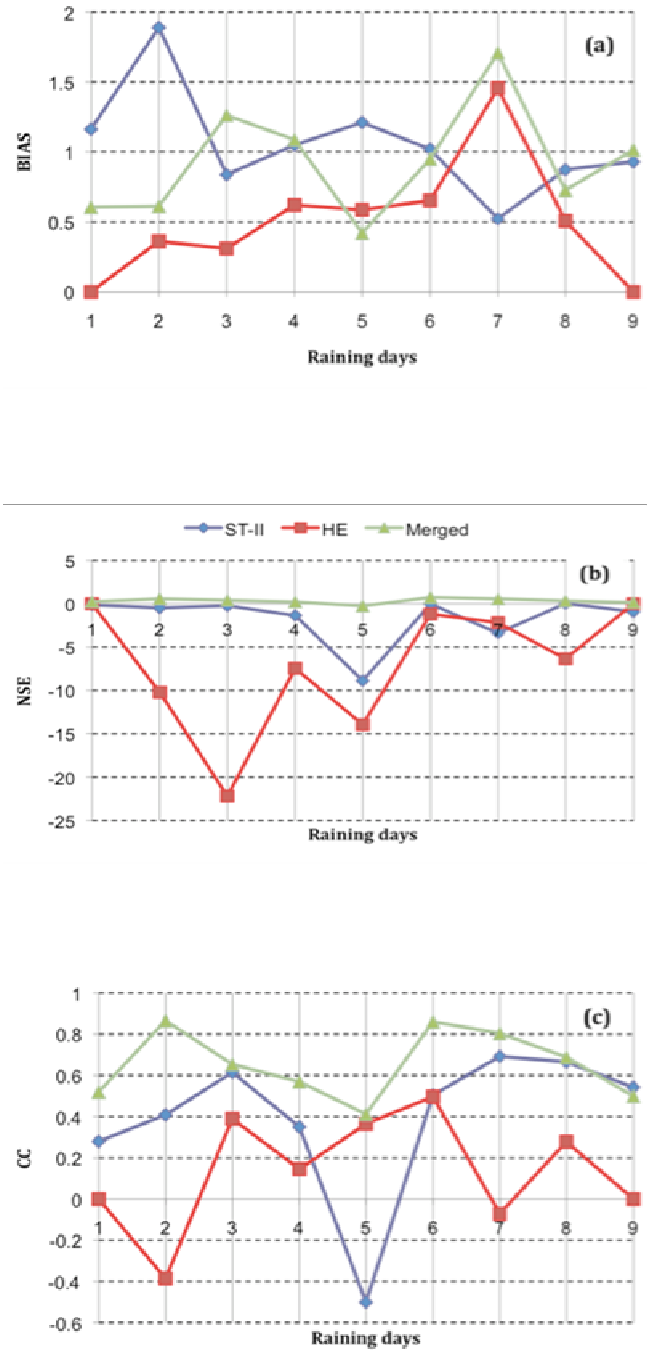

Figure 4-33 A time series of the three statistical criteria (Bias, Nash-Sutcliff Efficiency (NSE) and Correlation Coefficient (CC))

Table 4-5 Summary of statistics of ST-II, HE and Merged product compared with Mesonet gauges. CC(correlation Coefficient), NSE (Nash-Sutcliff Efficiency). Values are mean of the 9 rainy days considered.

Data source	CC	Bias	NSE
ST-II	0.40	1.06	-1.70
HE	0.36	0.64	-9.07
Merged product	0.65	0.94	0.33

4.4.3. Summary of Bayesian-SCM

The multi-source rainfall products produced by combining different existing precipitation estimates have shown better accuracy and correlation than the individual rainfall fields (the radar-only product (ST-II) and Satellite product (HE)) against independent mesonet gauges (Figure 4-31 and Table 4-5). The correlations obtained for these multi-source product ranged from 0.4 to 0.86. In some cases a correlation value of 0.4 was obtained. This occurs because the original inputs, ST-II, HE and PRISM are highly biased at the calibration gauge spots. The NSE and Bias for the model is much better than the individual rainfall products.

5. Application of the methodology in real radar gap cases

Rain gauges have been crucial in estimating precipitation in the western part of the United States. Their availability is most important because radar coverage is limited in these regions. However, sub-daily rain gauge measurements are very sparse in mountainous regions such as the western United States. And hence near real-time rain gauge measurements in those regions have difficulties to capture the true distribution of precipitation. For this reason we are forced to develop our technique on a daily basis. Daily accumulated measurements of precipitation estimates are equally essential for hydrological and climatological studies. Daily precipitation products are important to the development of long term climatological trends which in turn helps to manage water resources.

This chapter describes how the developed techniques are applied to fill real gaps over the radar network using satellite estimates, rain gauges, climatological data PRISM and the surrounding available radar estimates on a daily basis.

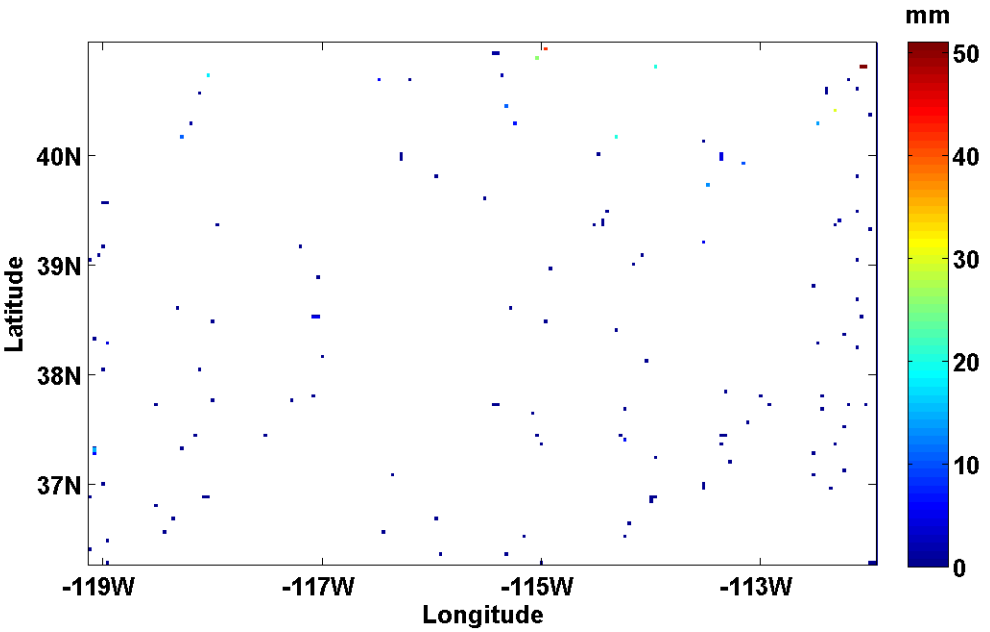

Figure 5-1 Areal distribution of rain gauges for Study Area-II (SA-II) for 20060527 UTC

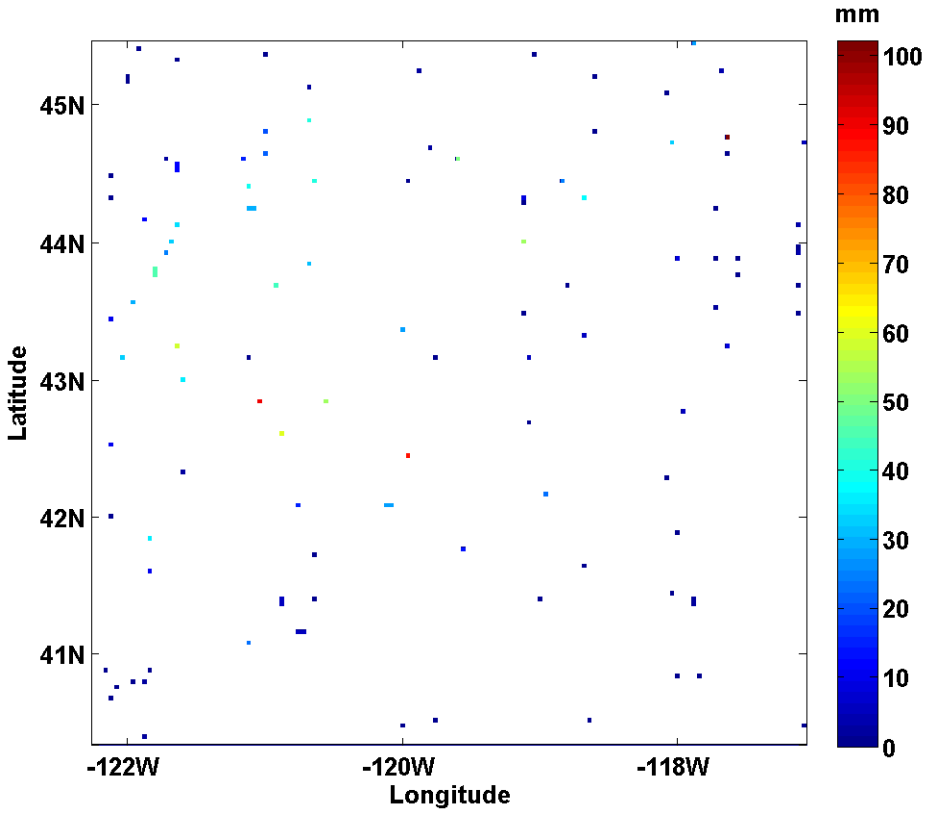

Figure 5-2 Areal distribution of gauges in Study Area-III (SA-III), for 20060629.

The Bayesian-SCM model, explained in Chapter 4 and 5 is used to simulate daily precipitation estimates in real gap areas. In daily precipitation estimation, the Bayesian-SCM model is calibrated using two-third of the available COOP rain gauges (Figure 5-1) in the study area. The remaining one-third of the rain gauge dataset is used for validation. Both validation and calibration gauges are selected randomly throughout the study area, so that the selected gauges represent the 'true' areal precipitation distribution. For spatial match up between point rain gauges and 4 km resolution radars, rain gauges within a 4 km square area are averaged to represent the nearest pixel.

The model is tested for several rainy days from 2006 to 2008 for three different locations where real gaps are available. The method is applied:

- First the satellite estimates are adjusted for spatial error and bias using the surrounding radar-gauge data.
- Next, the bias corrected SPE is merged with the radar PE to fill gaps over the radar rainfall field.
- The radar-satellite merged product is further merged with disaggregated PRISM, HE and rain gauges.

In this Chapter, in section 5-2, the process of covariate preparation for Bayesian model is explained. Section 5-3, describes the model results. In section 5-4, it is also explained how the model performed against independent rain gauge measurements. Section 5-5, summarizes the results of the chapter.

5.1. Study area

Three different study areas are considered for this study (Figure 5-1):

1. Study Area-I (SA-I), covering the area from -111^{o}E to -107^{o}E longitude and 35^{o}N to 38^{o}N latitude. It covers part of the states of Colorado, Utah, New Mexico and Arizona (Figure 5-3 (Green box)).

2. Study Area-II (SA-II), Figure 5-3 (Blue box), an area covering parts of Nevada, Utah, Arizona and California. The area is contained in a rectangular area bounded by -119^{o} to -112^{o} longitude, 36^{o} to 41^{o} latitude.

3. study Area-III (SA-III),

Figure 5-3 (Red box), covering most part of the Oregon State. The area is geographically bounded by -121^{o} to -116^{o} longitude, 40^{o} to 44^{o} latitude.

The study areas were selected because they represent real gaps created by signal blockage and other causes. They also represent different geographic and meteorological conditions. This is useful to test the capability of the proposed model under different conditions.

For model calibration and validation, 20 days of data (Table 5-1) for SA-I was selected. For SA-II 15 days of data were selected. For SA-III 15 days of data were selected. These selected data are heavily based on availability of radar data surrounding the gap. Because, Stage-II products from NCEP are not quality controlled, it offered a challenge to us to find proper rainy cases.

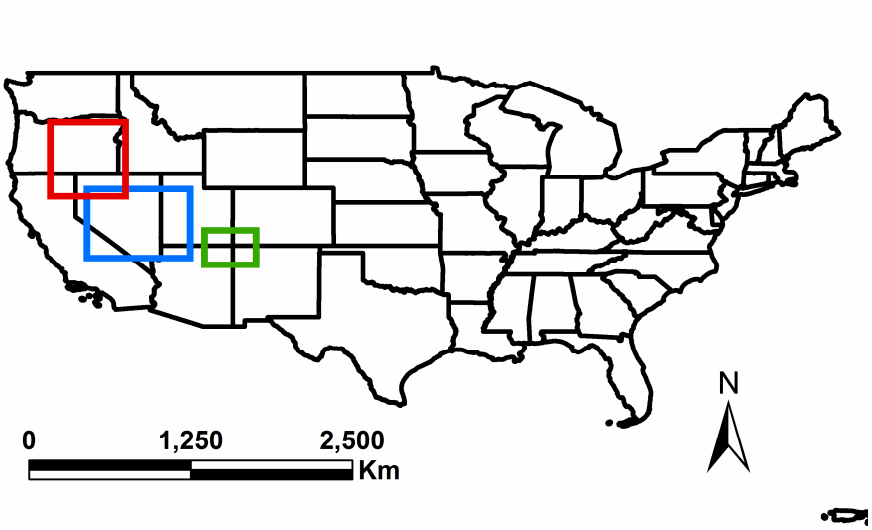

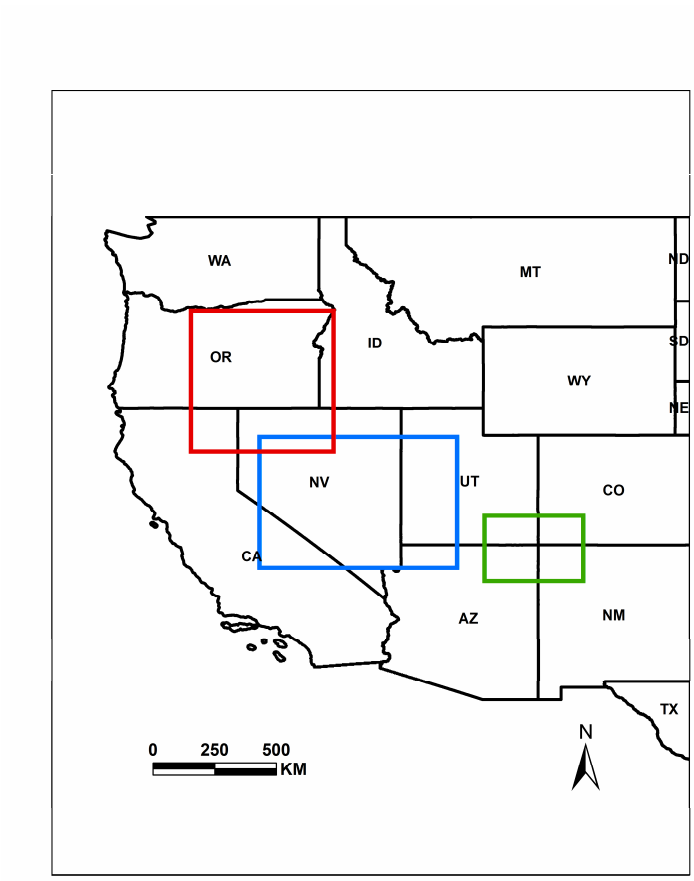

Figure 5-3 The conterminous United States (top); Study Area (bottom). The Green, Blue and Red boxes represent Study Area-I (SA-I), -II (SA-II) and -III (SA-III) respectively.

5.2. Statistical analysis

Three statistical criteria, correlation coefficient, root mean squared error and bias were selected to evaluate the performance of the overall model. For daily simulations, the estimated precipitations at independent gauge locations are compared with the observed gauge values.

5.3. Results and discussion

5.3.1. Study Area-I (SA-I)

Bias correction of HE is carried out against radar ST-II using the method of ensembles (Tesfagiorgis et al., 2011). The method of ensembles is slightly modified to use it in partial radar data. Corresponding rainy radar and satellite pixels are randomly selected as explained in the method of ensembles (Figure 5-4). Using the sampled rainy pixels, precipitation fields of radar and satellite are generated by the method of interpolation (Figure 5-5 and 5-6). Assuming that the method of inverse distance interpolation technique is unbiased, additional rainy pixels are sampled inside of the gap area (Figure 5-7). Now we can follow the normal procedure of the method of ensembles.

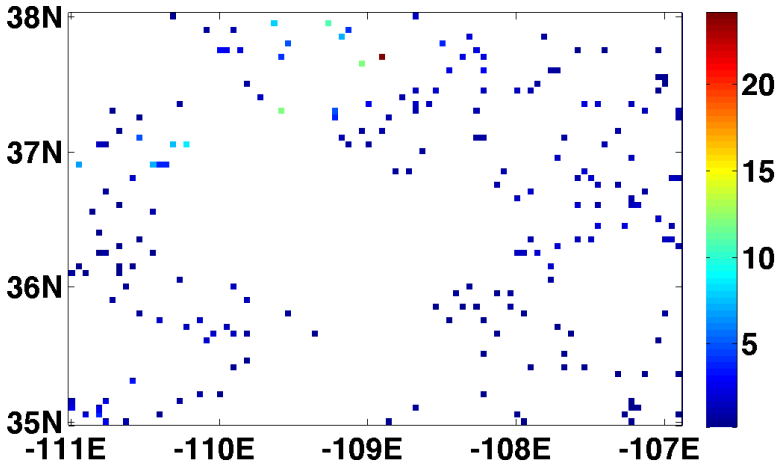

Figure 5-4 Bias ratios between HE and the surrounding ST-IV at randomly selected pixels.

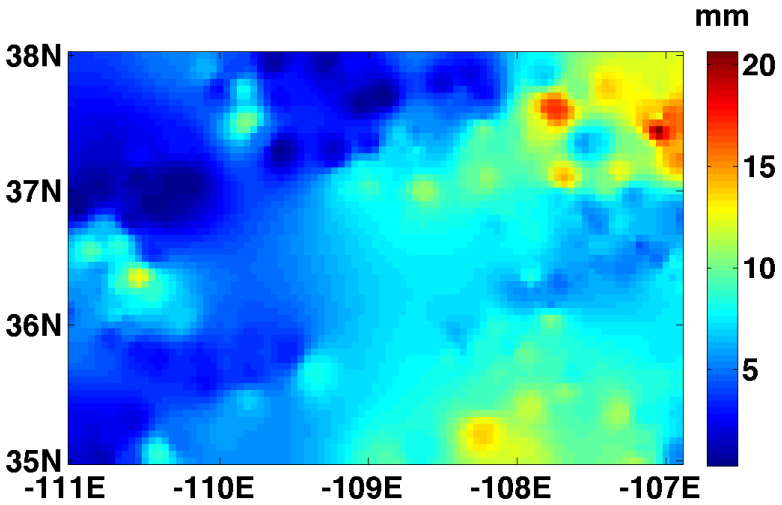

Figure 5-5 Satellite precipitation field generated by interpolation of pixels at the sampled locations.

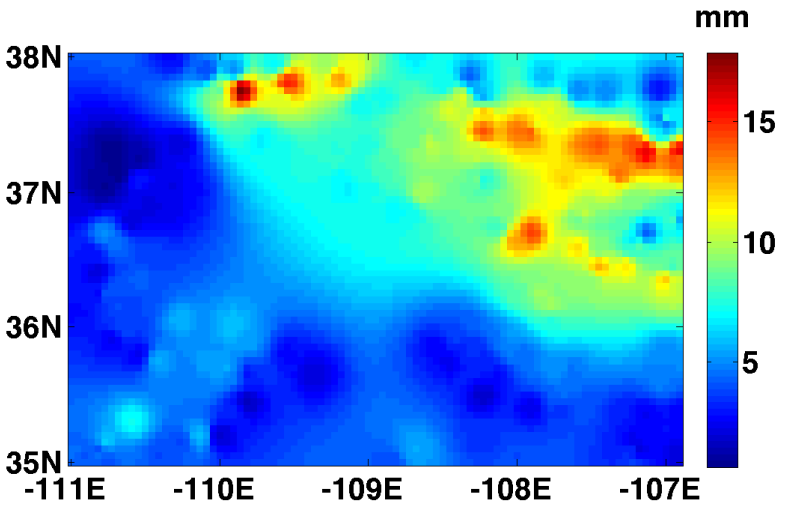

Figure 5-6 Radar precipitation field generated by using interpolation of pixels at the sampled locations.

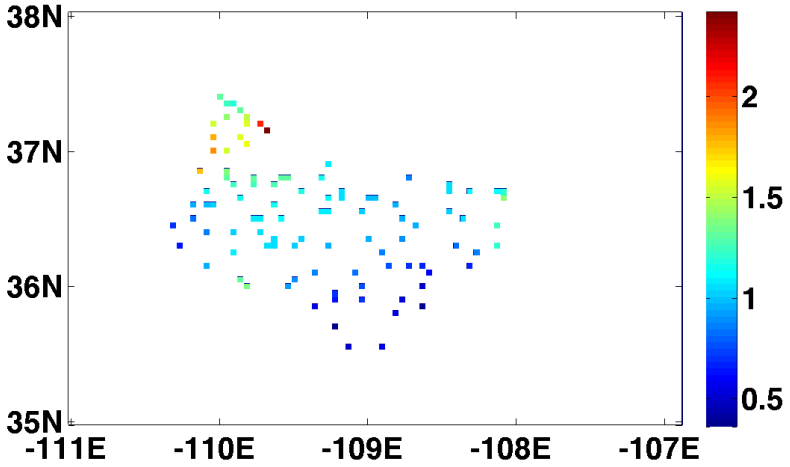

Figure 5-7 Bias factors randomly selected inside the radar gap. This is created by taking the ratio of Figure 5-6 to Figure 5-5.

The bias corrected HE is merged with ST-II to fill missing pixels in ST-II (Figure 5-8). The method of DOE was instrumental to fill gaps in this research. Its statistical development

helped to incorporate spatial variation in the estimated missing pixels. Figure 5-8 (second row left) shows a HE-ST-II merged product for the day 20080204.

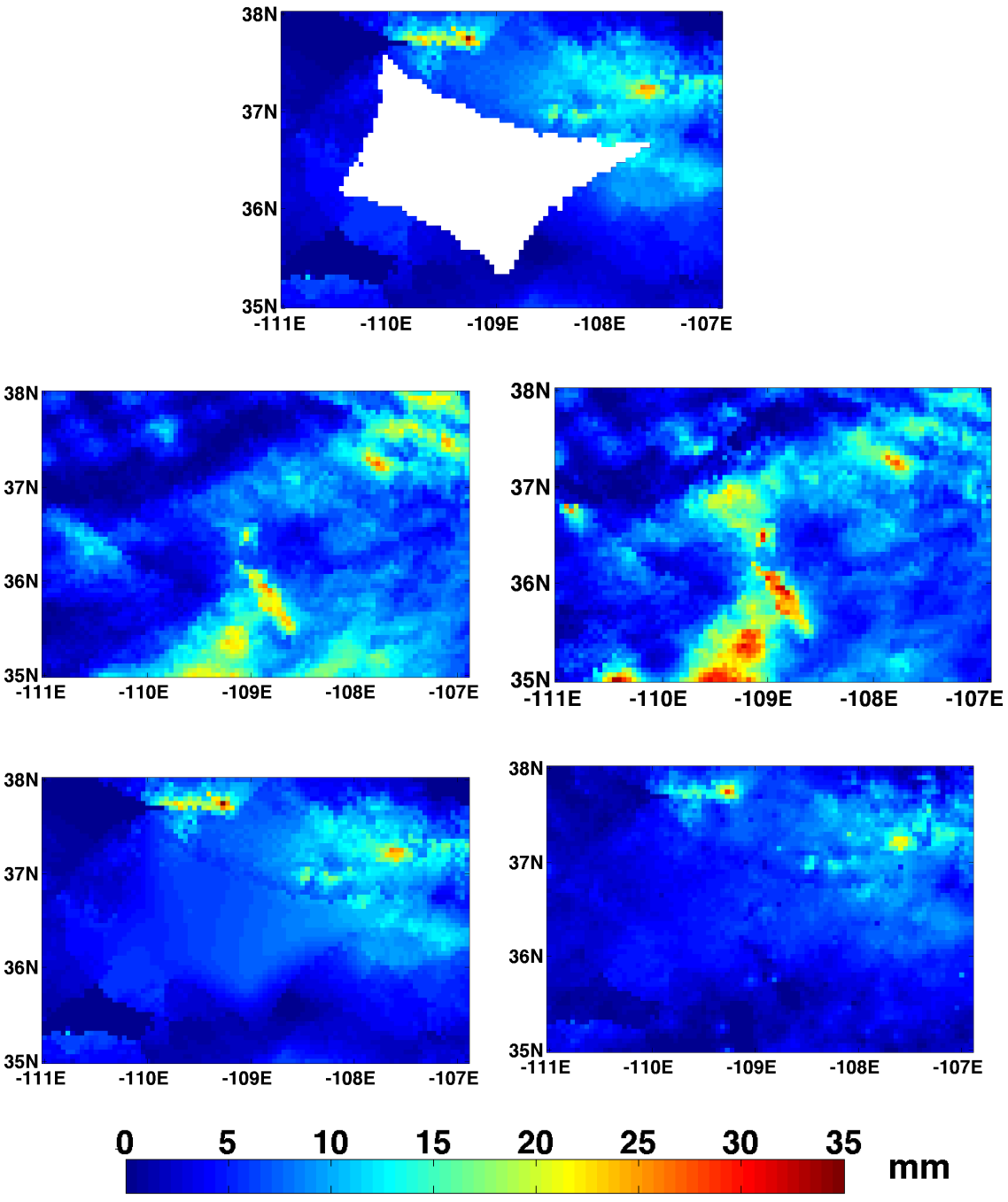

Figure 5-8 Radar Stage II (ST-II) (top), Original Hydro Estimator (HE) (Second row left), Bias Corrected HE (Second row right), HE-ST-II merged (bottom left), Merged (Rain gauges, HE, HE-ST-II and PRISM) (bottom right) for 20080204.

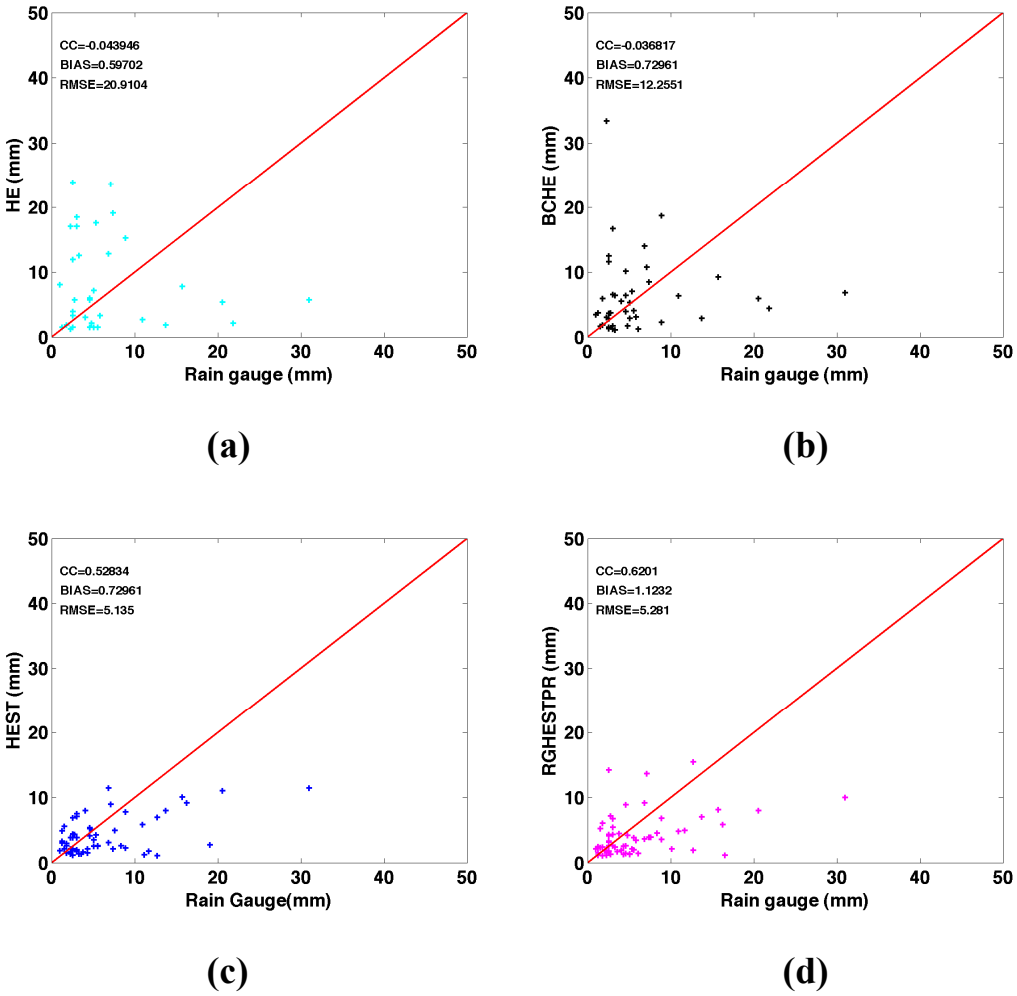

Figure 5-9 Comparison of the different precipitation outputs for Study Area-I. (a) HE against Rain gauges, (b) Bias corrected HE (HEBC), (c) Radar-Satellite merged preofuct (HEST), and (d) Gauge-Radar-Satellite-PRISM (RGHESTPR).

Figures 5-9 (a to d) show the validation results for all rainy days selected to SA-I. Validation was carried out using independent rain gauges. Because of the limited number of gauges in gap regions, we chose to use all the validation gauges in a single scatter plot (Figure 5-9). Figure 5-9 (a) shows the scatter plot between the original HE and independent rain gauges.

The scatter plot in Figure 5-9 (b) shows that bias corrected HE is a better estimate than HE. Figure 5-9 (c) shows the scatter plot between the HE-ST-II merged product and the independent rain gauges selected for validation. From this scatter plot, it is observed that the HE-ST-II is better than bias corrected HE. This shows that radar-satellite estimates can be used to fill gaps instead of satellite only products. In Figure 5-9 (d), it is depicted that the gauge-radar-satellite-PRISM product versus independent rain gauges. This figure shows that by incorporating gauges and PRISM, a much better matching result was obtained.

Rain gauges are very sparse, mostly unavailable in those radar gap regions for individual validation work. For this reason radar-gauge product ST-IV (ST-IV), an independent measurement is used to validate daily products. Figures 5-10 to 5-11 show randomly selected rainy cases that used ST-IV as validation. Those sample results show (from scatter plot), the model output shows a better result than HE and bias corrected HE. In Figure 5-10, the correlation coefficients improved from 0.08 for HE and 0.706 for HE-ST-II to 0.77 for model output. Similarly, Bias and RMSE are improved from 0.77 to 1.00 and 4.16 to 1.30 respectively. Some results do not show that much improvement. This problem can arise from the lack of good quality precipitation data. For instance for event shown in Figure 5-9, radar and HE precipitation show low values of precipitation. Many lower HE and ST-II pixel estimates can skew the parameters to lower values, resulting in lower estimates of precipitation. The characteristics of radar and gauge measurements are different. For instance radar measures precipitation in a wider area when it is compared to point rain gauges. Moreover, radar measurements are updated every several minutes (~5 minutes) where as gauges measure precipitation continuously. This may have some unwarranted validation results on our study.

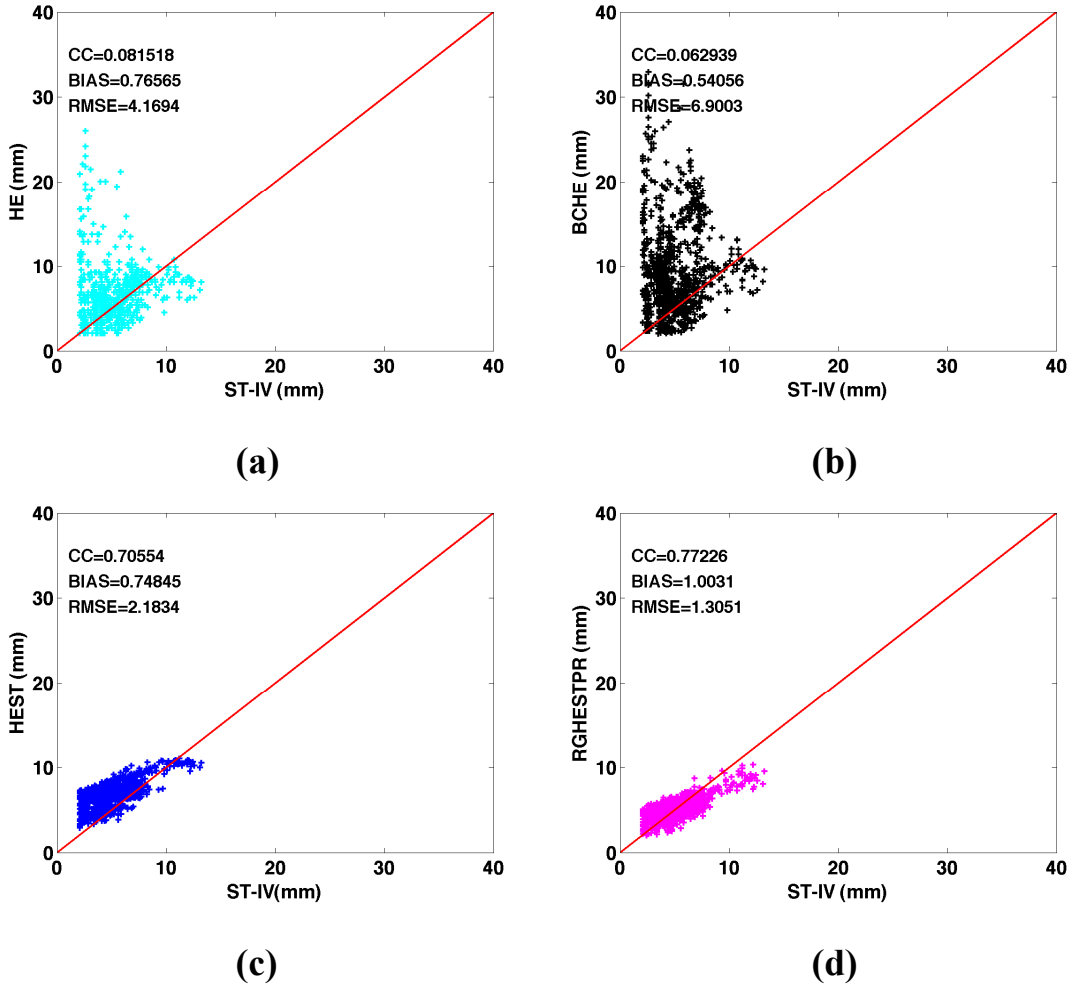

Figure 5-10 Comparison of the different precipitation outputs for Study Area-I. (a) HE against Radar ST-IV (ST-IV), (b) Bias corrected HE (HEBC) against ST-IV, (c) Radar-Satellite merged product (HEST) against ST-IV, and (d) Gauge-Radar-Satellite-PRISM (RGHESTPR) against ST-IV. This plot is for day 20080204.

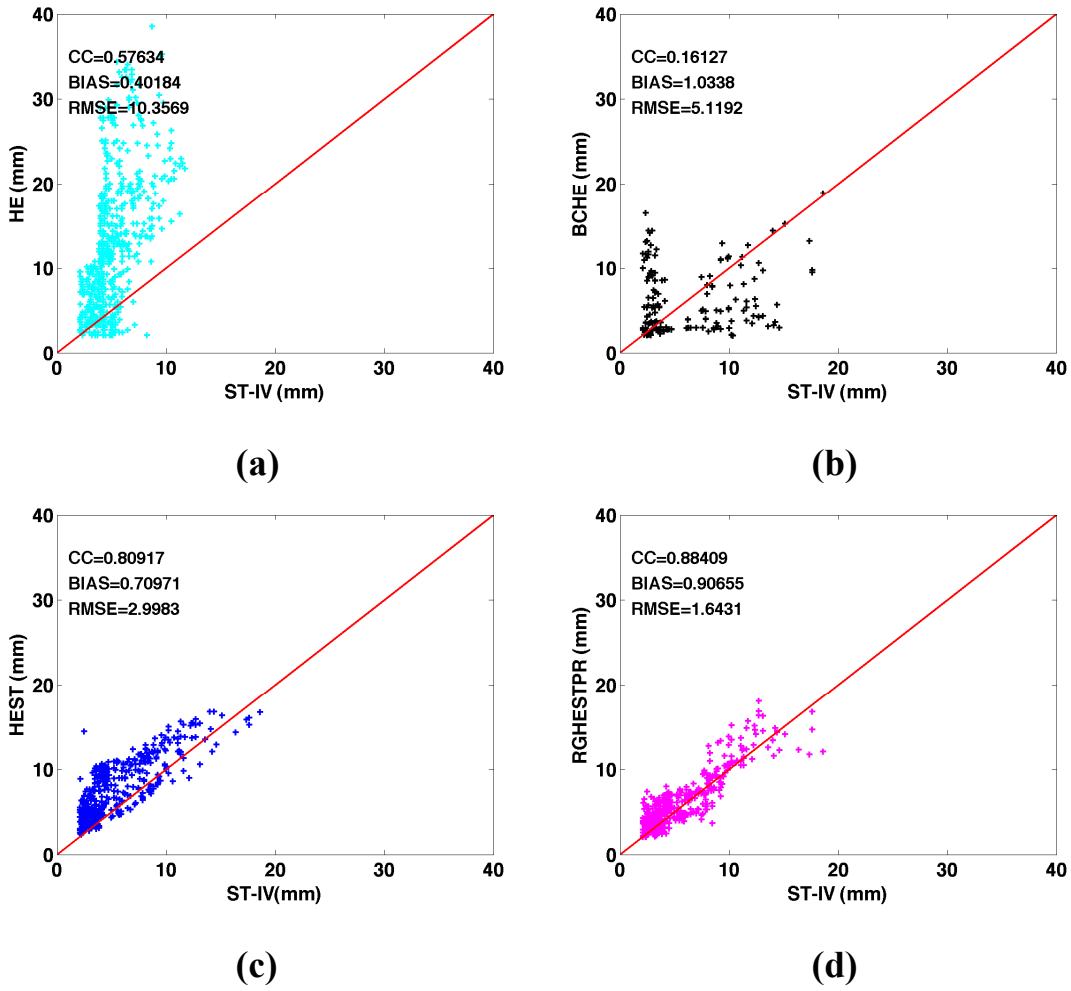

Figure 5-11 Comparison of the different precipitation outputs for Study Area-I. (a) HE against Radar ST-IV (ST-IV), (b) Bias corrected HE (HEBC) against ST-IV, (c) Radar-Satellite merged product (HEST) against ST-IV, and (d) Gauge-Radar-Satellite-PRISM (RGHESTPR) against ST-IV. This plot is for day 20080726.

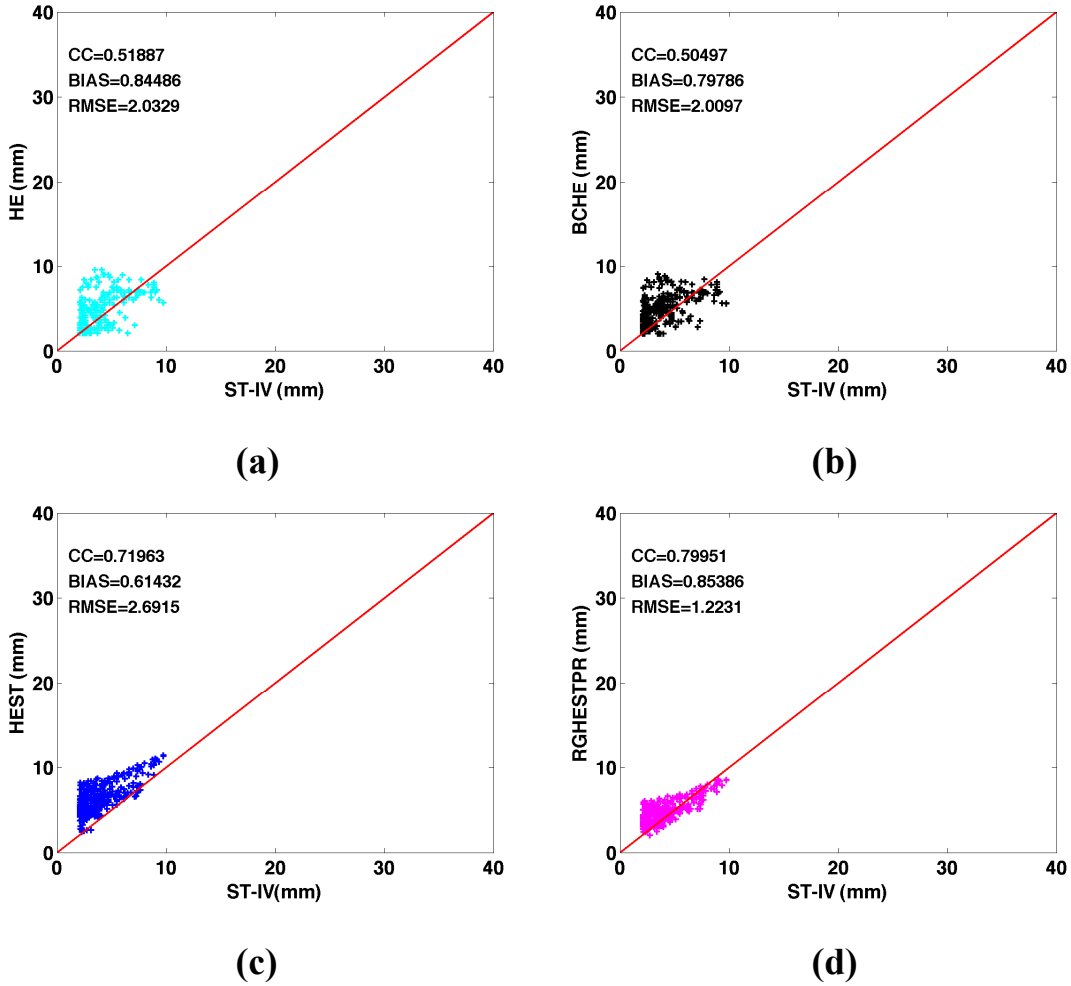

Figure 5-12 Comparison of the different precipitation outputs for Study Area-I. (a) HE against Radar ST-IV (ST-IV), (b) Bias corrected HE (HEBC) against ST-IV, (c) Radar-Satellite merged product (HEST) against ST-IV, and (d) Gauge-Radar-Satellite-PRISM (RGHESTPR) against ST-IV. This plot is for day 20080409.

Tables 5-1, 5-2 and 5-3 detail statistical outputs for each rainy day considered for SA-I. In those cases, it is indicated that the model outputs are working well in terms of providing precipitation in gap area I.

Table 5-1 Correlation coefficient of the different precipitation estimates against ST-IV

Rainy Days	MRGD	BCHE	HE	ST-HE
20080203	0.694	0.479	0.435	0.614
20080204	0.772	0.063	0.082	0.706
20080214	0.435	0.215	-0.214	0.417
20080221	0.523	0.319	0.576	0.528
20080302	0.426	0.972	1.000	NaN
20080409	0.800	0.505	0.519	0.720
20080410	0.528	0.177	-0.397	0.216
20080703	0.591	NaN	NaN	0.212
20080712	0.787	NaN	NaN	0.727
20080713	0.588	NaN	NaN	0.717
20080714	0.391	0.644	NaN	0.358
20080715	0.374	0.463	0.277	0.387
20080721	0.258	0.488	-1.000	0.525
20080722	0.428	0.607	0.589	0.439
20080723	0.515	0.082	0.134	0.498
20080724	0.412	0.441	NaN	0.035
20080725	0.102	0.609	-0.046	0.197
20080726	0.884	0.161	-0.541	0.809
20080727	0.327	0.222	NaN	0.285
Mean	0.518	0.403	0.109	0.466

Table 5-2 RMSE of the different precipitation estimates for SA-I

Rainy Days	MRGD	BCHE	HE	ST-HE
20080203	1.872	3.460	12.000	1.743
20080204	1.305	6.900	4.169	2.183
20080214	5.392	0.690	0.883	1.339
20080221	2.368	7.856	10.357	3.334
20080302	2.323	0.122	0.000	2.414
20080409	1.223	2.010	2.033	2.692
20080410	2.475	4.401	2.006	1.261
20080703	1.367	NaN	NaN	0.823
20080712	1.196	NaN	NaN	0.050
20080713	1.240	NaN	NaN	1.556
20080714	1.400	1.603	NaN	2.475
20080715	3.535	3.139	3.004	1.683
20080721	1.467	3.862	2.755	0.858
20080722	2.702	31.767	16.206	2.900
20080723	1.934	55.835	38.891	0.829
20080724	1.206	7.155	NaN	9.656
20080725	7.522	10.046	4.578	3.166
20080726	1.643	5.119	7.162	2.998
20080727	1.960	NaN	NaN	2.919
Mean	2.323	9.598	8.003	2.362

Table 5-3 Bias of the different precipitation estimates against ST-IV

Rainy Days	MRGD	BCHE	HE	ST-HE
20080203	0.609	0.510	0.217	0.658
20080204	1.003	0.541	0.766	0.748
20080214	0.342	1.015	1.026	0.692
20080221	1.332	0.489	0.402	0.633
20080302	0.581	0.953	1.000	NaN
20080409	0.854	0.798	0.845	0.614
20080410	0.441	0.563	1.019	0.978
20080703	1.385	NaN	NaN	0.849
20080712	0.672	NaN	NaN	0.997
20080713	2.571	NaN	NaN	0.814
20080714	2.224	1.272	NaN	0.691
20080715	0.875	0.642	0.662	0.754
20080721	1.538	0.618	0.934	1.132
20080722	2.838	0.212	0.338	0.665
20080723	0.710	0.074	0.098	0.933
20080724	1.131	1.719	NaN	0.755
20080725	0.619	0.397	1.884	1.069
20080726	0.907	1.034	1.173	0.710
20080727	0.677	NaN	NaN	0.572
Mean	1.121	0.722	0.797	0.792

In some case, poor detection of precipitation by radar can lead poor simulation of results. For instance for day 20080725, the original HE produced a correlation of -0.045. After bias corrected estimation of HE improved the correlation to 0.61. However, the HE-ST-II simulation produced a correlation of 0.196. Further incorporation of gauge and PRISM didn't help much. This implies that quality control of some of the products is highly recommended.

5.3.2. Study Area-II (SA-II) and Study Area-III (SA-III)

Unlike SA-I, SA-II and SA-III could not be validated using ST-IV. The main reason is ST-IV data in this region contain HE. Instead, we used all the available rain gauge measurements to validate the merged product (Figure 5-14). As shown in Figure 5-14 (SA-II), it is observed that the incorporation of rain gauge further degraded the correlations. However, we observed improvement in bias and RMSE. This is because of the large difference between gauge and HE measurements over the study area. For instance, as shown in Figure 5-15, HE and ST-IV (which is the same as HE for this case) measured significant amount of precipitation, whereas the rain gauge measured not so much precipitation. This study area (SA-II) has many similar cases, which made the general analysis more difficult.

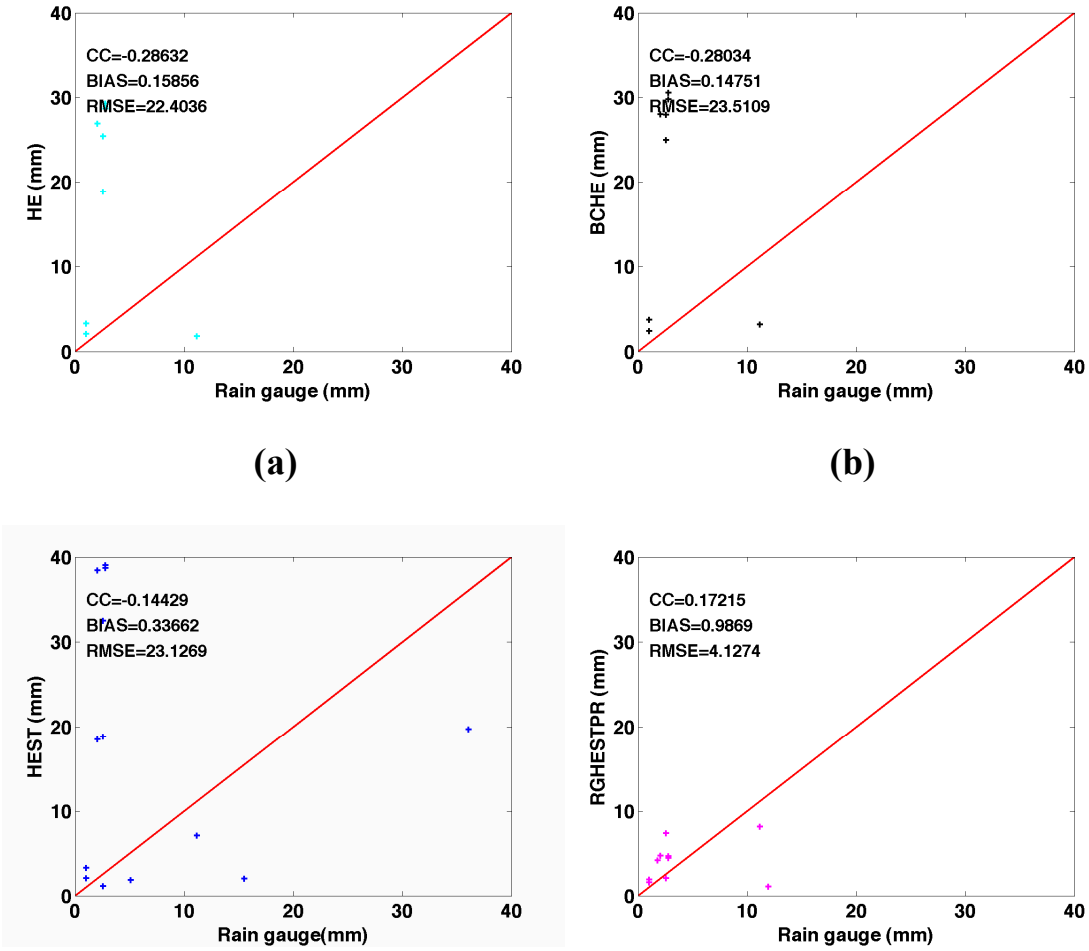

Figure 5-13 Comparison of the different precipitation outputs for Study Area-II. (a) HE against Rain gauges, (b) Bias corrected HE (HEBC), (c) Radar-Satellite merged product (HEST), and (d) Gauge-Radar-Satellite-PRISM (RGHESTPR).

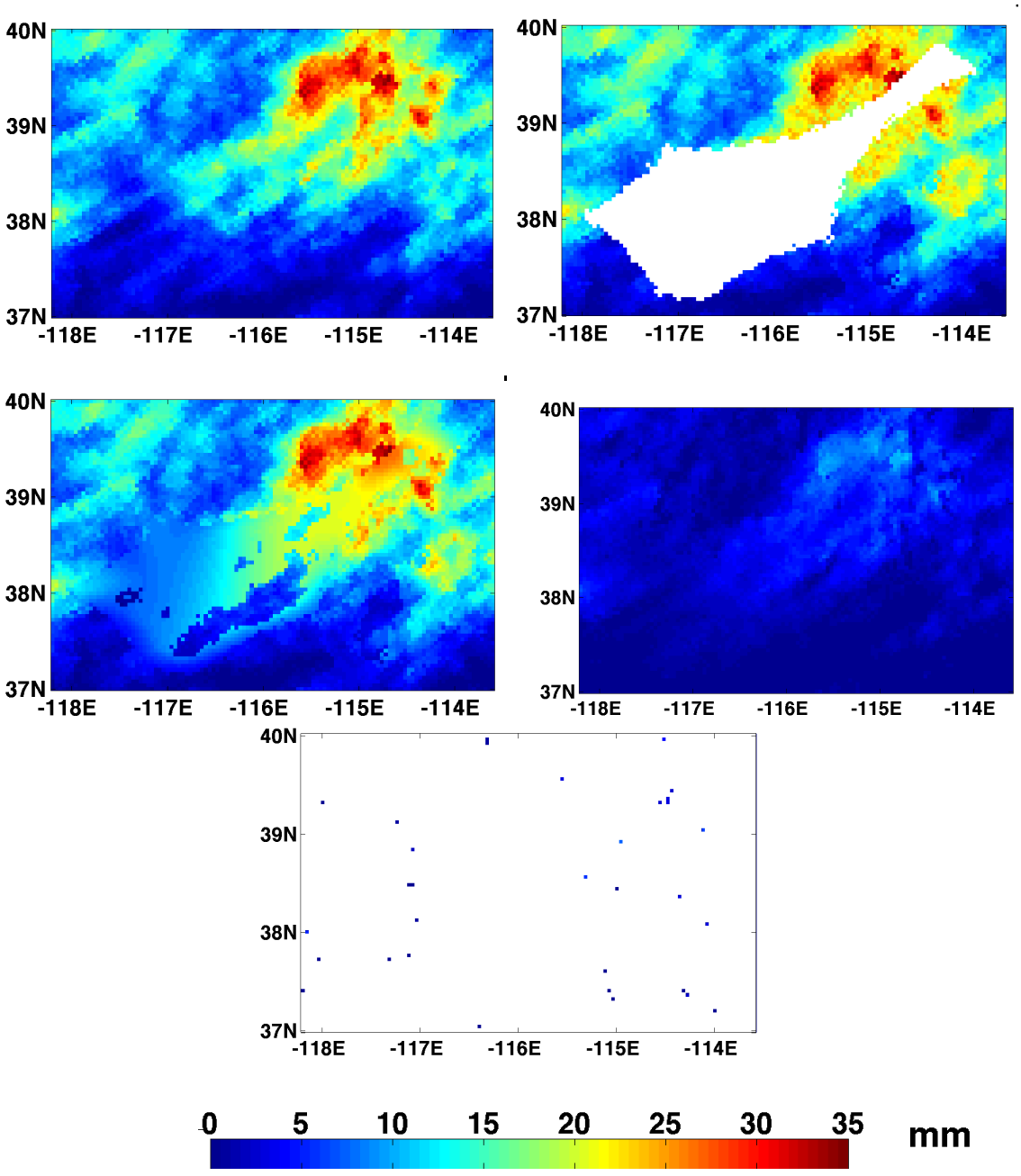

Figure 5-14 Spatial comparison of the distribution of precipitation from different products. Original HE (top left); ST-II (top right); HE-ST-II merged product (middle left); Gauge-HE-ST-II-PRISM merged product (middle right); and Rain gauges (bottom). This plot is for the day 20080330.

Figure 5-16, depicts the comparison between rain gauge measurements and the different remotely sensed precipitation out puts over SA-III. As shown in the figure, the model out put showed a better agreement with independent rain gauges than the rest of the models. Indicating

that, with better rain gauge measurements, it is possible to provide a precipitation estimate better than the satellite estimates.

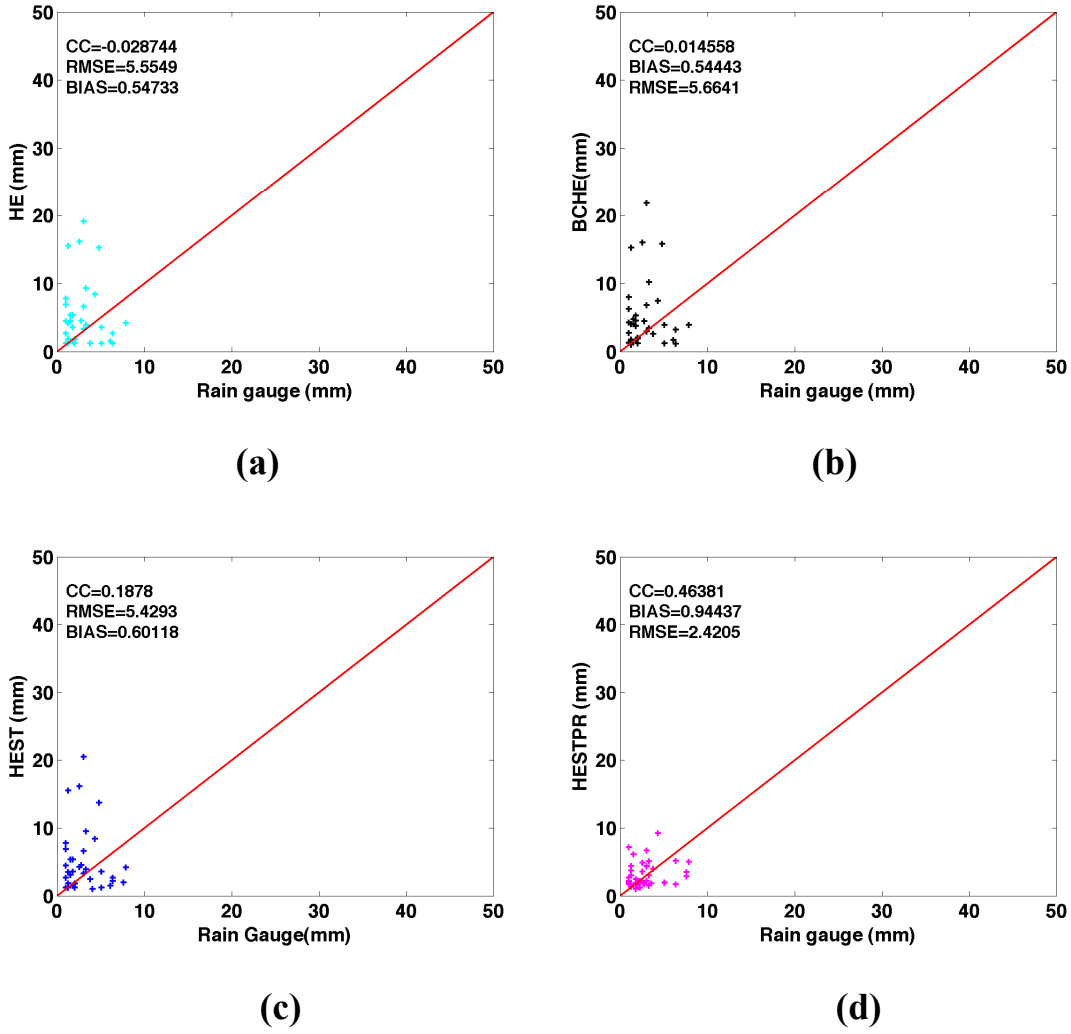

Figure 5-15 Spatial comparison between HE (ST-IV) and rain gauge for Study Area-III (SA-III) 20080330.

6. Summary and Conclusions

The goal of this study was to develop an approach to fill gaps over the radar precipitation field. The study was originally carried out by creating artificial radar gaps over the state of Oklahoma because radars and gauges are not available in real gap areas to validate our work. Once the study is carried out in Oklahoma, the proposed technique is tested over real gap areas. Three different real gaps in the western United States were selected. The first real gap area is located between -111^{o}E to -107^{o}E and 34^{o}N-37^{o}N. The second gap is located -119^{o} to -112^{o} longitude, 36^{o} to 41^{o} latitude and third gap is -121^{o} to -116^{o} longitude, 40^{o} to 44^{o} latitude. Several daily and hourly products were produced, and it is demonstrated that the proposed procedure is capable of producing precipitation estimates better than satellite estimates in radar gaps.

In order to fill the real gap areas, we used different precipitation products. 1. An InfraRed (IR) based satellite precipitation product Hydro Estimator (HE); 2. Radar-gauge products Stage-II and ST-IV; 3. Cooperatives Observers Program (COOP) gauge measurements; and 4. PRISM monthly climatological data were used to fill the gaps. To test the performance of the bias correction method, an additional Microwave based data (CMORPH) was used.

In this research, a step-wise multi-source precipitation estimation was used to fill gaps over the radar precipitation field. From the beginning of this project towards the end, our overall procedure is summarized as:

1. Detection and correction of spatial errors in satellite rainfall estimations. A

linear image registration technique was used to adjust the spatial mis-match between the satellite and the radar based precipitation field.

2. Bias estimation and correction in satellite precipitation estimates. A new ensemble based bias correction algorithm was developed to adjust the bias in the satellite estimate against the radar-gauge estimate.

3. Merging corrected satellite precipitation estimate with radar based precipitation estimate for radar gap regions. An objective based Successive Correction Method (SCM) with different schemes was used to fill gaps using the satellite precipitation estimate. Three different schemes: Inverse distance, Brandes and Single Optimal Estimation (DOE) were tested to fill the gaps.

4. Merging the satellite-radar merged product with rain gauges and PRISM. The satellite-radar, PRISM and satellite were used as covariates in a linear Bayesian spatial model.

5. The final merged product was validated using independent rain gauge and radar-gauge products.

Here we presented the technique to estimate the spatial error statistics of satellite rainfall data HE by validating it with ST-IV rainfall data. To estimate the spatial error, we used the field alignment algorithm to align the satellite-based rainfall measurements with ST-IV data. The spatial correction helped to reduce the False Alarm Ratio of satellite precipitation estimates.

In this study, a bias correction approach with spatially varying bias factors pre-smoothed using an ensemble was proposed and compared to the mean field and maximum ratio approaches as well as to interpolation without pre-smoothing. For improved spatial coverage and sampling, instead of rain gauge measurements a radar-gauge mosaicked rainfall product (ST-IV) was used to correct SPEs.

The sensitivity of spatial parameters was checked by varying each parameter around its optimal value while keeping the others constant. Results showed that all three parameters seem to have significant impacts on the bias correction quality. As one of the efficiencies of the method, it was shown that daily update of parameters was sufficient to adjust biases in hourly satellite products. Once the parameters were obtained, ensembles of bias factors were imposed to represent random errors in bias factors.

The performance of the proposed bias correction method was evaluated using root mean squared error, absolute bias, and correlation coefficient between the ST-IV and the corrected SPEs. Compared to the other methods tested, the proposed method of ensembles showed more improvement in bias ratio, correlation coefficient and RMSE. The method produced a correlation coefficient of 0.9 in one case while the other techniques did not show as much improvement over the original satellite product.

By adjusting biases in satellite products, radar-like satellite rainfall products can be produced. This is highly desirable in many operational settings where radar and satellite products being merged can differ sharply in terms of bias even though both undergo gauge-based bias adjustments before merging. It has also a considerable advantage in producing radar-like

products in radar gap areas and during radar outages. During radar outages, the approach can provide radar-like products using bias factors determined from radar data from the previous hour and satellite products from the present hour. This method can complement the existing operational bias corrections which are rain gauge based.

Two Successive Correction Method (SCM) schemes (Brandes and Single Optimal Estimation (SOE)) in combination with a bias correction technique was introduced for merging a satellite and a radar-gauge rainfall product to fill gaps in the radar-gauge rainfall field. Radars are good sources of precipitation data, but have gaps in mountainous regions. On the other hand, satellites produce a continuous precipitation field in such regions. The methodology introduced in this work uses radar precipitation pixels surrounding the gap and satellite information in and around the gap to fill missing pixels in the radar rainfall field. Primarily, the results of the SCM show that the method of ensembles for bias correction in conjunction with bias correction can be used to fill gap areas over the radar networks. Results of using the merged precipitation product showed that this method produce a more agreeable rainfall comparing with the original radar-gauge rainfall product than the SPE. In using SOE in the SCM, there is no guarantee that the covariance matrices will not be singular. It is not necessarily because the method has drawbacks. However, it looks like the problem stems from the fact that we are using 9 x 9 pixels centered at the point of estimation. If we have all 5 data points available and if the 4 noncollocating data points are exactly symmetric, that will lead to singularity. This has nothing to do with the particular formulation of SOE or Double Optimal Estimation (DOE), but with the fact that the resulting linear system is collinear. One remedy is to add small random perturbations to the locations or drop one of the surrounding 4 to make the geometry asymmetric.

Finally, the daily precipitation estimates were simulated using the Bayesian-SCM model to incorporate gauges and PRISM for real gap area. The simulated results are validated using independent rain gauge measurements. For Study Area-I (SA-I), in addition to independent gauge measurements, we used radar-gauge ST-IV as validation data. In this particular study, ST-IV is based mainly on the mountain mapper (personal communication with Robert Kuligowski). For Study Area-II (ST-II) and Study Area-III (SA-III) mountain mapper is not available. And hence we could not use mountain mapper as a validation data for SA-II and SA-III. Because the mountain mapper is generated using rain gauges and PRISM, it was not possible to independently validate the mountain mapper or our merged product directly with rain gauge measurements. In stead, we compared our merged product against the mountain mapper and they appear to be reasonably similar.

The results show that the Gauge-HE-ST-II-PRISM model is much more accurate than the satellite HE and its bias corrected version. Even if in some case the number of rain gauges is few, the method was more effective to produce precipitation estimates over radar gaps. These results indicate that daily precipitation estimates can be produced by combining different existing precipitation estimates and measurements. In the near future, the stand alone precipitation estimation may switch to a more advanced multi-source paradigm to produce more accurate estimates over radar gaps.

Based on the statistics of the analyzed daily and hourly products it is demonstrated that the step-wise procedure proposed in this work has produced results that could be used to fill gaps

over the radar precipitation field. The spatial adjustment has improved the False Alarm Ratio in the satellite precipitation estimate. The bias adjustment has significantly improved the magnitude differences between the satellite and the radar products. By incorporated rain gauges and PRISM climatological data, the model was further improved. This result indicates that the proposed model has the potential to be used over gaps in the radar precipitation field where direct measurements such as radar and gauge are unavailable.

Future Work:

a. Satellite precipitation estimates perform variably depending on season. The model may further be improved by using different satellite precipitation estimates in different season of the year.

b. Improve the developed SCM-Bayesian based on merging algorithm incorporating ensembles and additional parameters such as topography.

c. Convert the final work to an operational algorithm at NOAA-CREST centers.

d. Correlate spatial errors with caused sources such as related meteorological parameters (e.g. wind, parallax and geography).

e. Incorporate a time parameter in the model using Auto-regressive models.

Appendix

Satellite Rainfall Estimations	**Radar Rainfall Estimation**	
	Yes	**No**
Yes	Hits	False Alarms
No	Misses	Correct negatives
	Observed yes	**Observed no**

$$\textit{Bias}\ \text{Score} = \frac{\text{Hits} + \text{False Alarms}}{\textit{Hits} + \textit{Misses}}$$

$$\text{False Alarm Ratio} = \frac{\text{False Alarms}}{\text{Hits} + \text{False Alarms}}$$

$$\text{Probability of Detection (POD)} = \frac{\text{False Alarms}}{\text{Hits} + \text{Misses}}$$

7. Scientific contributions

1. Tesfagiorgis, K., Mahani, S. E., Krakauer, N. Y., and Khanbilvardi, R.: Bias correction of satellite precipitation estimates using a radar-gauge product – a case study in Oklahoma (USA), Hydrol. Earth Syst. Sci., 15, 2631-2647, doi:10.5194/hess-15-2631-2011, 2011.

2. Tesfagiorgis, K., Mahani, S. E., and Khanbilvardi, R: Multi-source Precipitation Estimation: Mitigating gaps over the radar network. 2011 IEEE-International Geoscience and Remote Sensing Symposium, Vancover, Canada, July 24-29, 2011. (Proceeding)

3. Tesfagiorgis, K., Mahani, S. E., and Khanbilvardi, R: Testing capability of successive correction method and Bayesian spatial model to fill gaps over the radar network. 2011 AMS-35th conference on Radar Meteorology, Pittsburgh, PA, Sept 26-30, 2011. (Proceeding)

4. Tesfagiorgis, K., Mahani, S. E., and Khanbilvardi, R: Testing multi-source precipitation estimates to fill gaps over the radar network. American Geophysical Union, Fall Meeting 2010, San Fransisco, CA., December 5-9, 2011. (Oral)

5. Tesfagiorgis, K., Mahani, S. E., and Khanbilvardi, R: Bias correction of satellite rainfall estimation using a radar adjusted product. American Geophysical Union, Fall Meeting 2010, abstract #H23B-1190, San Fransisco, CA., December 13-17, 2010. (Poster)

7. Tesfagiorgis, K., Mahani, S. E., and Khanbilvardi, R.: Multi-source Precipitation Estimation. NOAA-NESDIS Cooperative Research Program (CoRP) 7th Annual Symposium, Fort Collins, CO., August 10-11, 2010. (Oral)

8. Tesfagiorgis, K., Mahani, S. E., and Khanbilvardi, R: Multi-source Precipitation Estimation. NOAA Educational Partnership Program, the Fifth Education & Science Forum, Howard University, Washington D. C., November 12-14, 2009. (Oral)

9. Tesfagiorgis, K., Mahani, S. E., and Khanbilvardi, R.: Multi-source Precipitation Estimation. NOAA CREST board meeting, CUNY, New York, May, 2009. (Oral)

10. Mahani, S. E., Tesfagiorgis, K., and Khanbilvardi, R: Multi-Sources Precipitation Estimates, American Geophysical Union, Fall Meeting 2008, San Fransisco, CA., December 13-17, 2010.

8. References

Ahnert, P., Krajewski, W. F., and Johnson, E.: Kalman filter estimation of radar-rainfall field bias, 23rd Conference on Radar Meteorology, Snowmass, CO, 1986.

Anagnostou, E. N., Morales, C. A., and Dinku, T.: The use of TRMM precipitation radar observations in determining ground radar calibration biases, Journal of Atmospheric and Oceanic Technology, 18, 616-628, 2001.

Anagnostou, P., Krajewski, W. F., Seo, D. J., and Johnson, E. R.: Mean-field rainfall bias studies for wsr-88d, J. Hydrol. Eng. , 3, 149-159, 1998.

Ba, M. B., and Gruber, A.: Goes Multispectral Rainfall Algorithm (GMSRA), J. Appl. Meteor., 40, 1500-1514, 2001.

Barnes, S. L.: A technique for maximizing details in numerical weather map analysis, J. Appl. Meteor, 3, 396-409, 1964.

Binaghi, E., Brivio, P. A., Rampini, A., and Schowengerdt, R. A.: Special issue on non-conventional pattern analysis in remote sensing, Pattern Recognition Letters, 17, 1323-1324, 1996.

Bolen, S. M., and Chandrasekar, V.: Methodology for aligning and comparing spaceborne radar and ground-based radar observations, Journal of Atmospheric and Oceanic Technology, 20, 647-659, 2003.

Boushaki, F. I., Hsu, K.-L., Sorooshian, S., Park, G.-H., Mahani, S., and Shi, W.: Bias adjustment of satellite precipitation estimation using ground-based measurement: A case study evaluation over the southwestern United States, J. Hydrometeor. , 10, 1231-1242, 2009.

Brandes, E. A.: Optimizing precipitation estimates with aid of radar, Journal of Applied Meteorology, 14, 1339-1345, 1975.

Chumchean, S., Sharma, A., and Seed, A.: Radar rainfall error variance and its impact on radar rainfall calibration, Physics and Chemistry of the Earth, 8, 27-29, 2003.

Cressie, N. A. C.: Statistics for spatial data revised edition, John Wiley & Sons, Inc., New York, 900 pp., 1993.

Dai, A., Giorgi, F., and Trenberth, K. E.: Observed and model-simulated diurnal cycles of precipitation over the contiguous United States, J. Geophys. Res., 104, 6377–6402, 1999.

Daly, C., Gibson, W. P., Taylor, G. H., Doggett, M. K., and Smith, J. I.: Observer bias in daily precipitation measurements at United States cooperative network stations, Bull. Amer. Meteor. Soc., 88, 899–912, 2007.

Daly, C., Taylor, G., and Gibson, W.: The PRISM Approach to Mapping Precipitation and Temperature, 10th Conf. on Applied Climatology, Reno, NV, Amer. Meteor. Soc., 10-12, 1997.

Doviak, R. J., and Zrnic, D. S.: Doppler radar and weather observations, Academic Press, San Diego, CA, 458 pp., 1984.

Duan, Q. A., Gupta, V. K., and Sorooshian, S.: Shuffled complex evolution approach for effective and efficient global minimization, J. Optimization Theory and Appl. , 76, 501-521, 1993.

Ebert, E. E., Janowiak, J. E., and Kidd, C.: Comparison of near-real-time precipitation estimates from satellite observations and numerical models, Bull. Amer. Meteor. Soc., 88, 47-64, 2007.

Ferraro, R. R.: SSM/I derived global precipitation estimates for climatological applications, J. Geophys. Res., 102, 16715-16735. , 1997.

Ferraro, R. R., Weng, F., Grody, N. C., and Zhao, L.: Precipitation characteristics over land from the NOAA-15 AMSU sensor, Geophys. Res. Ltr., 27, 2669-2672., 2000.

Finley, A., Banerjee, S., and Carlin, B.: Spbayes: An R package for univariate and multivariate hierarchical point-referenced spatial models, Journal of Statistical Software, 19, 1-20, 2007.

Fulton, R. A., Breidenbach, J. P., Seo, D. J., Miller, D. A., and O'Bannon, T.: The WSR-88D rainfall algorithm, Wea. Forecast, 13, 377-395, 1998.

Germann, U., Berenguer, M., Sempere-Torres, D., and Salvade, G.: Ensemble radar precipitation estimation-a new topic on the radar horizon, Fourth ERAD Conference, Barcelona, Spain, 559-562, 2006b.

Gottschalck, Jon, Jesse Meng, Matt Rodell, Paul Houser, 2005: Analysis of multiple precipitation products and preliminary assessment of their impact on global land data Assimilation System Land Surface States. J. Hydrometeor, 6, 573–598.

Gourley, J. J., Hong, Y., Flamig, Z. L., Wang, J., Vergara, H., Anagnostou, A. N.: Hydrologic evaluation of rainfall estimates from radar, satellite, gauge, and combinations on Ft. Cobb Basin, Oklahoma. J. Hydrometeor, 12, 973–988, 2011.

Gourley, J. J., Maddox, R. A., Howard, K. W., and Burgess, D. W.: An exploratory multisensor technique for quantitative estimation of stratiform rainfall, Journal of Hydrometeorology, 3, 166-180, 2002.

Grassotti, C., Iskenderian, H., and Hoffman, R. N.: Fusion of surface radar and satellite rainfall data using feature calibration and alignment, Journal of Applied Meteorology, 38, 677-695, 1999.

Grassotti, C., Leidner, S. M., Louis, J. F., and Hoffman, R. N.: Development and application of a visible-infrared rain flag for scatterometer data, Journal of Applied Meteorology, 38, 665-676, 1999.

Hoffman, R. N., and Grassotti, C.: A technique for assimilating SSM/I observations of marine atmospheric storms: Tests with ECMWF analyses, Journal of Applied Meteorology, 35, 1177-1188, 1996.

Iguchi, T., Meneghini, R., Awaka, J., Kozu, T., and Okamoto, K.: Rain profiling algorithm for TRMM precipitation radar data, Remote Sensing and Applications: Earth, Atmosphere and Oceans, 25, 973-976, 2000.

Johns, C. J., and Mandel, J.: A two-stage ensemble Kalman filter for smooth data assimilation, Environmental and Ecological Statistics, 15, 101-110, Doi 10.1007/S10651-007-0033-0, 2008.

Joyce, R. J., Janowiak, J. E., Arkin, P. A., and Xie, P.: CMORPH: A method that produces global precipitation estimates from passive microwave and infrared data at high spatial and temporal resolution, J. Hydromet., 5, 487-503, 2004.

Kessinger, C., Ellis, S., and Andel, J. V.: A fuzzy logic, radar echo classification scheme for the wsr-88d, 29th Int'l Conf. Radar Meteorology, Montreal, Canada, 12-16 July 1999, 1999.

Kitanidis, P. K.: Parameter uncertainty in estimation of spatial functions: Bayesian analysis, Water Resources, 22, 499-507, 1986.

Krajewski, W. F., and Smith, J. A.: Radar hydrology: Rainfall estimation, Advances in Water Resources, 25, 1387-1394, 2002.

Kuligowski, R. J.: A self-calibrating real-time GOES rain fall algorithm for short-term precipitation estimates, J. Hydrometeorol. , 3, 112-130, 2002.

Kummerow, C., Hong, Y., Olson, W. S., Yang, S., Adler, R. F., McCollum, J., Ferraro, R., Petty, G., Shin, D.-B., and Wilheit, T. T.: Evolution of the Goddard profiling algorithm (GPROF) for rainfall estimation from passive microwave sensors, J. Appl. Meteor., 40, 1801-1820., 2001.

Lawson, W. G., and Hansen, J. A.: Alignment error models and ensemble-based data assimilation, Monthly Weather Review, 133, 1687-1709, 2005.

Lee, G. W. and Zawadzki, I.: Variability of drop size distributions: time-scale dependence of the variability and its effects on rain estimation, J. Appl. Meteorol., 44, 241–255, 2005.

Lee, K. Z., Chuang, W. C., and Ho, S. Y.: A non-parametric image segmentation algorithm using an orthogonal experimental design based hill-climbing, Intelligent Data Engineering and Automated Learning, 2690, 1076-1081, 2003.

Levizzani, V.: Satellite precipitation estimates: New perspectives for meteorology and climate from the eurainsat project, Annals of Geophysics, 46, 363-372, 2003.

Mahani, S. E., and Khanbilvardi, R.: Generating multi-sensor precipitation estimates over radar gap areas, WSEAS (World Scientific and Engineering Academy and Society) Transactions on Systems, 8, 96-106, 2009.

Mandel, J., Beezley, J. D., Coen, J. L., and Kim, M.: Data assimilation for wild land fires: Ensemble kalman filters in coupled atmosphere-surface models, IEEE Control Systems Magazine, 29, 47-65, 2009.

Marshall, J., and Palmer, W. M.: The distribution of raindrops with size, J. Meteorol. , 5, 165-166, 1948.

McCollum, J. R., Krajewski, W. F., Ferraro, R. R., and Ba, M. B.: Evaluation of biases of satellite rainfall estimation algorithms over the continental United States, J. App. Meteorol., 41, 1065-1080, 2002.

Nehrkorn, T., Hoffman, R. N., Grassotti, C., and Louis, J. F.: Feature calibration and alignment to represent model forecast errors: Empirical regularization, Quarterly Journal of the Royal Meteorological Society, 129, 195-218, Doi 10.1256/Gj.02.18, 2003.

Ravela, S., Emanuel, K., and McLaughlin, D.: Data assimilation by field alignment, Physica D-Nonlinear Phenomena, 230, 127-145, Doi 10.1016/J.Physd.2006.09.035, 2007.

Rosenfeld, D., and Mintz, Y.: Evaporation of rain falling from convective clouds as derived from radar measurements, J. Appl. Meteor 27, 209-215, 1988.

Rozumalski, R. A.: A quantitative assessment of the NESDIS auto-estimator, Wea. Forecasting, 15, 397-408, 2000.

Ryzhkov, A., Giangrande, S., and Schuur, T.: Rainfall measurements with the polarimetric WSR-88D radar, Report of the National Severe Storms Laboratory, Norman, OK, 73069, 98 pp, 2003.

Sapiano, Smith, and Arkin P.: A new merged analysis of precipitation utilizing satellite and reanalysis data, J. Geophys. Res., 113, D22103, 2008.

Schuur, T., Ryzhkov, A., Heinselman, P. , Zrnic, D., Burgess, D., and Scharfenberg, K.: Observations and classification of echoes with the Polarimetric WSR-88D radar, Report of the National Severe Storms Laboratory, Norman, OK, 45 pp, 2003.

Scofield, R. A., and Kuligowski, R. J.: Status and outlook of operational satellite precipitation algorithms for extreme-precipitation events, Mon. Wea. Rev., 18, 1037-1051, 2003.

Seo, D.-J., and Breidenbach, J. P.: Real-time correction of spatially nonuniform bias in radar rainfall data using rain guage measurements, J. Hydrometeorol. , 3, 93-111, 2002.

Seo, D.-J., Ding, F., and Fulton, R.: Final report interagency memorandum of understanding among the NEXRAD program, the WSR-88D radar operations center, and the NWS office of hydrologic development, Office of Hydrologic Development, National Weather Service, Silver Spring, MD, 2002.

Seo, D. J.: Real-time estimation of rainfall fields using radar rainfall and rain gage data, Journal of Hydrology, 208, 37-52, 1998.

Shepard, D.: A two dimensional interpolation function for regularly spaced data, 23rd National Conf. of the Association for Computing Machinery, 1968, 517-524,

Smith, C. J.: The reduction of errors caused by bright bands in quantitative rainfall measurements made using radar. J. Atmos. Oceanic Technol., 3, 129–141, 1986.

Smith, J. A. and Krajewski,W. F.: A modeling study of rainfall rate reflectivity relationships, Water Resour. Res., 29, 2505–2514, 1993.

Smith, J. A., and Krajewski, W. F.: Estimatioin of the mean field bias of radar precipitation estimates, J. Appl. Metorol. , 30, 397-412, 1990.

Smith, T. M., Arkin, P. A., Bates, J. J., and Huffman, G. J.: Estimating bias of satellite-based precipitation estimates, J. Hydrometeor. , 7, 841-856, 2006.

Smith, T. M., Arkin, P. A., Bates, J. J., and Huffman, G. J.: Estimating bias of satellite-based precipitation estimates, Journal of Hydrometeorology, 7, 841-856, 2006.

Stein, M. L.: Spatial interpolation of high-frequency monitoring data, Annals of Applied Statistics, 3, 272-291, Doi 10.1214/08-Aoas208, 2009.

Steiner, M., Smith, J. A., Burges, S. J., Alonso, C. V., and Darden, R. W.: Effect of bias adjustment and rain gauge data quality control on radar rainfall estimation, Water Resources Research, 35, 2487-2503, 1999.

Stellman, K. M., Fuelberg, H. E., Garza, R., and Mullusky, M.: An examination of radar and rain gauge–derived mean areal precipitation over Georgia watersheds, Wea. Forecasting, 16, 133-144, 2001.

Tesfagiorgis, K., Mahani, S. E., Krakauer, N. Y., and Khanbilvardi, R.: Bias correction of satellite precipitation estimates using a radar-gauge product - a case study in Oklahoma (USA), Hydrology and Earth System Sciences, 15, 2631-2647, Doi 10.5194/Hess-15-2631-2011, 2011.

Tuttle, J. D., Carbone, R. E., Arkin, P. A.: Comparison of ground-based radar and geosynchronous satellite climatologies of warm-season precipitation over the United States J. Appl. Meteor. Climatol., 47, 3264–3270, 2008.

Vasiloff, S. V., Howard, K. W., and Zhang, J.: Difficulties with correcting radar precipitation estimates based on rain gauge data: A case study of severe weather in Montana on 16-17 June 2007, Weather and Forecasting, 24, 1334-1344, Doi 10.1175/2009waf2222154.1, 2009.

Vicente, G. A., Scofield, R. A., and Menzel, W. P.: The operational GOES infrared rainfall estimation technique, Bull. Amer. Meteor. Soc., 79, 1883-1898, 1998.

Vignal, B., and Krajewski, W. F.: Large-sample evaluation of two methods to correct range-dependent error for wsr-88d precipitation estimates, J. Hydrometeor., 2, 490–504, 2001.

Westrick, K. J., Clifford F. Mass, C. F., and Colle B. A.: The Limitations of the WSR-88D Radar network for quantitative precipitation measurement over the coastal western United States, Bull. Ame. Meteor. Soc., 80, 2289-2298, 1999.

Wilson, J. W.: Integration of radar and raingage data for improved rainfall measurement, J. Appl. Meteor, 9, 489-497, 1970.

Xie, P. P., and Arkin, P. A.: Analyses of global monthly precipitation using gauge observations, satellite estimates, and numerical model predictions, Journal of Climate, 9, 840-858, 1996.

Xie, P. P., and Arkin, P. A.: Global precipitation: A 17-year monthly analysis based on gauge observations, satellite estimates, and numerical model outputs, Bulletin of the American Meteorological Society, 78, 2539-2558, 1997.

Young, C. B., Nelson, B. R., Bradley, A. A., Smith, J. A., Peters-Lidard, C. D., Kruger, A., and Baeck, M. L.: An evaluation of nexrad precipitation estimates in complex terrain, Journal of Geophysical Research- Atmospheres 104, 19691-19703, 1999.